MODELLING, COMPENSATION AND APPLICATION OF GYRATOR CIRCUITS

Kolloru Srihivasulu Naidu

A THESIS

in

The Faculty

of

Engineering

Presented in Partial Fulfillment of the Requirements
for the Degree of Doctor of Engineering at
Concordia University
Montreal, Canada

March, 1975

MODELLING, COMPENSATION AND APPLICATION OF GYRATOR CIRCUITS

KOLLORU SRINIVASULU NAIDU

ABSTRACT

The thesis proposes a new approach for the analysis and modelling of operational amplifier gyrator circuits. Two gyrator circuits are considered. Assuming a typical range of amplifier specifications, a model is derived for each gyrator circuit comprising resistances, capacitances and inductances. The validity of the models is established using an exact computer-aided analysis and then by experiment.

The derived models indicate clearly the influence of each amplifier imperfection on the performance of the gyrator circuits. The effects of temperature and supply voltage variations on the simulated inductance are studied. A method for evaluating the voltage handling capabilities of gyrator circuits is proposed.

Low and high frequency operation of a gyrator circuit is studied. A compensation technique is developed whereby the useful bandwidth of the gyrator can be increased. The compensation technique is verified first by computer-aided analysis and then by experiment.

The modelling considerations and the compensation technique are applied in the design of a critical twelfth order channel bandpass filter. A design procedure is given for gyrator-C filters which can be used for filters with grounded inductors. The influence of dc supply voltage and ambient temperature variations on the performance of the filter is examined.

ACKNOWLEDGEMENTS

The author is deeply indebted to Dr. A. Antoniou for his supervision and suggestions throughout the preparation of this thesis.

Thanks are due to J. Valihora, J. Rinel and J.T. Lim for useful discussions and comments.

The author also gratefully acknowledges the patience and sacrifices offered by his wife during the preparation of this thesis.

Thanks are due to Miss Margaret MacKinnon for her excellent job in typing the thesis.

This work is supported under the Bell-Northern Research Ltd. grant, and National Research Council of Canada grant awarded to Dr. A. Antoniou.

TABLE OF CONTENTS

LIST OF FIGURES

CHAPTER 1

INTRODUCTION

1.1 General

The state-of-the-art of designing passive RLC filters can be said to be quite mature [1]-[3]. Most properties of passive networks are well understood, and many methods have been devised to obtain various network functions. However, there are several problems encountered in the design of RLC filters. One of them is the magnetic coupling between elements which may introduce errors in instruments such as those carried in satellites for measuring very weak signals. Probably the major difficulty arises in the case of low-frequency applications, such as control systems and instrumentation. At low frequencies, less than 1 kHz, practical inductors of reasonable Q-factor tend to become very bulky and expensive.

Active inductorless filters were first considered in the late Thirties [4] when they were built using vacuum tubes, resistors and capacitors. Because of the bulky size and large power consumption of vacuum tubes, active filters did not receive much attention. Development of transistors in the late Forties revitalized the interest in this area. The research and development efforts in active filters in recent years have been influenced primarily by the progress and breakthroughs in the rapidly developing area of integrated circuit technology. Now-a-days many network elements and their functional interconnections are fabricated as single devices. The main advantages of integrated microcircuits are the following [5]-[6]:

(i) Increased system reliability

(ii) Reduction of size and weight

(iii) Reduction in power dissipation

It is perhaps in the area of integration that one is confronted with the major drawback in the use of inductors. This is due to the fact that it has not yet been possible to fabricate inductors with reasonable value of inductances and quality factors by integrated circuit techniques [6]-[7]. On the other hand, conventional inductors, when miniaturized to be consistent in size with other integrated circuit components, are extremely poor in quality to be of any use for many applications [8]. These problems can be overcome by eliminating inductors through active RC filter design. Active RC filters have the following additional advantages over RLC filters [7]:

(i) Use of active elements removes two fundamental restrictions from RLC networks, namely, passivity and reciprocity. As a result, active networks can realize network functions which can not be realized by passive RLC networks.

(ii) Active filters often provide insertion gain, thereby eliminating the need for additional amplifiers.

(iii) The filter output impedance can be made very low. Consequently, the filters can be cascaded without additional buffer stages.

Active RC networks, however, may have two problems associated with them. These are [7]:

(i) An improperly designed active filter can become unstable, while passive RLC networks are absolutely stable.

(ii) If proper attention is not given to their design, active filters may turn out to be highly sensitive to element variations. For resistively terminated LC filters the sensitivity problem is not serious.

Active RC filters are now commercially available in hybrid integrated circuit forms [9]. They are used extensively in many areas, for example, in telephone and data communication systems, as they are more economical for low frequency applications.

1.2 Active Network Elements

The commonly used active network elements are the various controlled sources, the negative impedance converter, the operational amplifier, the gyrator [10] and the frequency-dependent negative resistance (FDNR) [11]. The ideal characteristics of these devices are summarized in Table 1.1. Since this thesis is concerned with gyrators implemented with operational amplifiers, the properties of operational amplifiers are discussed next.

1.3. Operational Amplifier

One of the most versatile active network element is the operational amplifier which finds applications in such diverse areas as control systems, communications, precision instruments and analog computers. The ideal operational amplifier is basically an infinite gain, voltage controlled voltage source. The input impedance is infinite and output impedance is zero. The model and symbolic representation of an ideal operational amplifier are shown in Fig. 1.1, where

ACTIVE NETWORK ELEMENT	INPUT-OUTPUT RELATIONS	NETWORK SYMBOL
VOLTAGE-CONTROLLED VOLTAGE SOURCE, VCVS OR VOLTAGE AMPLIFIER	$V_2 = \mu V_1$ $I_1 = 0$	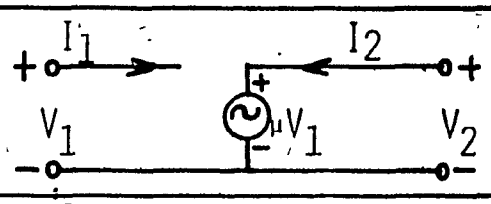
CURRENT-CONTROLLED CURRENT SOURCE, CCCS OR CURRENT AMPLIFIER	$I_2 = \alpha I_1$ $V_1 = 0$	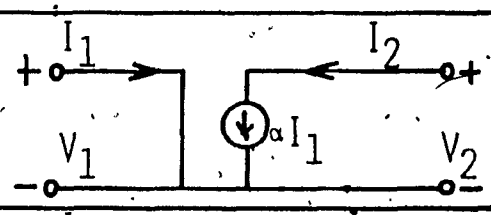
VOLTAGE-CONTROLLED CURRENT SOURCE, VCCS	$I_2 = gV_1$ $I_1 = 0$	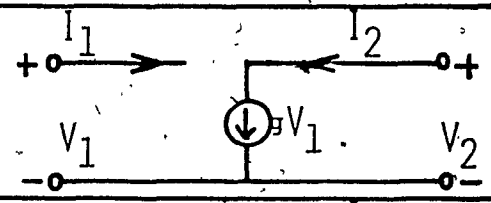
CURRENT CONTROLLED VOLTAGE SOURCE, CCVS	$V_2 = rI$ $V_1 = 0$	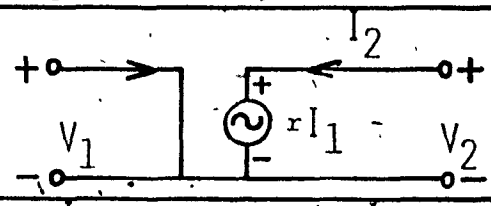
NEGATIVE-IMPEDANCE CONVERTER NIC	$V_1 = K_1 V_2$ $I_2 = K_2 I_1$	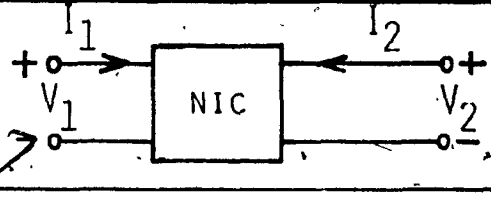
POSITIVE-IMPEDANCE INVERTER, PIV (ACTIVE GYRATOR)	$I_1 = g_1 V_2$ $I_2 = -g_2 V_1$	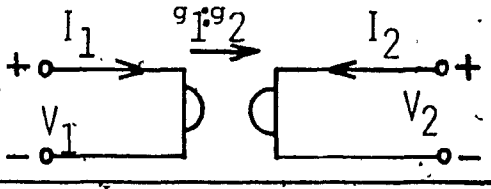
OPERATIONAL AMPLIFIER	$V_o = A(V_2 - V_1)$ $A \to \infty$ $I_1 = I_2 = 0$	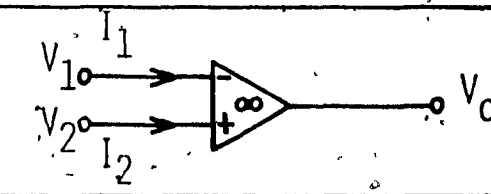
FREQUENCY DEPENDENT NEGATIVE RESISTANCE FDNR	$I_1 = V_1 s^2 D$	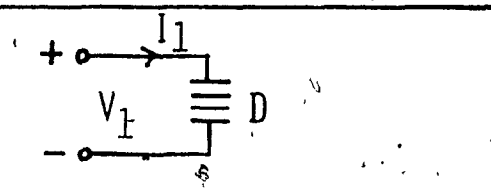

TABLE 1.1 COMMONLY USED LINEAR ACTIVE ELEMENTS.

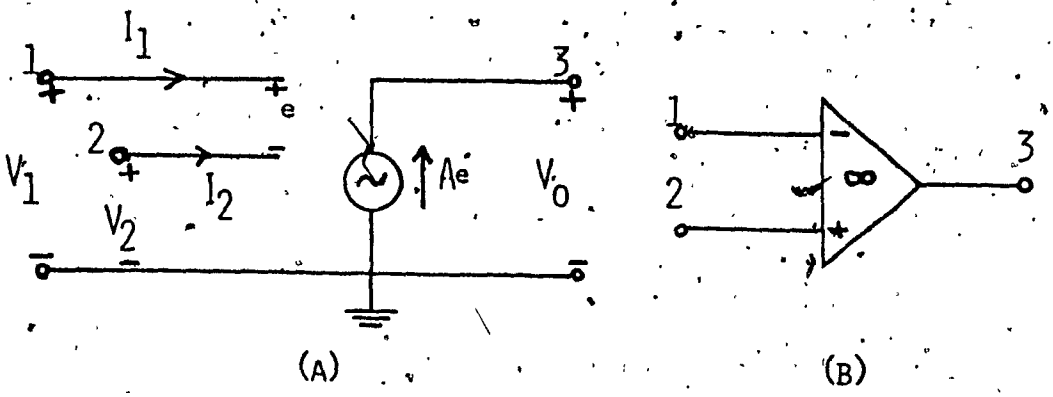

FIG. 1.1 THE OPERATIONAL AMPLIFIER
(A) CONTROLLED-SOURCE REPRESENTATION
(B) SYMBOLIC REPRESENTATION

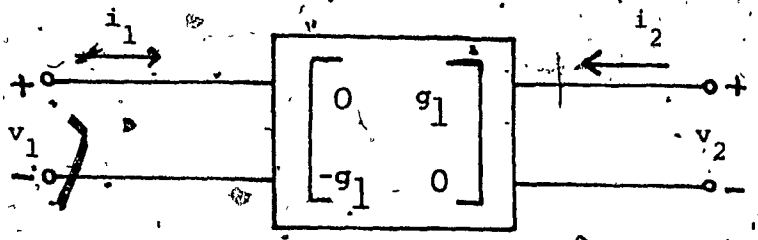

FIG. 1.2 IMPEDANCE INVERTING CIRCUIT

$$V_o = A(V_1 - V_2) = Ae \qquad A \to \infty \qquad (1.1)$$

$$I_1 = I_2 = 0 \qquad V_o = 0 \text{ when } V_2 = V_1 \qquad (1.2)$$

The practical operational amplifier is characterized by a frequency-dependent voltage gain, monotonically decreasing with frequency from a high value at dc, and having finite input and output impedances. There is usually an upper limit on the input and output signal levels. Other sources of nonidealness include the finite input offset voltage and finite unequal common-mode impedances of the two input terminals.

The gain characteristic in almost all uncompensated operational amplifiers rolls off faster than 12dB/octave. This inevitably creates a stability problem. For stable operation, external compensating networks must be added to modify the amplifier gain characteristics. In using the μA709 operational amplifier it is usually necessary to use a resistor and two capacitors for compensation purposes. However, internally compensated operational amplifiers are also available (e.g. the μA741). The μA741 operational amplifier is input over-voltage and output short-circuit protected. It has an input resistance of 2MΩ, output resistance of 75Ω and gain-bandwidth product of 1MHz. Its price is less than $1.00, compared with $70.00 for μA709 in 1965, and there is every indication that costs will reduce further in future.

1.4 Gyrator

Gyrator is a two-port device described by the admittance matrix

$$[y] = \begin{bmatrix} 0 & g_1 \\ -g_2 & 0 \end{bmatrix} \qquad (1.3)$$

where g_1 and g_2 are positive real numbers and are known as the gyration conductances. The prime property of the gyrator is its nonreciprocity. An expression for the total power absorbed at the two ports in Fig. 1.2 can be obtained as

$$v_1 i_1 + v_2 i_2 = v_1 v_2 (g_1 - g_2) \qquad (1.4)$$

If $g_1 \neq g_2$, the total power delivered to the two ports becomes negative for some suitably chosen excitations and, as a result, in general, the gyrator is an active device (active gyrator). If $g_1 = g_2 = g$, the expression for the total power vanishes for all values of V_1 and V_2. The network can then neither supply nor absorb any power (ideal gyrator). This special network was first conceived by Tellegen [10] as an ideal circuit element. Symbolic representations of active and ideal gyrators are given in Fig. 1.3.

The input impedance Z_i of a gyrator is proportional to the load admittance Y_L, that is

$$Z_i = kY_L \qquad (1.5)$$

where k is a positive constant referred to as the gyration constant. Eqns. 1.3 and 1.5 show readily that

$$k = 1/g_1 g_2$$

For impedance inversion it is primarily the product $g_1 g_2$ that is important. Evidently, a capacitance C at the output port will be converted to an inductance $L = C/g_1 g_2$, as illustrated in Fig. 1.4a. A floating inductance can be simulated using two grounded gyrators [12],

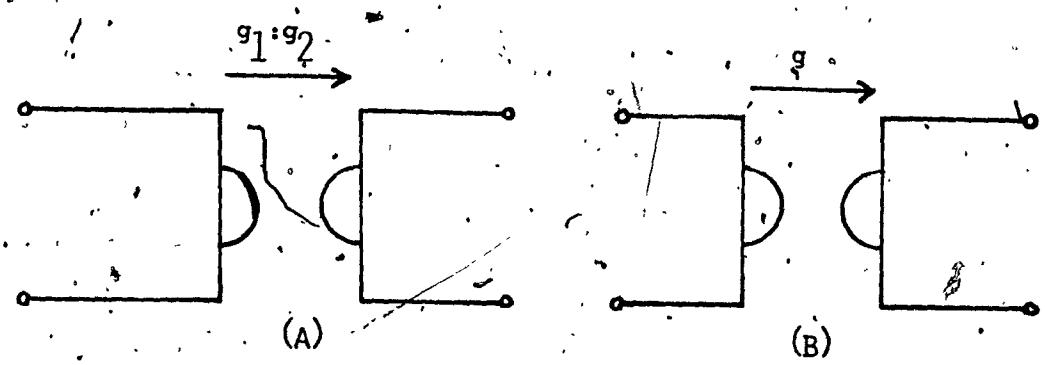

FIG. 1.3 SYMBOLIC RESPRESENTATIONS OF GYRATORS
(A) ACTIVE GYRATOR
(B) IDEAL GYRATOR

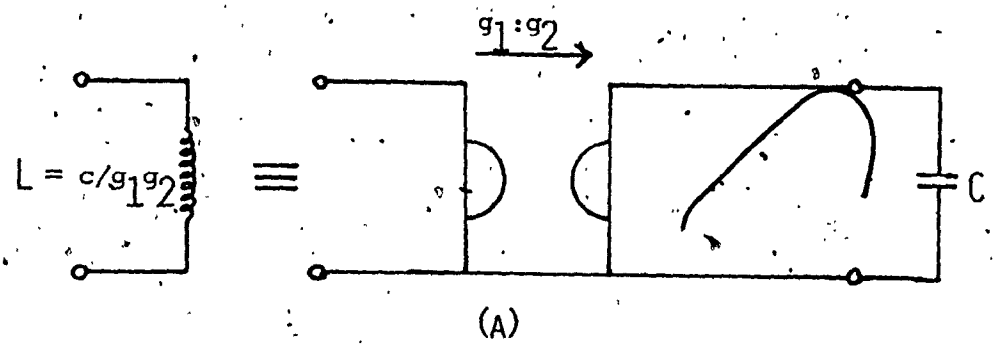

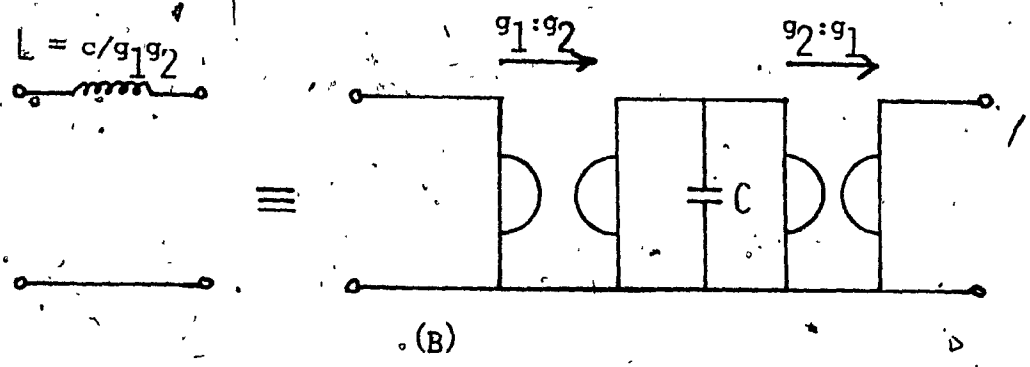

FIG. 1.4 USE OF GYRATORS
(A) TO SIMULATE A GROUNDED INDUCTOR
(B) TO SIMULATE A FLOATING INDUCTOR

as shown in Fig. 1.4b.

1.5 Active RC Network Synthesis

Many methods of active RC network synthesis have been proposed mostly using operational amplifiers [13]-[16], fixed gain amplifiers [17]-[19], or negative impedance converters [20]-[30] as active elements. The majority of these tend to give filters which are very sensitive to element variations [31]-[34]. This is especially serious for high selectivity and close-tolerance filters. Active RC filters having low sensitivity to component variations have also been proposed [35]-[37]. They illustrate the method of obtaining reduced sensitivity at the cost of more active and passive elements. In many of these configurations [35], [36], spread of component values is quite large [6].

Orchard [32] has demonstrated that doubly terminated LC ladder filters are inherently insensitive to element variations. Thus, a simple way of designing a low-sensitivity active RC filter is to design a conventional LC filter first for the prescribed specifications, and then replace the inductances by simulated inductances [38]-[42]. This approach offers the following additional advantages:

(1) The design is simple due to the availability of tabulated data and filter design programs for LC filters [43]-[44].

(2) Filters are easy to align because simulated inductances can be adjusted by trimming resistors [40].

An inductance can be simulated by a capacitively terminated gyrator [40], [45]-[51]. Consequently, with the availability of good quality gyrator circuit, inductorless filters can be designed which are

as insensitive as passive RLC filters [6], [11], [38]-[40], [49], [52], [53], [82]. Bruton has also advanced similar philosophy to design active filters using frequency dependent negative resistance elements.

In the last few years, gyrator circuits have been applied to the implementation of low-pass and bandpass filters [38], [52]-[57]. However, in these implementations custom designed amplifiers were used to construct gyrator circuits and hence the cost per filter was quite high. Alternative methods of constructing good quality, cheap gyrator circuits are thus required to produce inexpensive inductorless active filters.

The use of operational amplifiers leads to inexpensive gyrator circuits. This is due to the fact that integrated-circuit operational amplifiers are readily available as off-the-shelf components and are very cheap, owing to the enormous demand.

1.6 Scope of the Thesis

The present work investigates a new approach for the analysis and modelling of operational amplifier gyrator circuits. Models are derived for two gyrator circuits and their validity is established by using an exact computer-aided analysis. The models are then used to examine the performance of gyrator circuits. A compensation technique is next proposed to increase gyrator bandwidth. A critical twelfth order channel bandpass filter is designed and tested using compensated circuits.

The thesis is divided into five main chapters. In Chapter 2, various gyrator realizations are studied. The disadvantages associated with transistor gyrator circuits are pointed out. The properties,

advantages and disadvantages of different operational amplifier gyrator circuits are then discussed.

In Chapter 3, available gyrator models are reviewed. These models are unsatisfactory for many practical applications, such as to analyze and optimize highly-selective gyrator-C filters. A new approach for the analysis and modelling of gyrator circuits is presented next. Models, comprising resistances, capacitances and inductances, are derived for two gyrator circuits reported in reference [63]. The validity of the derived models is next established using an exact computer-aided analysis. Experimental results given substantiate the validity of the model.

The gyrator models developed are useful in four respects as follows:

(1) The influence of each operational amplifier imperfection on the performance of the gyrator circuit can be clearly understood.

(2) They can be used for computer-aided analysis of capacitively terminated gyrator circuits.

(3) They can be used for the optimization of the gyrator circuits.

(4) They can be used for the computer-aided analysis of gyrator-C filters.

In Chapter 4, the derived models are used to evaluate the performance of the gyrator circuits. First the influence of each operational amplifier imperfection on the simulated inductance is examined. It is shown that the most significant parameter of the

amplifier is the gain-bandwidth product. Next, the influence of temperature and dc supply voltage variations on the simulated inductance is investigated. Equations are derived for the temperature coefficient of the simulated inductance. The performance of a gyrator circuit to temperature and dc supply voltage variations is examined experimentally to verify the theoretical results. Further, in this chapter, a method for evaluating the voltage handling capabilities of gyrator circuits is proposed. The two gyrators of Reference [63] are then compared.

Chapter 5 proposes a compensation technique whereby the useful bandwidth of the gyrator can be increased significantly. The technique is verified first by computer-aided analysis and then by experiment.

Chapter 6 uses the modelling consideration of Chapter 3 and the compensation technique of Chapter 5 in the design of a critical twelfth order gyrator-C channel bandpass filter. The filter is constructed using low cost μA741 operational amplifiers. The chapter is concluded with a presentation of experimental results and it is shown that the entire filter can be fabricated using the hybrid integrated circuit technology.

The results obtained and possible extensions of the work are summarized in Chapter 7.

CHAPTER 2

GYRATOR CIRCUITS

In this chapter various gyrator realizations are studied. The disadvantages associated with transistor gyrator circuits are pointed out. The properties, advantages and disadvantages of different operational amplifier gyrator circuits are then discussed.

2.1 Transistor Gyrator Realizations

The admittance matrix of an ideal gyrator circuit can be split up as

$$\begin{bmatrix} 0 & g_1 \\ -g_2 & 0 \end{bmatrix} = \begin{bmatrix} 0 & 0 \\ -g_2 & 0 \end{bmatrix} + \begin{bmatrix} 0 & g_1 \\ 0 & 0 \end{bmatrix} \tag{2.1}$$

where the two matrices on the right-hand side represent ideal voltage controlled current sources with transconductances $-g_2$ and g_1, repectively. It follows that a gyrator can be realized as a parallel and back-to-back connection of two voltage controlled current sources as shown in Fig. 2.1.

The preceding technique has been used extensively for the design of transistor gyrator circuits [58]-[61]. Some of the published circuits, such as those advanced by Rao and Newcomb [60], and Sheahan and Orchard [61] shown in Figs. 2.2 and 2.3, can be readily integrated. In general, however, transistor gyrator circuits are subject to the following disadvantages:

(a) It is necessary to fabricate a special purpose integrated circuit and, consequently, the cost per device will be relatively high.

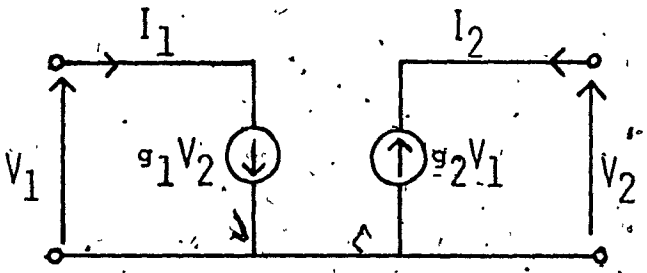

FIG. 2.1 GYRATOR REALIZATION USING VCCS'S

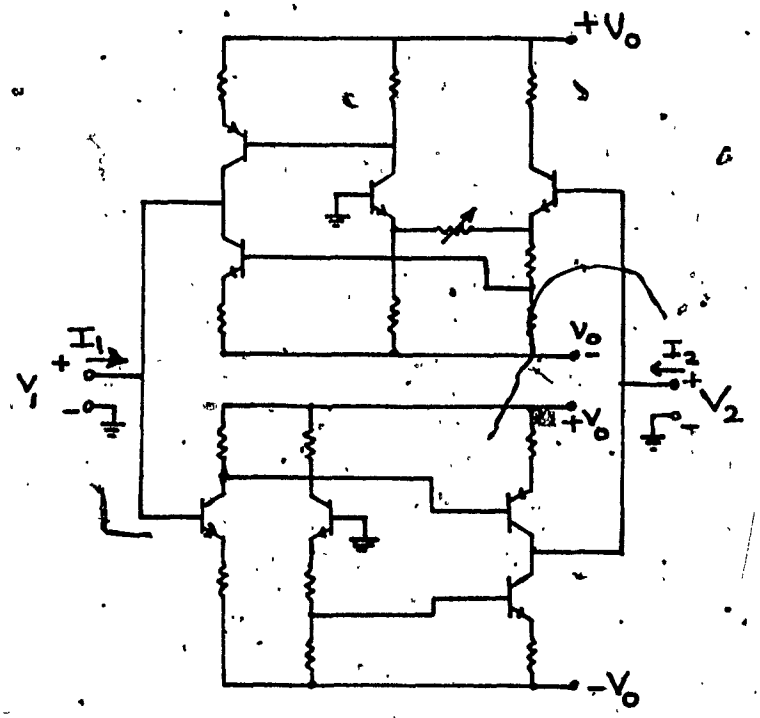

FIG. 2.2 A DIRECT-COUPLED GYRATOR SUITABLE FOR INTEGRATED CIRCUITS AND TIME VARIATIONS

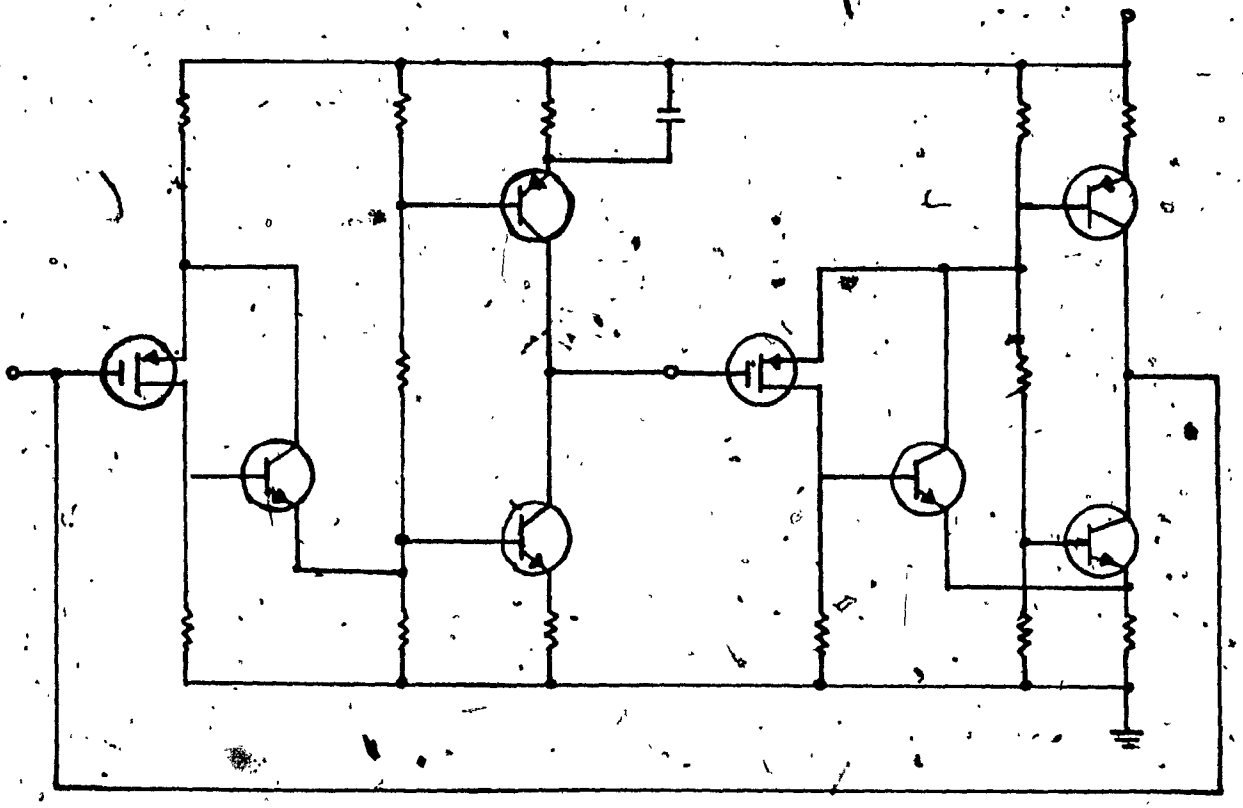

FIG. 2.3 INTEGRABLE GYRATOR USING M.O.S. AND BIPOLAR TRANSISTORS

(b) In practice, an adjustable gyration constant is required and it becomes necessary to make resistance adjustments within the gyrator circuit. This can be overcome by fabricating the gyrator as a hybrid circuit where resistances needing adjustments are fabricated as external thin-film or thick-film components. In transistor gyrator circuits two sets of adjustments are, in general, necessary. First to control the gyration constant and second to set the operating points of individual transistor stages. It is found that five or six and sometimes more resistance adjustments are, in general, needed.

(c) The stability of the gyration constant depends on the amount of negative feedback that can be applied to each voltage controlled current source. An over all feedback from output to input has been found difficult to apply [62]. Instead, local feedback is applied at each individual transistor stage and, consequently, variations in coupling elements between transistor stages can cause variations of a similar magnitude in the transconductance and accordingly in gyration constant.

(d) To achieve proper transistor biasing both pnp and npn transistors are needed. Integrated circuits with both pnp and npn transistors are more expensive to fabricate.

On account of these disadvantages interest has been directed towards gyrator circuits using readily available integrated operational amplifiers.

2.2 Gyrators Using Operational Amplifiers

An alternative gyrator realization to that outlined in Section 2.1 can be obtained by cascading a negative-impedance converter (NIC) in which

$$Z_i = -\frac{R_1}{R_4} Z_L \qquad (2.2)$$

and a negative-impedance inverter (NII) in which

$$Z_i = -\frac{R_2 R_3}{Z_L} \qquad (2.3)$$

as shown in Fig. 2.4a. Eqns. 2.2 and 2.3 give the input impedance of the gyrator as

$$Z_i = \frac{R_1 R_2 R_3}{R_4 Z_L} \qquad (2.4)$$

Another gyrator realization can be obtained by using two voltage-controlled voltage-sources as shown in Fig. 2.4b. A simple analysis shows readily that the input impedance is again given by Eqn. 2.4.

NIC's and NII's and voltage-controlled voltage-sources can be readily implemented by using operational amplifiers and, therefore, the circuits of Fig. 2.4a and 2.4b can be implemented as shown in Figs. 2.5a and 2.5b. These circuits were first proposed in [64] and [67], respectively. It is observed from Eqn. 2.4 that the operation of the circuits of Fig. 2.5 remain unchanged if R_4 and Z_L are interchanged and hence nodes 33' can also be used as the output port.

The circuits of Fig. 2.5 have been found to be conditionally stable [40], [65] in a sense similar to that of Bode [66] and the amplifiers can lock in an unstable mode or latched-up condition during activation. This effect has also been observed by Riordan [67] and

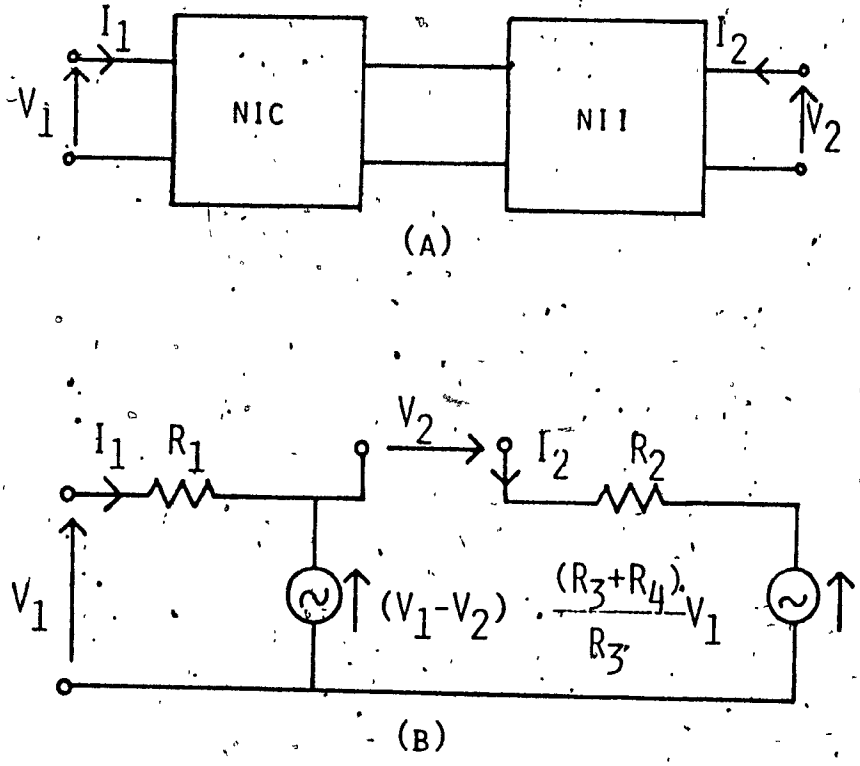

FIG. 2.4 GYRATOR REALIZATIONS

(A) CASCADING AN NIC AND AN NII.
(B) USING VCVS'S.

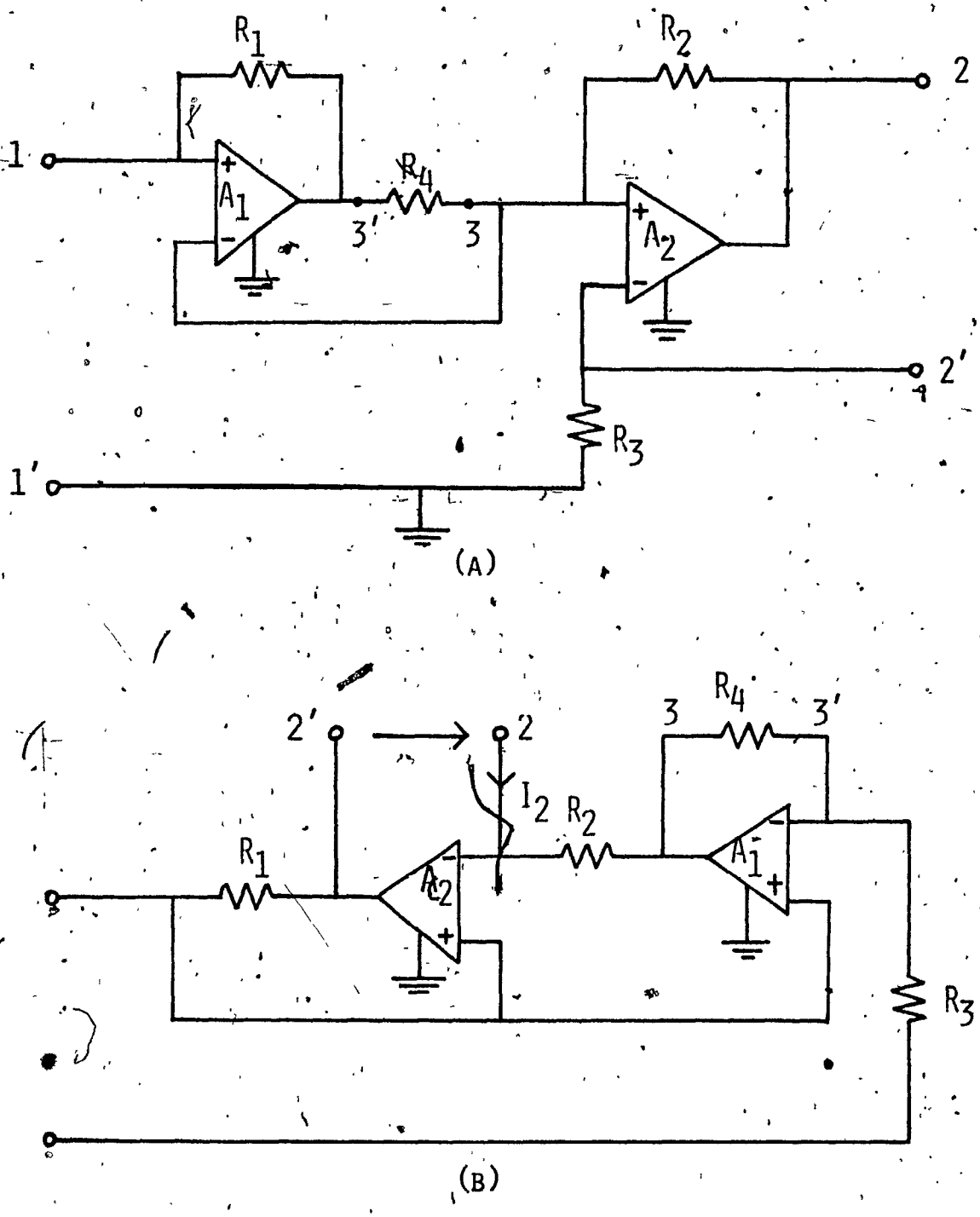

FIG. 2.5 GYRATOR REALIZATIONS USING OPERATIONAL AMPLIFIERS

(A) CIRCUIT OBTAINED FROM FIG. 2.4A

(B) CIRCUIT OBTAINED FROM FIG. 2.4B

Orchard and Sheahan [38] in Riordan's circuit given in Fig. 2.5b but it was erroneously attributed to a weakness in the amplifiers used rather than a weakness in the gyrator circuit.

Two other gyrator circuits, illustrated in Figs. 2.6a and 2.6b have been derived from those of Figs. 2.5a and 2.5b, respectively by using the nullor transformation [40], [63], [65]. For ideal operational amplifiers, the circuits of Figs. 2.6a and 2.6b are equivalent to those of Figs. 2.5a and 2.5b respectively, and hence the input impedance of circuits in Figs. 2.6a and 2.6b is given by Eqn. 2.4. In analogy to the original circuits R_4 and Z_L can be interchanged. A stability analysis [40], [65] has shown that the derived circuits are unconditionally stable and, in practice, the tendency for a latched-up condition is completely absent. The circuits of Fig. 2.6 have all the advantages of those of Fig. 2.5 and so far none of the disadvantages. Therefore, the former should be preferred. For ideal amplifiers, the y parameters for the circuits of Figs. 2.5a and 2.6a are given by

$$[y] = \begin{bmatrix} 0 & \dfrac{R_4}{R_1 R_2} \\ -\dfrac{1}{R_3} & 0 \end{bmatrix} \qquad (2.5)$$

and similarly for the circuits of Figs. 2.5b and 2.6b by

$$[y] = \begin{bmatrix} 0 & \dfrac{1}{R_1} \\ -\dfrac{R_4}{R_2 R_3} & 0 \end{bmatrix} \qquad (2.6)$$

From Eqns. 1.5, 2.5 and 2.6 the ideal gyration constant is obtained as

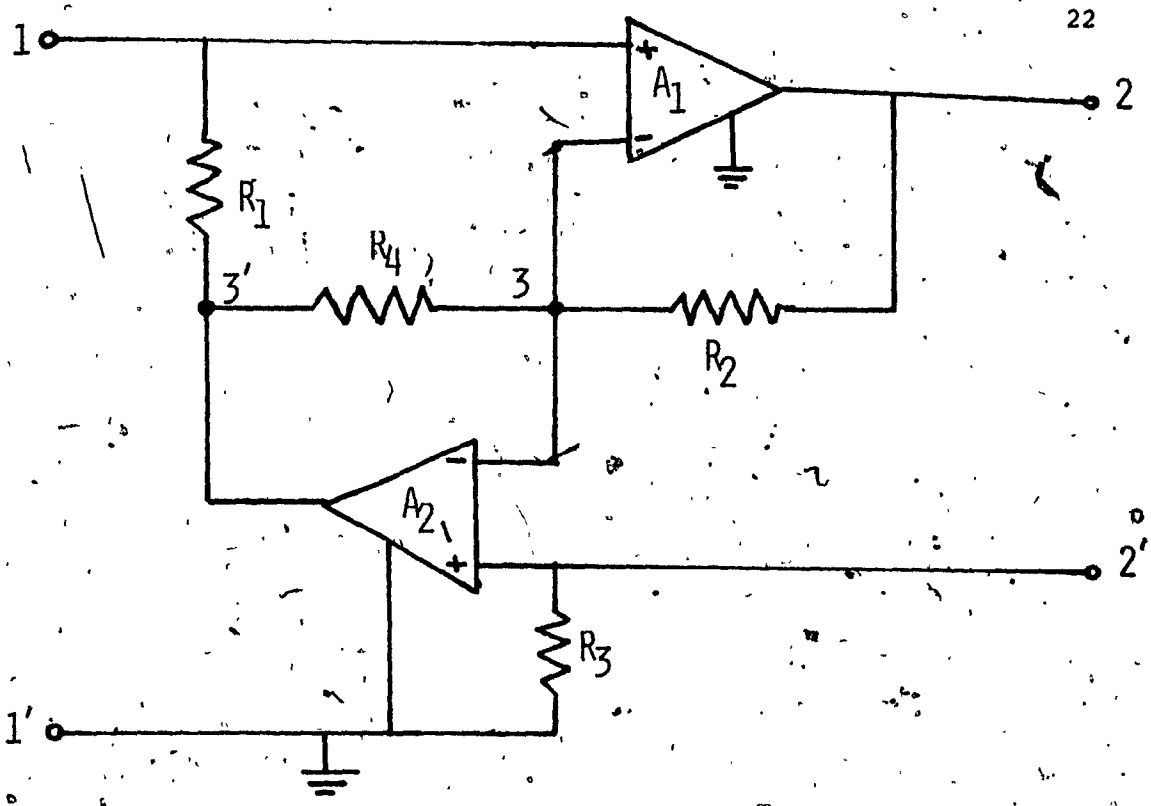

(A)

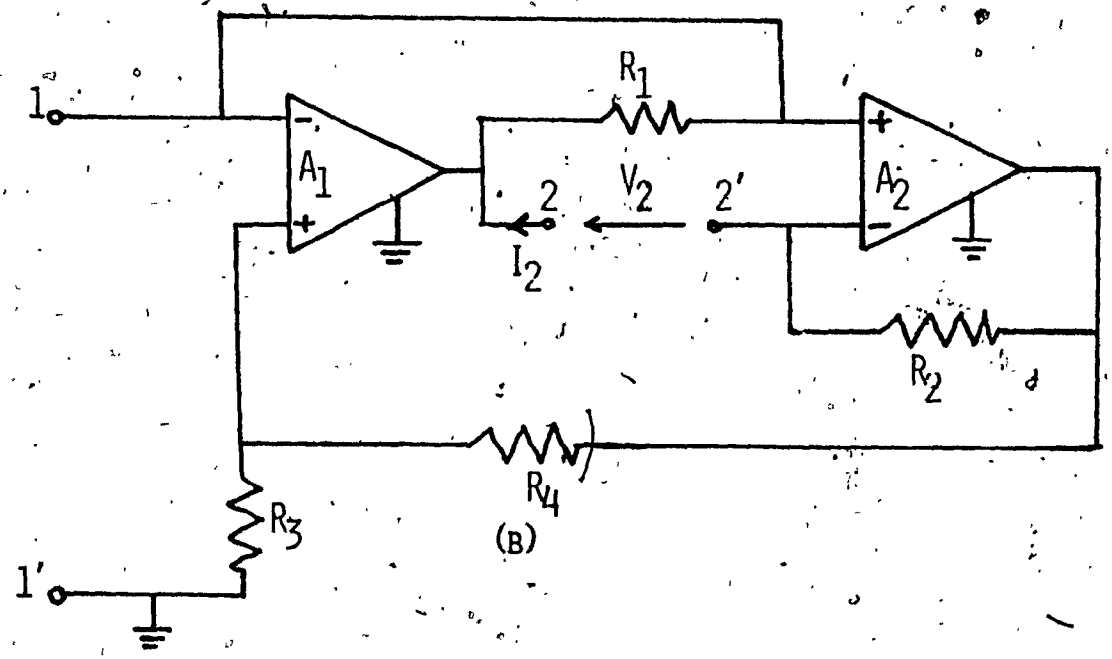

(B)

FIG. 2.6 ALTERNATE GYRATOR CIRCUITS
(A) DERIVED FROM FIG. 2.5A
(B) DERIVED FROM FIG. 2.5B

$$k = \frac{R_1 R_2 R_3}{R_4} \tag{2.7}$$

The following advantages can be attributed to the gyrator circuits made with operational amplifiers:

(a) It is unnecessary to fabricate a special purpose integrated circuit since integrated-circuit chip operational amplifiers are readily available as off-the-shelf components. To fabricate a gyrator circuit it is only necessary to design a thin-film or thick-film substrate with four resistors upon which a chip dual operational amplifier is bonded. The low cost of the operational amplifier and the substrate lead to an inexpensive gyrator circuit.

(b) Adjustments of the simulated inductances and the gyration constant are very simple since they can be carried out by trimming any one of the four resistors. The resistors are external to the amplifiers and hence the operation of the amplifiers is not influenced. Also tolerance variations in the four resistors can be compensated by adjusting only one of the four resistors.

The gyrator circuits of Figs. 2.5 and 2.6 are seen to be four-terminal devices with the output port floating. However, this is unimportant for the simulation of grounded inductances. Three-terminal gyrator circuits have been proposed by Morse and Huelsman [68], Deboo [69], and Antoniou [70]. In these circuits y_{11} and y_{22} are reduced to zero by cancelling positive by negative resistances and for high Q-factors it is necessary to adjust and maintain distinct resistances to a very precise match. Effectively, the circuits are sensitive to

element variations. On the other hand, no matching is required in the gyrator circuits of Figs. 2.5 and 2.6. The gyrator circuit of Fig. 2.5a has been found to give stable and high Q-factor inductances [28], [40], [71]-[74]. It has been used for the design of a new digitone detector [71] which is currently manufactured.

CHAPTER 3

MODELLING OF GYRATOR CIRCUITS

Circuit elements are often represented by simple models so as to facilitate analysis procedures, design methods and synthesis techniques to a manageable size. In this chapter, modelling of gyrator circuits is investigated [78], [79].

In Section 3.1, the old method of modelling gyrator circuits is reviewed. The old model is based on the assumption that the imperfection due to nonzero y_{11} and y_{22} in the admittance matrix are real, constant and equal. Also y_{12} and y_{21} are assumed to be equal and constant in magnitude. These assumptions are not true for the practical gyrator circuits. The y parameters are complex and depend on the parameters of the active elements employed for the gyrator circuit.

A more exact method of analyzing gyrator circuits is presented in Section 3.2. The method is demonstrated for a gyrator circuit (referred to as gyrator GA) constructed employing operational amplifiers. Each operational amplifier is replaced by a suitable model and exact equations are derived for the y parameters of the gyrator GA. Using suitable approximations based on the typical range of operational amplifier specifications, the y parameters are then simplified.

In Section 3.3 a model is derived for the capacitively terminated gyrator GA. In Section 3.4 the model is used for the analysis of gyrator GA. The frequency responses are in close agreement with those obtained by using an exact computer-aided analysis. The validity of the model is thus justified. The simplicity of the model by comparison

with an exact equivalent circuit leads to a significant reduction in the cost of computation. In Section 3.5 the model is verified by an experiment.

The new method of analyzing and modelling gyrator circuits is demonstrated for a second gyrator circuit (referred to as Gyrator GB) in appendix A.

3.1 Old Models

An ideal gyrator should have an admittance matrix

$$[y] = \begin{bmatrix} 0 & g \\ -g & 0 \end{bmatrix} \tag{3.1}$$

where g is the gyration conductance.

The first imperfection in a nonideal gyrator circuit is due to nonzero principal diagonal elements in the Eqn. 3.1. Assume that the admittance matrix is

$$[y] = \begin{bmatrix} \varepsilon g & g \\ -g & \varepsilon g \end{bmatrix} \tag{3.2}$$

where ε is a real constant less than unity. The equivalent circuit of such an nonideal gyrator circuit terminated by a lossless capacitor C is shown in Fig. 3.1.

The admittance Y_{in} seen at the input of Fig. 3.1 is given as

$$Y_{in} = y_{11} - \frac{y_{12}y_{21}}{y_{22} + Y_L}$$

$$= \varepsilon g + \frac{g^2}{\varepsilon g + Cs} \tag{3.3}$$

and can be represented as shown in Fig. 3.2.

Fig. 3.2 is similar to the equivalent circuit of a normal

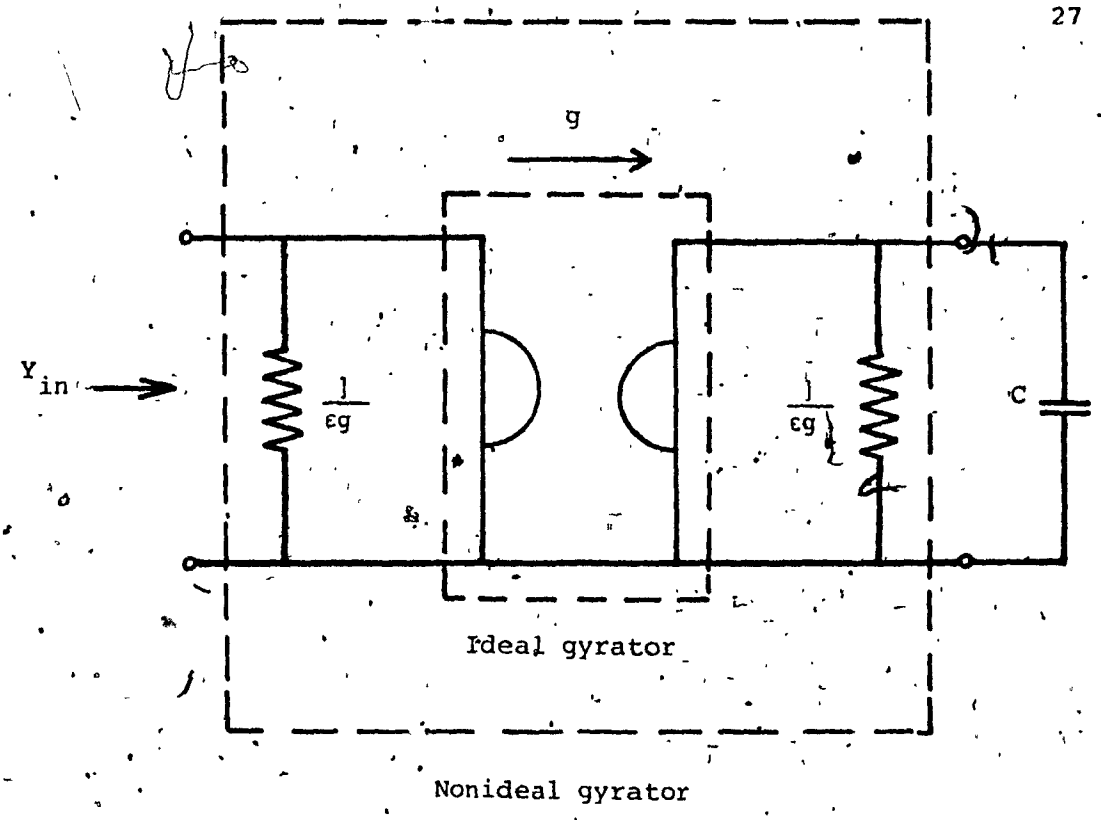

FIG. 3.1 CIRCUIT REPRESENTATION OF A NONIDEAL GYRATOR WITH NONZERO Y_{11} AND Y_{22}.

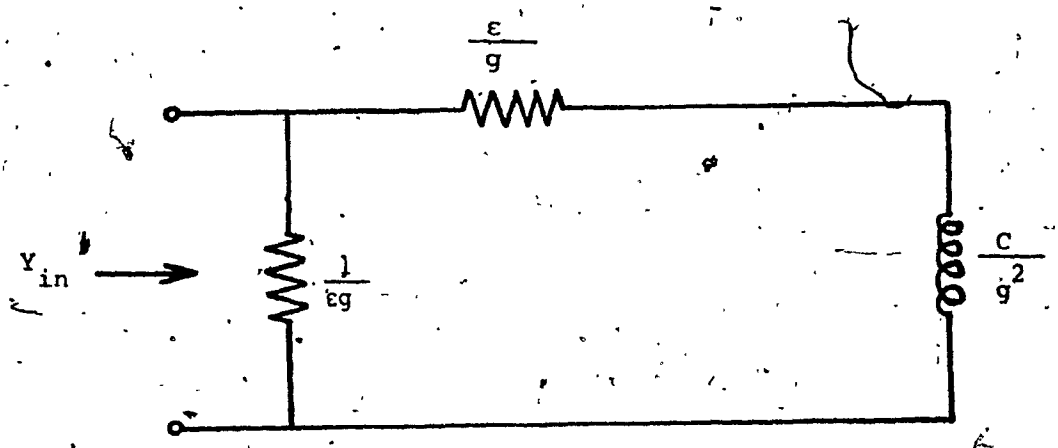

FIG. 3.2 MODEL FOR THE INDUCTANCE SIMULATED BY A GYRATOR WITH NONZERO Y_{11} AND Y_{22}.

iron-cored inductor in which core and winding losses are represented by shunt and series resistances, respectively.

Neglecting terms in ε^2, the Q-factor for the inductance simulated in Fig. 3.2 can be derived as

$$Q = \frac{\mathrm{Im}Z_{in}}{\mathrm{Re}Z_{in}}$$

$$= \frac{1}{\varepsilon} \frac{(\omega C/g)}{1 + (\omega C/g)^2} \qquad (3.4)$$

The maximum value of the Q-factor is $(2\varepsilon)^{-1}$ and occurs when $\omega C/g = 1$. Nonzero values in the principal diagonal elements of the admittance matrix in Eqn. 3.1 thus correspond to dissipation in the simulated inductance and limit the maximum achievable Q-factor.

The second imperfection in a nonideal gyrator is due to the fact that gyration conductances are not purely conductive but have a small phase angle ϕ. The admittance matrix for the nonideal gyrator can then be written as

$$[y] = \begin{bmatrix} 0 & ge^{-j\phi} \\ -ge^{-j\phi} & 0 \end{bmatrix} \qquad (3.5)$$

and hence for a lossless load capacitor the input admittance becomes

$$Y_{in} = \frac{1}{s} \frac{g^2}{Ce^{2j\phi}} \qquad (3.6)$$

By letting $s = j\omega$

$$Y_{in} = \frac{1}{j\omega} \frac{g^2}{Ce^{2j\phi}} \qquad (3.7)$$

or

$$Z_{in} = \frac{1}{Y_{in}} = \frac{Ce^{2j\phi}}{g^2} j\omega \qquad (3.8)$$

and by using the first two terms of the Taylor series expansion for $e^{2j\phi}$ Eqn. 3.8 can be rewritten as

$$Z_{in} = -\frac{2\phi C\omega}{g^2} + \frac{C}{g^2} j\omega \qquad (3.9)$$

The Q-factor of the simulated inductance is

$$Q = -\frac{1}{2\phi} \qquad (3.10)$$

and the equivalent circuit represented by Eqn. 3.9 is shown in Fig. 3.3. A negative phase angle ϕ in each gyration conductance g in Eqn. 3.1 produces a negative frequency dependent resistance as seen in Fig. 3.3.

When both the imperfections are present the admittance matrix for the nonideal gyrator can be written as

$$[y] = \begin{bmatrix} \varepsilon g & ge^{-j\phi} \\ -ge^{-j\phi} & \varepsilon g \end{bmatrix} \qquad (3.11)$$

The input admittance of a capacitively terminated gyrator is now given by

$$Y_{in}(s) = \varepsilon G + \frac{g^2 e^{-2j\phi}}{\varepsilon g + Cs} \qquad (3.12)$$

By using the first two terms of Taylor's series for $e^{-2j\phi}$ and then letting $s = j\omega$ Eqn. 3.12 can be reduced to

$$Y_{in}(j\omega) = \varepsilon G + \frac{1}{\frac{\varepsilon}{g} - \frac{2C\phi}{g^2}\omega + \frac{2\varepsilon\phi}{g\omega} j\omega + \frac{C}{g^2} j\omega} \qquad (3.13)$$

The equivalent circuit represented by the Eqn. 3.13 is shown in Fig. 3.4.

The preceding method of deriving models for nonideal gyrator circuits was discussed in many textbooks on active network synthesis

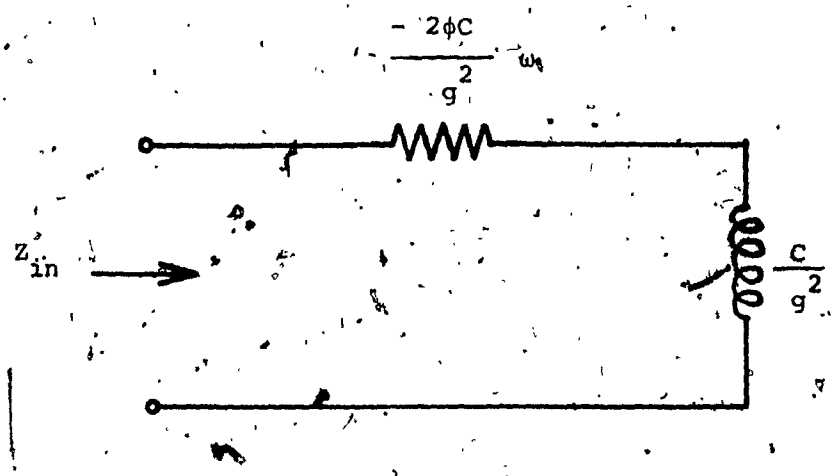

FIG.3.3 MODEL FOR THE INDUCTANCE SIMULATED BY A GYRATOR WITH NONIDEAL GYRATION CONDUCTANCE.

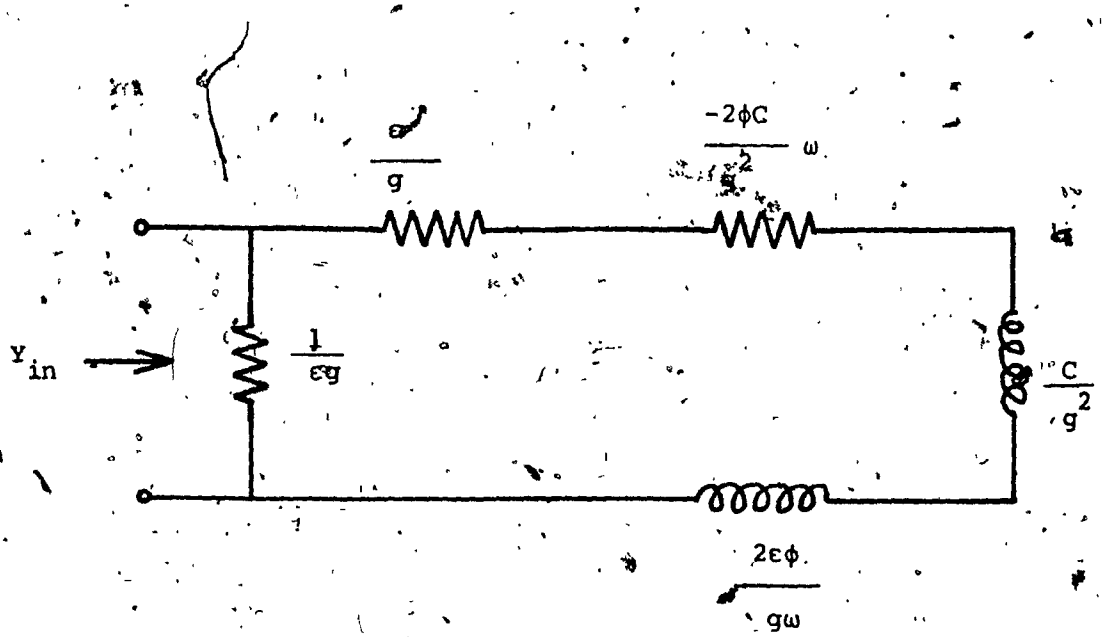

FIG.3.4 OLD MODEL FOR THE INDUCTANCE SIMULATED BY A GYRATOR.

[67], [79], and [62].

3.2 More Exact Method of Analyzing Gyrator Circuits

The models of Section 3.1 are unsatisfactory because y_{11} and y_{22} in the Eqn. 3.11 are assumed to be real, constant and equal. Also y_{12} and y_{21} are assumed to be constant in magnitude, equal and opposite. These assumptions are not true for most of the practical gyrator circuits. The y parameters are complex and depend on the parameters of the active elements employed. If operational amplifiers are employed their imperfections tends to influence the performance of the gyrator circuits significantly.

It is of significant practical interest to examine the influence of operational amplifier imperfections on the performance of gyrator circuits. Such an investigation has been carried out by Orchard and Sheahan [38], for Riordan's circuit. Also Bruton [72] has examined the performance of the gyrator circuits of Figs. 3.5 and A.1. In both the cases, however, only the frequency dependence of amplifier gains has been taken into account. A more exact method of analysis will now be presented where the amplifiers are assumed to have finite input and nonzero output resistances and also frequency dependent finite gains. The analysis tends to be somewhat tedious owing to the large number of parameters involved. However, after suitable approximations the equations can be simplified considerably.

The gyrator circuit considered for demonstrating the method of analysis and deriving a model is shown in Fig. 3.5. This circuit is referred to as gyrator GA. The alternate arrangement where R_4 is transferred from nodes 33' to nodes 22' will be referred to as gyrator GB.

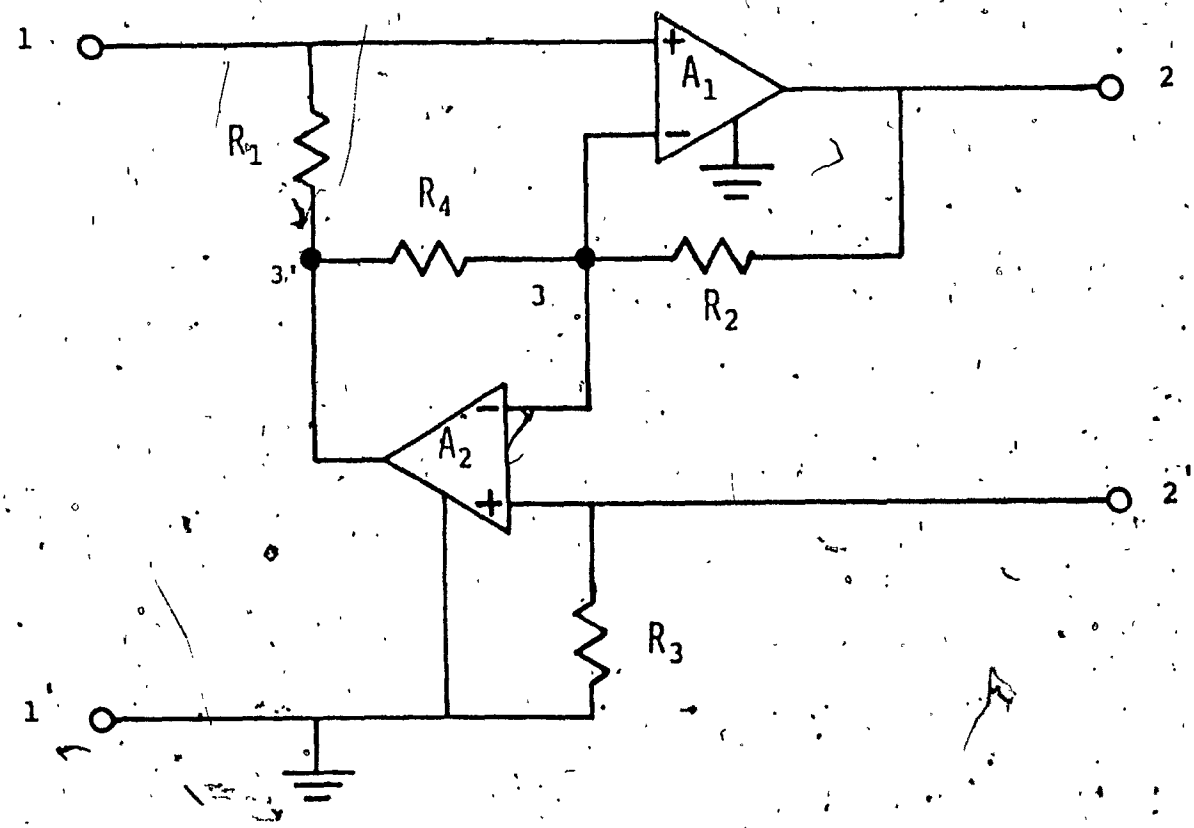

FIG.3.5 GYRATOR GA

The operational amplifiers are assumed to have finite input and nonzero output resistances and also frequency dependent finite gains. The amplifier model used is shown in Fig. 3.6. For compensated operational amplifiers the gain is given by

$$A = \frac{A_0 \omega_0}{s + \omega_0} \tag{3.14}$$

where A_0 is the dc gain, ω_0 is the cut-off frequency of the amplifier and s is the complex frequency variable.

To simplify the equations, the four gyration resistances are all assumed to be equal to R. By using the model of Fig. 3.6 for each operational amplifier, an equivalent circuit for the gyrator GA is obtained as illustrated in Fig. 3.7, where

A_1 is the gain of operational amplifier 1,

R_{01} is the output resistance of operational amplifier 1,

R_{I1} is the differential input resistance of operational amplifier 1,

R_{P1} is the input resistance at the non-inverting input terminal of the operational amplifier 1,

R_{N1} is the input resistance at the inverting input terminal of the operational amplifier 1,

A_2 is the gain of the operational amplifier 2,

R_{02} is the output resistance of the operational amplifier 2,

R_{I2} is the differential input resistance of the operational amplifier 2,

R_{P2} is the input resistance at the non-inverting input terminal of the operational amplifier 2,

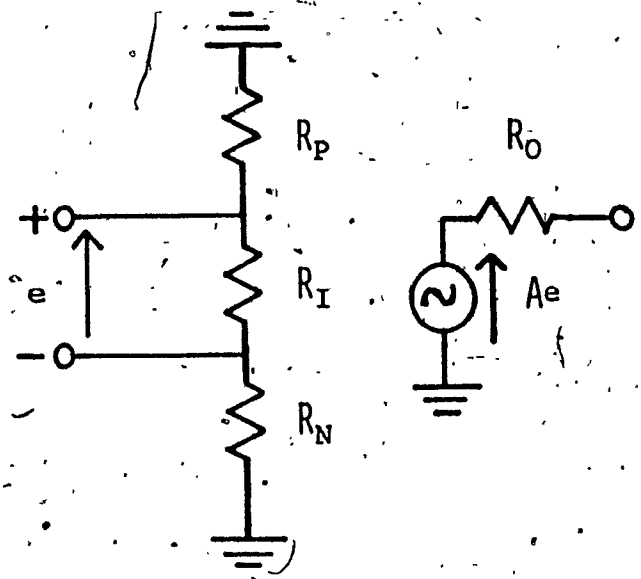

FIG.3.6 MODEL FOR NONIDEAL OPERATIONAL AMPLIFIER.

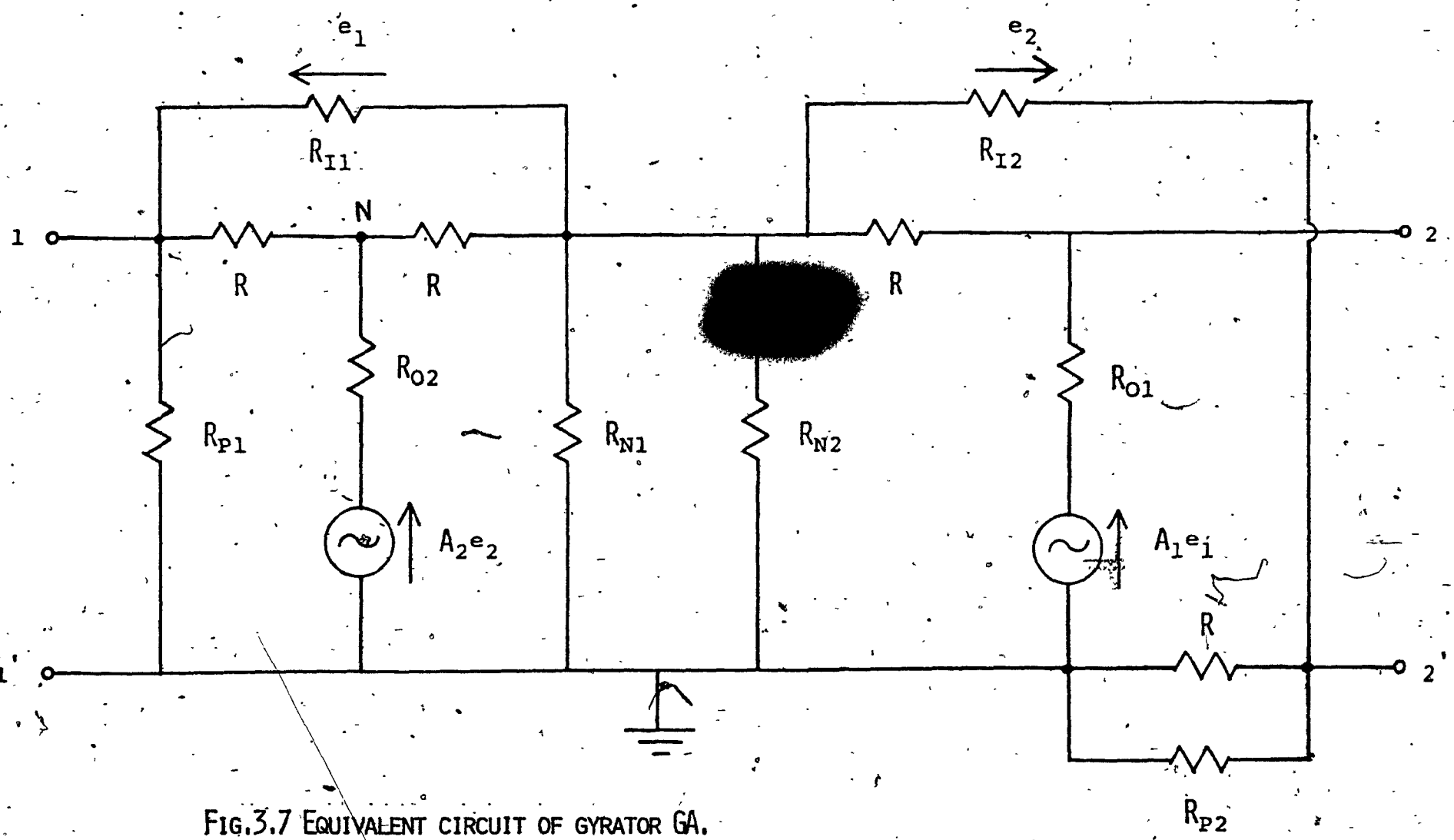

FIG.3.7 EQUIVALENT CIRCUIT OF GYRATOR GA.

R_{N2} is the input resistance at the inverting input terminal of the operational amplifier 2.

The analysis of the gyrator equivalent circuit will now be considered. After a star-delta transformation at node N, a signal flow graph analysis gives the y parameters as

$$y_{11} = \frac{1}{R_{P1}} + \frac{1}{DR_a}\left\{1 - A_1A_2 + \frac{A_1R_e}{R_c} + \frac{A_2R_e}{R_a} + \frac{A_2R_{01}R_e}{R_aR_b} + \frac{R_e}{R_a} + \frac{R_e}{R_c} + \frac{R_e}{R_a}\left(\frac{R_{01}}{R_b} + \frac{R_{01}}{R_c}\right) + \frac{R_e}{R_c}\left(\frac{R_{01}}{R_b} + \frac{R_d}{R_a}\right) + \frac{R_{01}}{R_b} + \frac{R_d}{R_a} + \frac{R_{01}}{R_c} + \frac{R_eR_{01}R_d}{R_aR_bR_c} + \frac{R_{01}R_d}{R_aR_b} + \frac{R_{01}R_d}{R_aR_c}\right\} \quad (3.15)$$

$$y_{12} = \frac{1}{D}\left(\frac{A_1A_2R_e}{RR_a} + \frac{A_2R_e}{R_aR_a} + \frac{A_2R_e}{RR_a} + \frac{A_2R_eR_{01}}{R_aR_aR} + \frac{A_2R_eR_{01}}{RR_aR_b} + \frac{A_2R_{01}}{RR_a} + \frac{A_2}{R_a} + \frac{R_dR_e}{R_a^2R_{I2}} + \frac{R_dR_eR_{01}}{R_a^2R_bR_{I2}} - \frac{R_dR_eR_{01}}{R_a^2R_bR_c}\right) \quad (3.16)$$

$$y_{21} = -\frac{1}{D}\left(\frac{A_1A_2R_e}{R_aR_b} + \frac{A_1R_e}{R_aR_b} + \frac{A_1R_e}{R_bR_c} + \frac{2A_1R_dR_e}{R_aR_bR_c} + \frac{A_1R_e}{R_{I2}R_a} + \frac{A_1}{R_b} + \frac{A_1}{R_{I2}} + \frac{2A_1R_d}{R_aR_b} + \frac{2A_1R_d}{R_aR_{I2}} + \frac{R_{01}R_dR_e}{RR_a^2R_b} - \frac{R_dR_e}{R_a^2R_{I2}}\right) \quad (3.17)$$

$$y_{22} = \frac{1}{D}\left(\frac{A_2R_e}{R_aR_b} + \frac{A_1R_e}{RR_b} + \frac{2A_1R_dR_e}{RR_aR_b} + \frac{A_2R_{01}R_e}{RR_aR_b} + \frac{A_1R_e}{RR_{I2}} + \frac{2A_1R_dR_e}{RR_aR_{I2}} + \frac{R_e}{R_aR_b} + \frac{R_e}{RR_b} + \frac{R_e}{R_bR_{I2}} + \frac{R_e}{R_aR_{I2}} + \frac{R_e}{RR_{I2}} + \frac{1}{R_b} + \frac{1}{R_{I2}} + \frac{R_{01}R_e}{RR_aR_b}\right)$$

$$+\frac{R_d R_e}{R_a^2 R_b}+\frac{2R_d R_e}{RR_a R_b}+\frac{R_{01}R_e}{RR_b R_{I2}}+\frac{R_d R_e}{R_a^2 R_{I2}}+\frac{R_{01}R_e}{RR_a R_{I2}}+\frac{2R_d R_e}{RR_a R_{I2}}+\frac{2R_d R_e}{R_a R_b R_{I2}}+\frac{R_{01}}{RR_b}$$

$$+\frac{2R_d}{R_a R_b}+\frac{R_{01}}{RR_{I2}}+\frac{2R_d}{R_a R_{I2}}+\frac{R_{01}R_d R_e}{RR_a^2 R_b}+\frac{R_{01}R_d R_e}{RR_a^2 R_{I2}}+\frac{2R_{01}R_d R_e}{RR_a R_b R_{I2}}+\frac{2R_{01}R_d}{RR_a R_b}$$

$$+\frac{2R_{01}R_d}{RR_a R_{I2}}\Bigg) \tag{3.18}$$

where

$$R_a = \frac{RR_{I1}}{2R + R_{I1}} \tag{3.19}$$

$$R_b = \frac{RR_{P2}}{R + R_{P2}} \tag{3.20}$$

$$R_c = \frac{RR_{I2}}{R + R_{I2}} \tag{3.21}$$

$$R_d = R_{02} + \frac{R^2}{2R + R_{I1}} \tag{3.22}$$

$$R_e = \frac{R_{N1}R_{N2}}{R_{N1} + R_{N2}} \tag{3.23}$$

and

$$D = \frac{A_1 A_2 R_e}{R_a}+\frac{A_1 R_e}{R_c}+\frac{A_2 R_e}{R_a}+\frac{2A_1 R_e R_d}{R_a R_c}+\frac{A_2 R_{01} R_e}{R_a R_b}+\frac{R_e}{R_a}+\frac{R_e}{R_c}$$

$$+\frac{R_d R_e}{R_a^2}+\frac{2R_d R_e}{R_a R_c}+\frac{R_{01}R_e}{R_a R_c}+\frac{R_{01}R_e}{R_a R_b}+\frac{R_{01}R_e}{R_b R_c}+1+\frac{2R_d}{R_a}+\frac{R_{01}}{R_b}$$

$$+\frac{R_{01}}{R_c}+\frac{R_{01}R_d R_e}{R_a^2}\left(\frac{1}{R_b}+\frac{1}{R_c}\right)+\frac{2R_{01}R_d R_e}{R_a R_b R_c}+\frac{2R_{01}R_d}{R_a R_b}+\frac{2R_{01}R_d}{R_a R_c} \tag{3.24}$$

In commercially available operational amplifiers the usual ranges for the parameters of the model shown in Fig. 3.6 are as follows:

$$\left.\begin{aligned} &A_0: \text{ 3000 to 200,000} \\ &\omega_0: \text{ 30 to } 15 \times 10^3 \text{ rad/sec} \\ &R_p, R_N: \text{ 50 to 500 M}\Omega \\ &R_I: \text{ 50 k}\Omega \text{ to 2M}\Omega \\ &R_0: \text{ 50 to 200 }\Omega \end{aligned}\right\} \qquad (3.25)$$

The frequency range of interest is usually much smaller than the gain-bandwidth product of the amplifier. So let us assume that

$$\omega << A_0\omega_0 \qquad (3.26)$$

For typical applications, the gyration constant is in the range 10^6 to 100×10^6, that is, R is in the range 1 to 10kΩ. Therefore from Eqns. 3.14 and 3.25-3.26, we can write

$$\left.\begin{aligned} &|A| >> 1 \\ &R_I >> R \\ &R_p, R_N >> R_I \\ &R >> R_0 \end{aligned}\right\} \qquad (3.27)$$

For the sake of simplicity, the two amplifiers will be assumed identical so that

$$\left.\begin{aligned} &A_1 = A_2 = A \\ &R_{P1} = R_{P2} = R_P \\ &R_{N1} = R_{N2} = R_N \\ &R_{I1} = R_{I2} = R_I \\ &R_{01} = R_{02} = R_0 \end{aligned}\right\} \qquad (3.28)$$

This assumption is reasonable since each gyrator will usually employ a single dual operational amplifier. Eqns. 3.19-3.22, 3.27 and 3.28 show that

$$\left.\begin{aligned} R_a &\simeq R_b \simeq R_c \simeq R \\ R_d &\simeq R_0 \end{aligned}\right\} \tag{3.29}$$

From Eqns. 3.15-3.18, 3.24, 3.27, 3.28 and 3.29 the y parameters can be approximated as

$$y_{11} \simeq \frac{1}{R_{P1}} + \frac{1}{DR}\left(\frac{2AR_e}{R} + \frac{AR_0R_e}{R^2} - A^2 + \frac{2R_e}{R}\right) \tag{3.30}$$

$$y_{12} \simeq \frac{AR_e}{DR}\left(\frac{A+2}{R} + \frac{2R_0}{R^2}\right) \tag{3.31}$$

$$y_{21} \simeq -\frac{AR_e}{DR^2}\left(A + 2 + \frac{2R_0}{R} + \frac{R}{R_I}\right) \tag{3.32}$$

$$y_{22} \simeq \frac{R_e}{DR}\left(\frac{2A+2}{R} + \frac{3AR_0}{R^2} + \frac{A}{R_I} + \frac{2AR_0}{RR_I}\right) \tag{3.33}$$

where

$$D \simeq \frac{R_e}{R}\left(A^2 + 2A + 2 + \frac{3AR_0}{R}\right) \tag{3.34}$$

By using Eqns. 3.27 and 3.34 the y parameters can now be written as

$$y_{11} \simeq \frac{1}{R_{P1}} - \frac{1}{R_e} + \frac{2}{AR} + \frac{R_0}{AR^2} + \frac{2}{AR_5} + \frac{3R_0}{ARR_5} - \frac{2}{A^2R} - \frac{8R_0}{A^2R^2} \tag{3.35}$$

$$y_{12} \simeq \frac{1}{R}\left(1 - \frac{R_0}{AR} - \frac{2}{A^2} + \frac{2R_0}{A^2R}\right) \tag{3.36}$$

$$y_{21} \simeq \frac{1}{R} - \frac{R_0}{AR^2} + \frac{1}{AR_I} - \frac{2}{A^2R} + \frac{2R_0}{A^2R^2} \tag{3.37}$$

$$y_{22} \simeq \frac{2}{AR} + \frac{3R_0}{AR^2} + \frac{1}{AR_I} + \frac{2R_0}{ARR_I} - \frac{2}{A^2R} - \frac{12R_0}{A^2R^2} \qquad (3.38)$$

By letting $s = j\omega$ in Eqn. 3.14 and then by using Eqns. 3.14, 3.26-3.27, the y parameters can be further reduced to

$$y_{11} \simeq G_f + G_g + G_h + \frac{2 + \frac{R_0}{R}}{A_0\omega_0 R} j\omega \qquad (3.39)$$

$$y_{12} \simeq \frac{1}{R} + \frac{2\omega^2}{A_0^2\omega_0^2 R}\left(1 - \frac{R_0}{R}\right) - \frac{R_0}{A_0\omega_0 R^2} j\omega \qquad (3.40)$$

$$y_{21} \simeq -\frac{1}{R} - \frac{2\omega^2(R - R_0)}{A_0^2\omega_0^2 R^2} + \frac{R_0R_I - R^2}{A_0\omega_0 R^2 R_I} j\omega \qquad (3.41)$$

$$y_{22} \simeq \frac{2}{A_0R} + \frac{3R_0}{A_0R^2} + \frac{2\omega^2(R + 6R_0)}{A_0^2\omega_0^2R^2} + \frac{2R + 3R_0}{A_0\omega_0R^2} j\omega \qquad (3.42)$$

where

$$G_f = \frac{1}{R_{P1}} + \frac{2 + \frac{R_0}{R}}{A_0R} \qquad (3.43)$$

$$G_g = -\left(\frac{1}{R_{N1}} + \frac{1}{R_{N2}}\right) \qquad (3.44)$$

$$G_h = \frac{2\omega^2}{A_0^2\omega_0^2 R}\left(1 + \frac{4R_0}{R}\right) \qquad (3.45)$$

3.3 New Model

The analysis of Section 3.2 can be used for the derivation of a gyrator model comprising resistances, capacitances and inductances. Such a model is useful in four respects as follows:

a) The influence of amplifier imperfections upon the simulated inductance can be clearly understood.

b) It can be used for computer-aided analysis of capacitively terminated gyrator circuits.

c) It can be used for the optimization of the gyrator circuits.

d) It can be used for the computer-aided analysis of gyrator-C filters.

Consider a gyrator circuit terminated by a lossy capacitor such that

$$Y_L(s) = G_L + sC \tag{3.46}$$

The input admittance of the gyrator is given by

$$Y_i(s) = y_{11}(s) - \frac{y_{12}(s)y_{21}(s)}{y_{22}(s) + G_L + sC} \tag{3.47}$$

If $s = j\omega$ we obtain

$$Y_i(j\omega) = y_{11}(j\omega) - \frac{y_{12}(j\omega)y_{21}(j\omega)}{y_{22}(j\omega) + G_L + j\omega C} \tag{3.48}$$

By using Eqns. 3.40-3.42 and 3.48 Y_i can be expressed as

$$Y_i(j\omega) = y_{11}(j\omega) + \frac{H(j\omega + k_1)(j\omega + k_2)}{(j\omega + k_3)} \tag{3.49}$$

where

$$H = \frac{R_0(R_0R_I - R^2)}{A_0\omega_0R^2R_I(2R + 3R_0 + A_0\omega_0R^2C)} \tag{3.50}$$

$$k_1 = -\frac{A_0^2\omega_0^2R + 2\omega^2(R - R_0)}{A_0\omega_0R_0} \tag{3.51}$$

$$k_2 = -\frac{A_0^2\omega_0^2 RR_I + 2\omega^2(RR_I - R_0R_I)}{A_0\omega_0(R_0R_I - R^2)} \tag{3.52}$$

$$k_3 = \frac{2A_0\omega_0^2 R + 3A_0\omega_0^2 R_0 + G_L A_0^2\omega_0^2 R^2 + 2\omega^2(R + 6R_0)}{A_0\omega_0(2R + 3R_0 + A_0\omega_0 R^2 C)} \tag{3.53}$$

Now Eqn. 3.49 can be written as

$$Y_i(j\omega) = y_{11}(j\omega) + Hj\omega + Hk_4 + \frac{Hk_5}{j\omega + k_3} \tag{3.54}$$

where

$$k_4 = k_1 + k_2 - k_3 \tag{3.55}$$

$$k_5 = k_1k_2 - k_3k_4 \tag{3.56}$$

For a low-loss load capacitor such that $G_L < 40$ μmho Eqns. 3.51-3.53, 3.26 and 3.27 show that

$$|k_1 + k_2| >> |k_3| \tag{3.57}$$

and therefore

$$k_4 \simeq k_1 + k_2$$

$$\simeq \frac{-1}{A_0\omega_0 R_0(R_0R_I - R^2)} \left\{ 2A_0^2\omega_0^2 RR_0R_I - A_0^2\omega_0^2 R^3 \right.$$

$$\left. + \omega^2(4RR_0R_I - 4R_0^2R_I - 2R^3 + 2R^2R_0) \right\} \tag{3.58}$$

From Eqns. 3.56 and 3.58 we get

$$k_5 \simeq k_1k_2 - k_1k_3 - k_2k_3 \tag{3.59}$$

Since it is assumed that $A_0\omega_0 >> \omega$, Eqns. 3.51-3.53 and 3.27 give

$$k_1 \simeq -\frac{A_0\omega_0 R}{R_0} \tag{3.60}$$

$$k_2 \simeq -\frac{A_0\omega_0 R_I R}{(R_0 R_I - R^2)} \tag{3.61}$$

and

$$k_3 \simeq \frac{2A_0\omega_0^2 + G_L A_0^2 \omega_0^2 R}{A_0\omega_0(2 + A_0\omega_0 RC)} \tag{3.62}$$

From Eqns. 3.59-3.62 we get

$$k_5 = \frac{A_0^2\omega_0^2 R^2 R_I}{R_0(R_0 R_I - R^2)} + \left\{\frac{2A_0\omega_0 R R_I R_0 - A_0\omega_0 R^3}{R_0(R_0 R_I - R^2)}\right\} \times \left\{\frac{2\omega_0 + G_L A_0\omega_0 R}{(2 + A_0\omega_0 RC)}\right\} \tag{3.63}$$

or

$$k_5 = \frac{\left\{A_0^2\omega_0^2 R^2 R_I(2 + A_0\omega_0 RC) + (2A_0\omega_0 R R_I R_0 - A_0\omega_0 R^3)(2 + A_0\omega_0 RC) + (2\omega_0 + G_L A_0\omega_0 R) R_0(R_0 R_I + R^2)\right\}}{(2 + A_0\omega_0 RC)(R_0 R_I - R^2) R_0} \tag{3.64}$$

By using Eqns. 3.26-3.27 we get

$$k_5 \simeq \frac{A_0^2\omega_0^2 R^2 R_I}{R_0(R_0 R_I - R^2)} \tag{3.65}$$

The input admittance of Eqn. 3.54 can now be expressed as

$$Y_i = Y_A + \frac{1}{Z_B + Z_C} \tag{3.66}$$

where

$$Y_A = y_{11} + Hj\omega + Hk_4 \tag{3.67}$$

$$Z_B = \frac{j\omega}{Hk_5} \tag{3.68}$$

$$Z_C = \frac{k_3}{Hk_5} \tag{3.69}$$

A network representation of Eqn. 3.66 is readily obtained as shown in Fig. 3.8.

From Eqns. 3.67, 3.39, 3.43-3.45, 3.50 and 3.58 we can write

$$Y_A = G_{p1} + G_{p2} + G_{p3} + j\omega C_p \tag{3.70}$$

where

$$G_{p1} = \frac{1}{R_{P1}} + \frac{1}{A_0 R}\left(2 + \frac{R_0}{R}\right) + \frac{R}{R_I(2R + 3R_0 + A_0\omega_0 R^2 C)} \tag{3.71}$$

$$G_{p2} = -\left\{\frac{1}{R_{N1}} + \frac{1}{R_{N2}} + \frac{2R_0}{R(2R + 3R_0 + A_0\omega_0 R^2 C)}\right\} \tag{3.72}$$

$$G_{p3} = \frac{2\omega^2}{A_0^2\omega_0^2 R}\left\{1 + \frac{4R_0}{R} - \frac{2RR_0R_I - 2R_0^2R_I - R^3 + R^2R_0}{RR_I(2R + 3R_0 + A_0\omega_0 R^2 C)}\right\} \tag{3.73}$$

$$= \frac{2\omega^2}{A_0^2\omega_0^2 R}\left\{1 + \frac{4R_0}{R} + \frac{1}{(2 + A_0\omega_0 RC)}\left(\frac{R}{R_I} - \frac{2R_0}{R}\right)\right\} \tag{3.74}$$

$$C_p = \frac{1}{A_0\omega_0 R}\left\{2 + \frac{R_0}{R} + \frac{1}{RR_I}\left(\frac{R_0(R_0R_I - R^2)}{2R + 3R_0 + A_0\omega_0 R^2 C}\right)\right\} \tag{3.75}$$

$$\simeq \frac{1}{A_0\omega_0 R}\left(2 + \frac{R_0}{R}\right) \tag{3.76}$$

The admittance Y_A can thus be split into three parallel conductances G_{p1}, G_{p2}, and G_{p3} and a parallel capacitance C_p.

From Eqns. 3.68, 3.50, and 3.65 we obtain

$$Z_B = (L_o + L_p)\, j\omega \tag{3.77}$$

where

$$L_o = R^2 C \tag{3.78}$$

$$L_p = \frac{2R}{A_0\omega_0} + \frac{3R_0}{A_0\omega_0} \tag{3.79}$$

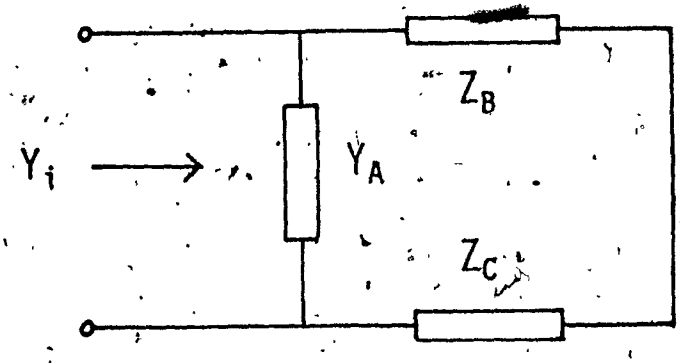

FIG. 3.8 NETWORK REPRESENTATION OF EQN. 3.66

and hence Z_B can be considered as a series arrangement of inductances L_o and L_p.

From Eqns. 3.69, 3.50, 3.53 and 3.65 we obtain

$$Z_C = r_{p4} + r_{p5} \tag{3.80}$$

where

$$r_{p4} = \frac{2R}{A_0} + \frac{3R_0}{A_0} + G_L R^2 \tag{3.81}$$

$$r_{p5} = \frac{2\omega^2 (R + 6R_0)}{A_0^2 \omega_0^2} \tag{3.82}$$

and thus Z_C can be split into two series resistances r_{p4} and r_{p5}.

A model for a capacitively terminated gyrator can now be obtained by connecting the components of Y_A, Z_B and Z_C as shown in Fig. 3.9.

3.4 Validity of the Gyrator Model

The model of Fig. 3.9 has been used for the analysis of the gyrator circuit GA. An exact computer-aided analysis has also been carried out using a network analysis program, known as NASAP, in order to examine the validity of the model. The Inductance Deviation is defined as

$$ID = \frac{L - L_o}{L_o} \times 100\% \tag{3.83}$$

where L is the actual inductance simulated and $L_o = R^2C$ is the nominal inductance. The Q-factor and the inductance deviation have been computed for a range of frequencies. The analysis was carried out for a μA741C type amplifier using the specifications of Table 3.1. The Q-factor of the load capacitance has been assumed to be equal to 10^4 at 1kHz. The parallel loss resistance of the load capacitor C was

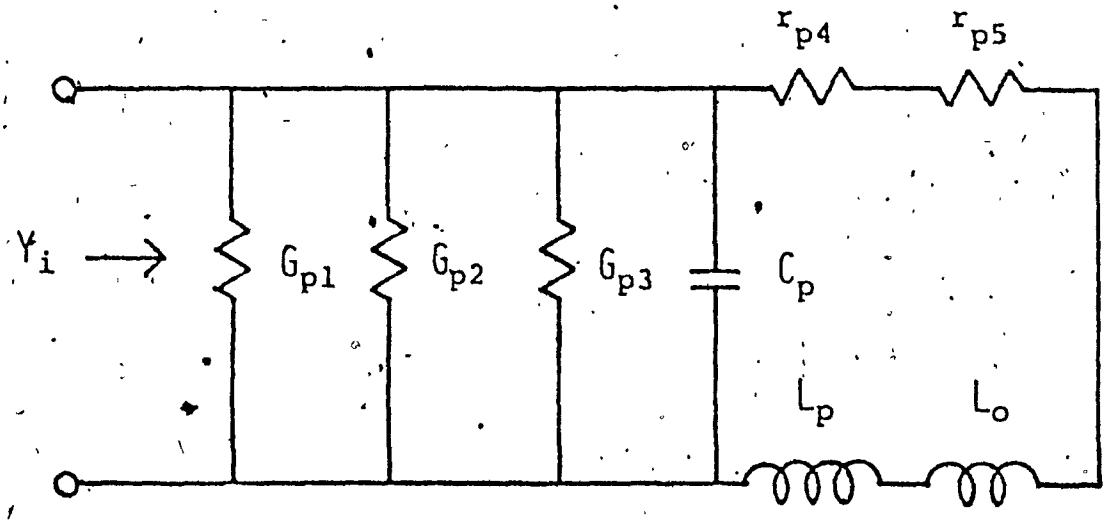

$$G_{p1} = \frac{1}{R_{p1}} + \frac{1}{A_0 R}\left(2+\frac{R_0}{R}\right) + \frac{R}{R_I(2R+3R_0+A_0\omega_0 R^2 C)}$$

$$G_{p2} = -\left\{\frac{1}{R_{N1}} + \frac{1}{R_{N2}} + \frac{2R_0}{R(2R+3R_0+A_0\omega_0 R^2 C)}\right\}$$

$$G_{p3} = \frac{2\omega^2}{A_0^2\omega_0^2 R}\left[1+\frac{4R_0}{R} + \frac{1}{(2+A_0\omega_0 RC)}\left\{\frac{R}{R_I} - \frac{2R_0}{R}\right\}\right]$$

$$C_p = \frac{1}{A_0\omega_0 R}\left(2+\frac{R_0}{R}\right)$$

$$r_{p4} = \frac{2R}{A_0} + \frac{3R_0}{A_0} + G_L R^2$$

$$r_{p5} = \frac{2\omega^2}{A_0^2\omega_0^2}(R+6R_0)$$

$$L_p = \frac{1}{A_0\omega_0}(2R+3R_0)$$

$$L_0 = R^2 C$$

FIG. 3.9 MODEL FOR THE CAPACITIVELY TERMINATED GYRATOR GA

assumed to be independent of frequency and equal to $10/2\pi C$ (i.e. Q = 10^4 at 1kHz). The results are shown in Figs. 3.10-3.13.

TABLE 3.1

Parameter	μA741C	μA715	μA702	Units
A_0	200×10^3	30×10^3	3.6×10^3	
ω_0	37.6	13.82×10^3	5.55×10^3	rad/sec
R_0	75	75	200	Ω
R_I	2×10^3	1×10^3	40	kΩ
R_p, R_N	500	500	500	MΩ

Figs. 3.10a and 3.10b show the variations of the inductance deviations and the Q-factor with frequency, respectively, for a fixed gyration resistance R = 2.5kΩ and a varying nominal inductance L_o.

As $\omega \to 0$ Eqns. 3.74 and 3.82 show that

$$G_{p3} \text{ and } r_{p5} \simeq 0 \tag{3.84}$$

Also Eqns. 3.26, 3.27, 3.71, 3.72, 3.76, 3.78 and 3.79 show that

$$\frac{1}{\omega C_p} >> \omega(L_o + L_p) \tag{3.85}$$

$$\left|\frac{1}{G_{p1} + G_{p2}}\right| >> \omega(L_o + L_p) \tag{3.86}$$

Consequently the effective input inductance for low frequencies is obtained as

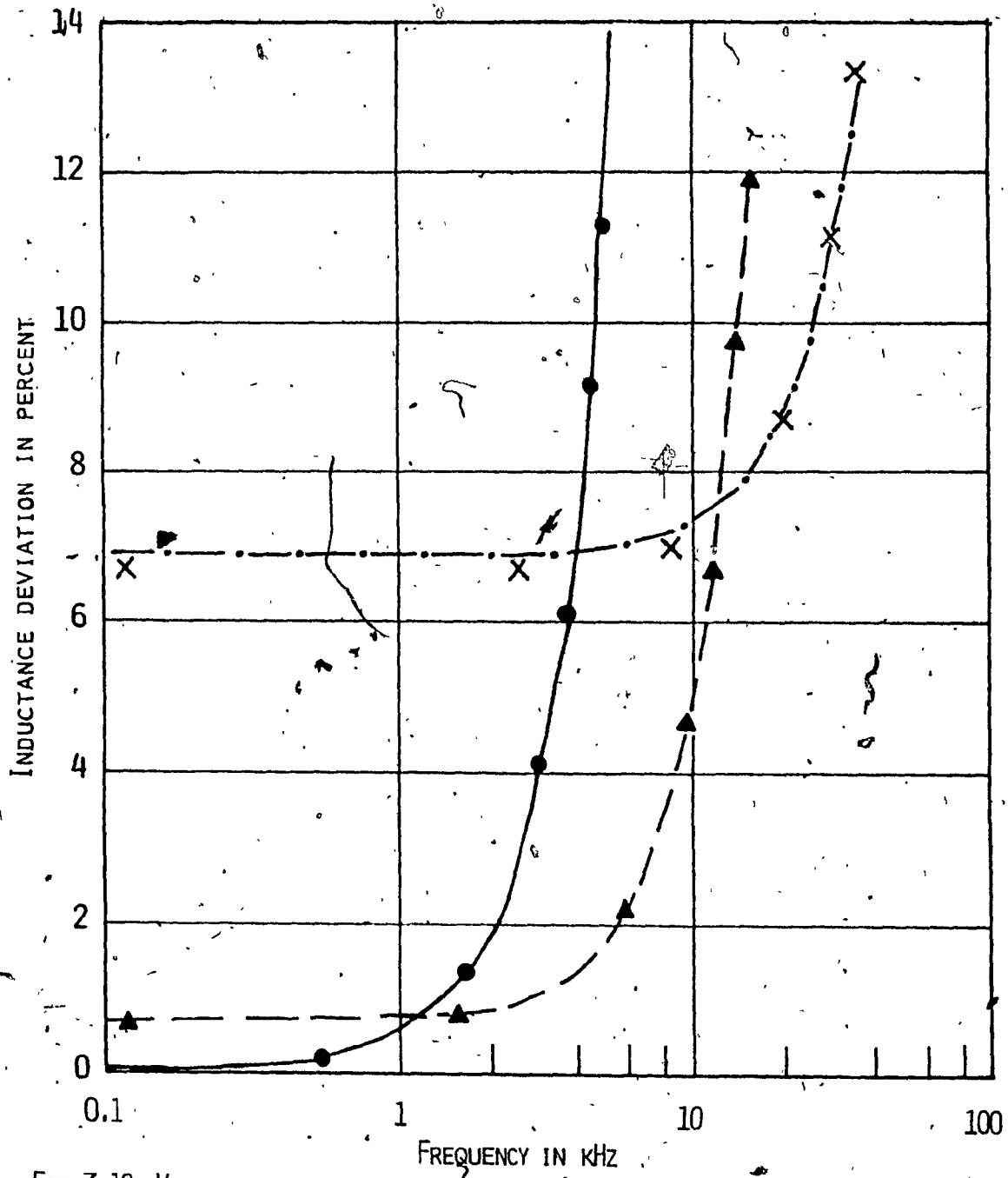

FIG.3.10A VARIATION OF INDUCTANCE DEVIATION WITH FREQUENCY FOR DIFFERENT NOMINAL INDUCTANCES(AMPLIFIER TYPE μA741C).

$R=2.5K\Omega, L_o$	EXACT ANALYSIS	MODEL ANALYSIS
1.0H	———	● ● ●
0.1H	— — —	▲ ▲ ▲
0.01H	—·—·—	× × ×

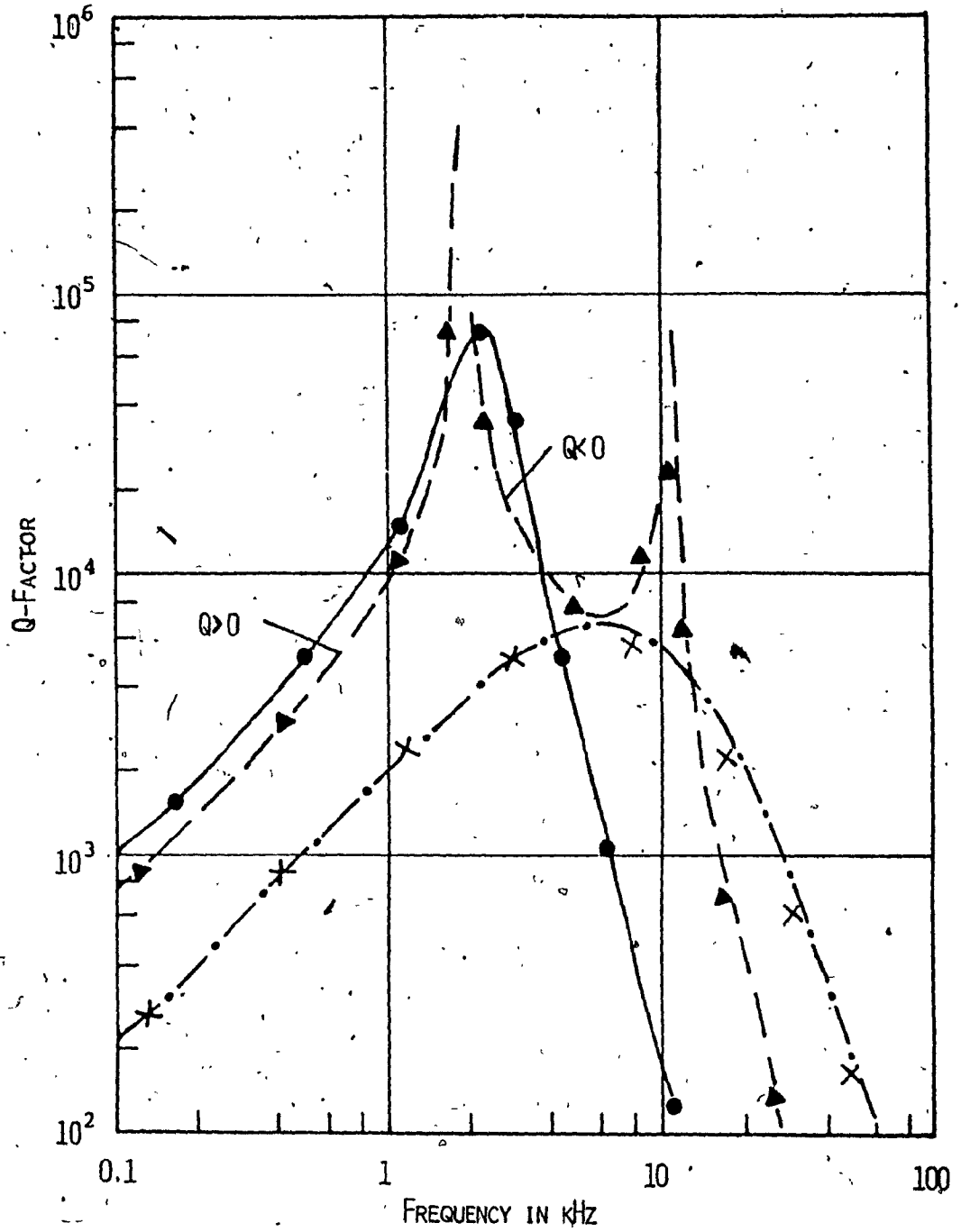

FIG.3.10B VARIATION OF Q-FACTOR WITH FREQUENCY FOR DIFFERENT NOMINAL INDUCTANCES(AMPLIFIER TYPE μA741C).

R=2.5kΩ L_o :	EXACT ANALYSIS	MODEL ANALYSIS
1.0H	———	● ● ● ●
0.1H	- - - - -	▲ ▲ ▲ ▲
0.01H	— - — - —	× × × ×

$$L \simeq L_o + L_p \tag{3.87}$$

and hence

$$ID \simeq \frac{L_p}{L_o} \times 100\% \tag{3.88}$$

For a fixed value of R Eqn. 3.79 shows that L_p is invariant. Therefore, as L_o is increased the low frequency inductance deviation is reduced. This is evident in Fig. 3.10a. For L_o = 0.1H the enhancment exceeds the total loss in the frequency range 2-10kHz and thus a negative Q-factor is obtained.

The influence of variations in gyration resistance for a constant nominal inductance is illustrated in Figs. 3.11a and 3.11b. The low frequency inductance deviation is reduced when R is reduced since L_p is reduced according to Eqn. 3.79. The amount of enhancement in Fig. 3.11b is seen to increase as R is reduced.

Figs. 3.12a and 3.12b illustrate the influence of variations in the dc gain of the amplifier. The low-frequency inductance deviation tends to be reduced as A_o is increased, according to Eqn. 3.79.

Gyrator responses for three different types of amplifiers are compared in Figs. 3.13a and 3.13b. The amplifiers used are μA702; μA715 and μA741C and their specifications are summarized in Table 3.1. The μA715 is essentially a wideband amplifier and, consequently, a wider useful gyrator bandwidth is obtained. Figs. 3.13a and 3.13b show that an inductance of 0.1H with a Q-factor of 700 at 80kHz is feasible.

Figs. 3.10-3.13 show that the gyrator responses predicted by the model agree closely with those obtained by the exact analysis and, therefore, the validity of the model is justified. The simplicity of

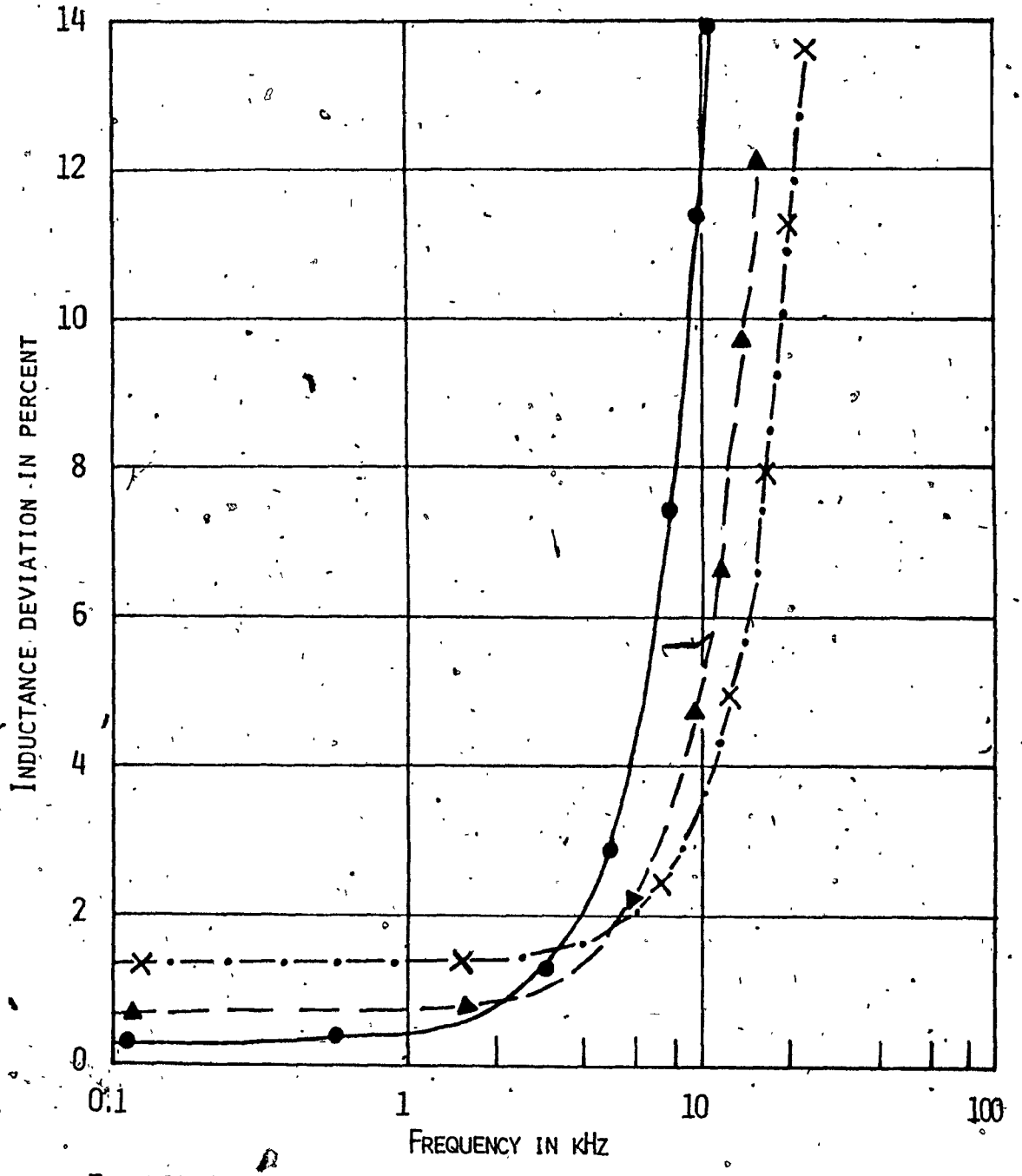

FIG.3.11A VARIATION OF INDUCTANCE DEVIATION WITH FREQUENCY FOR DIFFERENT GYRATION RESISTANCES (AMPLIFIER TYPE μA741C)

L_o=0.1H, R — EXACT ANALYSIS — MODEL ANALYSIS

1KΩ ——— • • •

2.5KΩ — — — ▲ ▲ ▲

5KΩ —·—·— × × ×

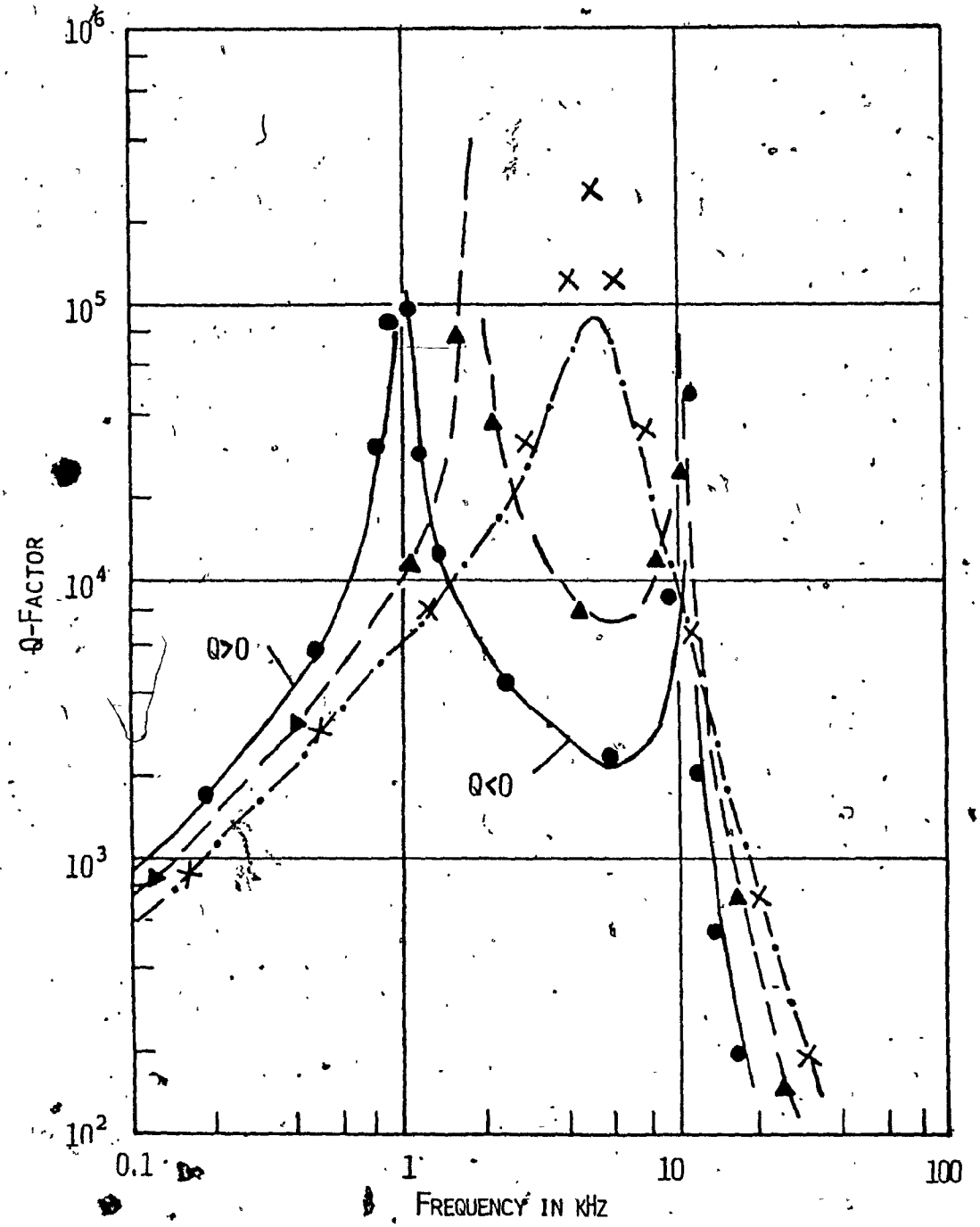

FIG.3.11B VARIATION OF Q-FACTOR WITH FREQUENCY FOR DIFFERENT GYRATION RESISTANCES(AMPLIFIER TYPE μA741C).

L_p=0.1H,R EXACT ANALYSIS MODEL ANALYSIS

1KΩ —————— • • •

2.5KΩ — — — — ▲ ▲ ▲

5KΩ — · — · — × × ×

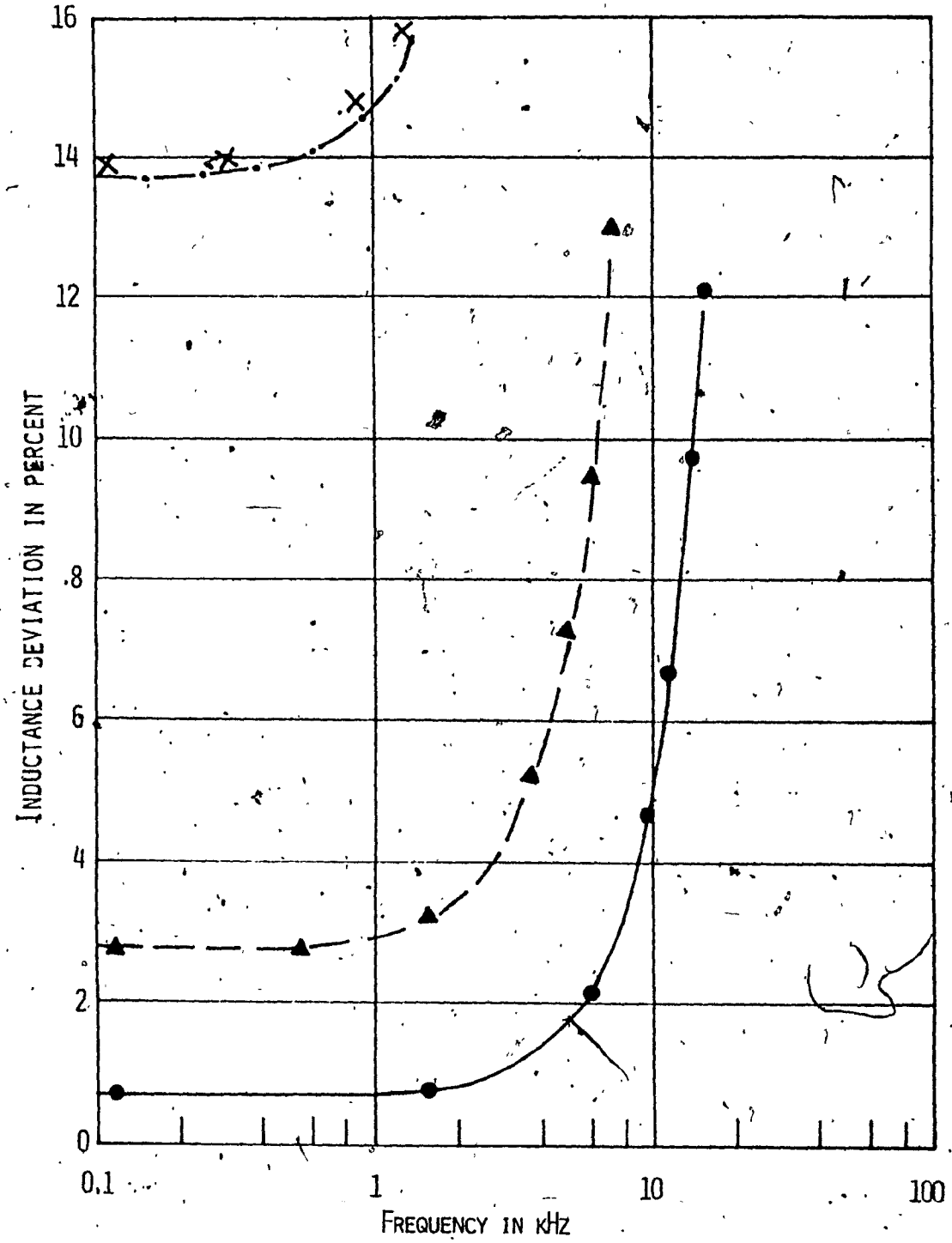

FIG.3.12A VARIATION OF INDUCTANCE DEVIATION WITH FREQUENCY FOR DIFFERENT DC GAINS(AMPLIFIER TYPE μA741C).
L_o=0.1H, R=2.5KΩ, A

	EXACT ANALYSIS	MODEL ANALYSIS
200K	———	• • •
50K	— — —	▲ ▲ ▲
10K	—·—·—	x x x

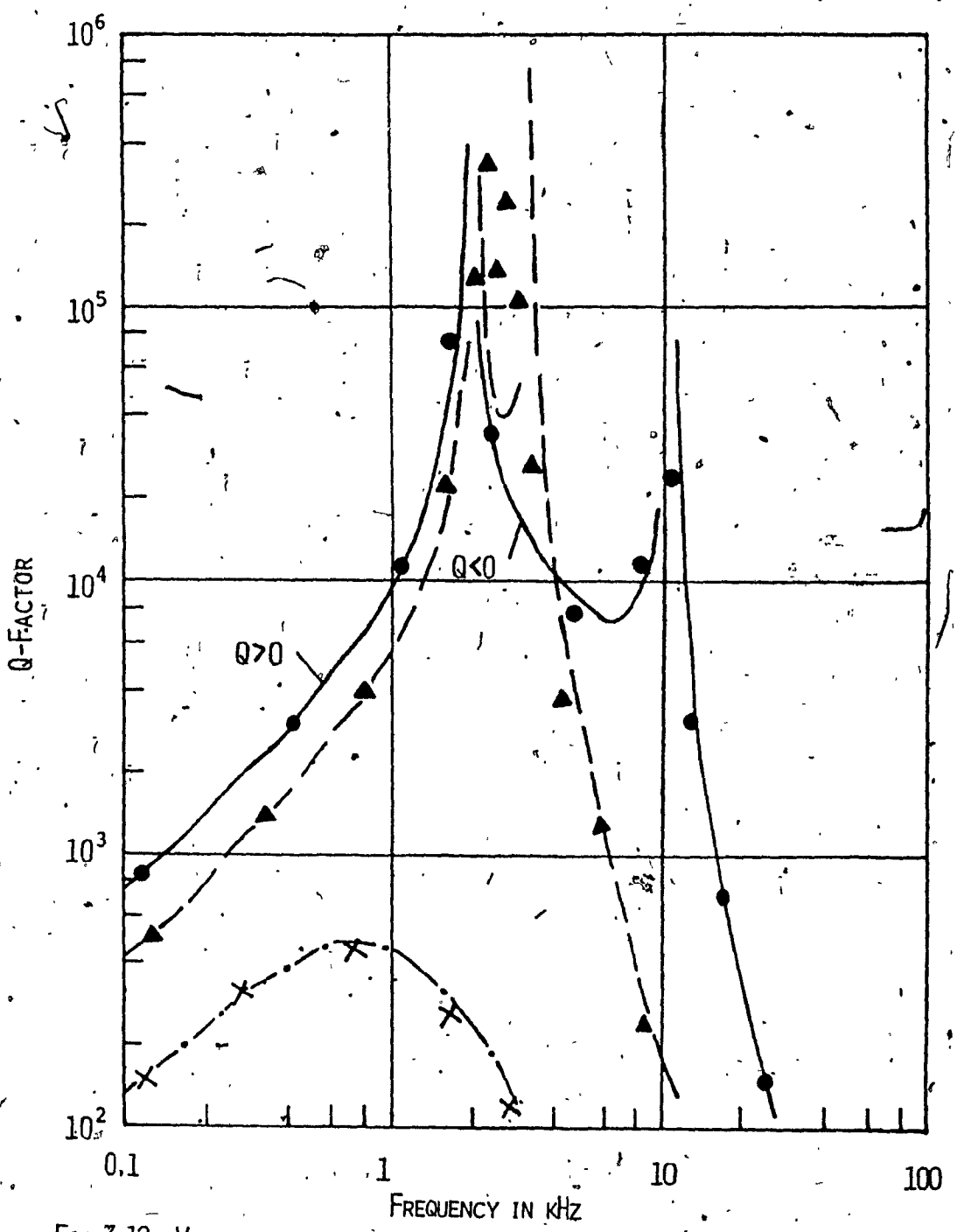

FIG.3.12B VARIATION OF Q-FACTOR WITH FREQUENCY FOR DIFFERENT DC GAINS (AMPLIFIER TYPE μA741C).

L_o=0.1H, R=2.5KΩ, A_0

	EXACT ANALYSIS	MODEL ANALYSIS
200K	———	● ● ● ●
50K	— — — —	▲ ▲ ▲ ▲
10K	—·—·—	× × × ×

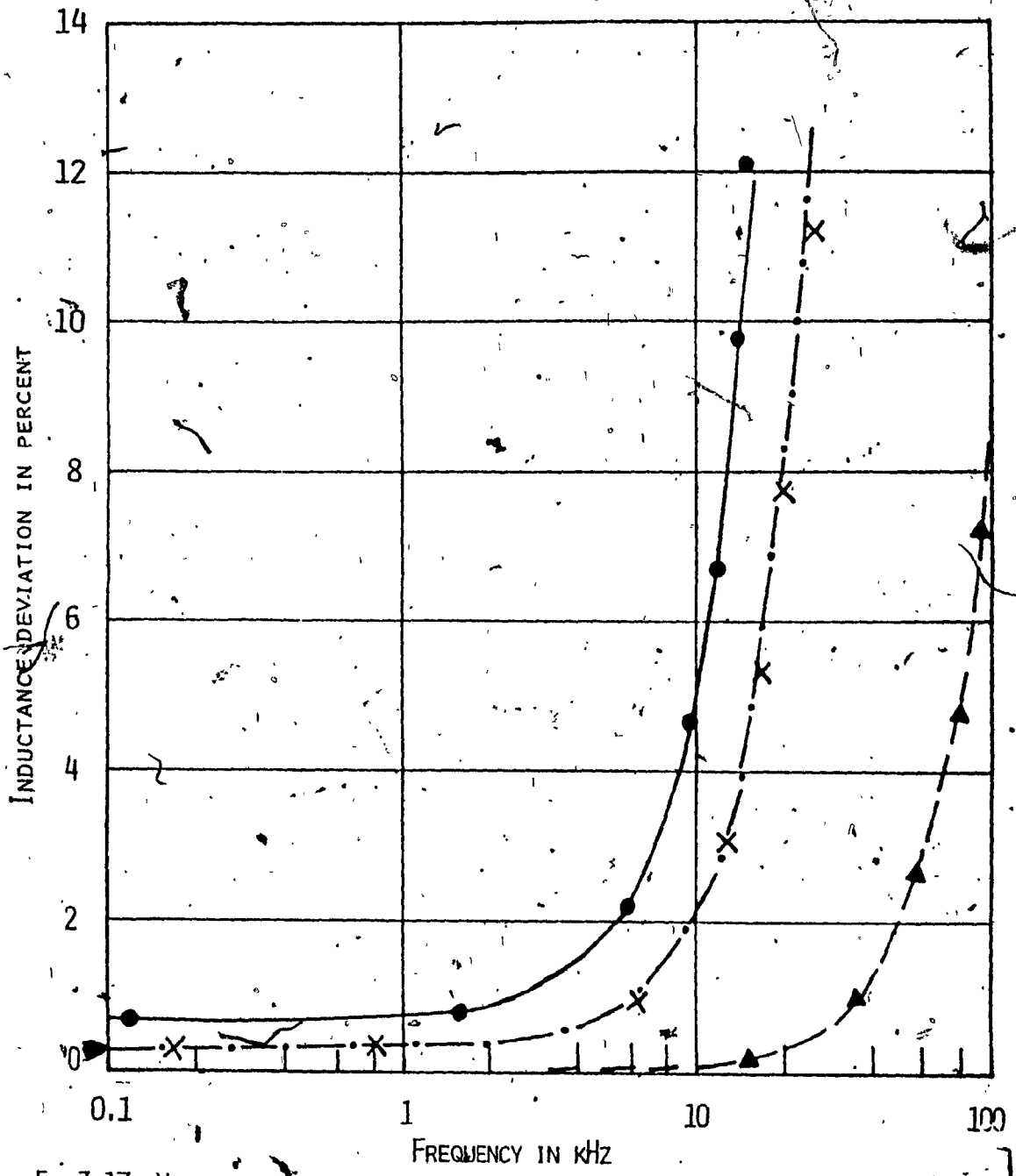

FIG.3.13A VARIATION OF INDUCTANCE DEVIATION WITH FREQUENCY FOR DIFFERENT AMPLIFIERS.

L_o=0.1H, R=2.5KΩ

EXACT ANALYSIS – MODEL ANALYSIS

μA741C ——— ● ● ●

μA715 — — — ▲ ▲ ▲

μA702 — · — · — × × ×

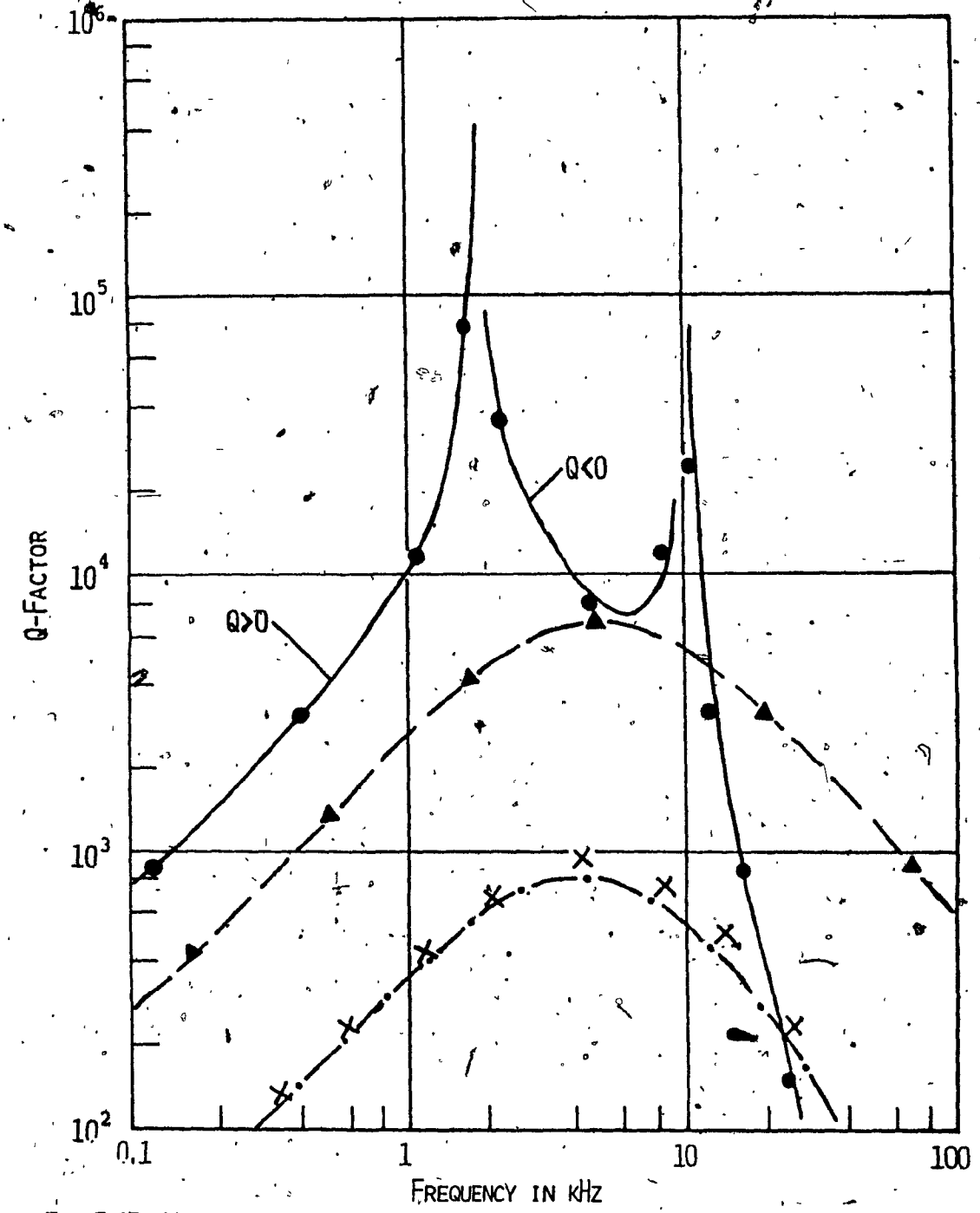

FIG.3.13B VARIATION OF Q-FACTOR WITH FREQUENCY FOR DIFFERET OPERATIONAL AMPLIFIERS.

L_o=0.1H, R=2.5KΩ

EXACT ANALYSIS — MODEL ANALYSIS

μA741C

μA715

μA702

the model by comparison with the exact equivalent circuit leads to a large saving in the cost of computation. It has been found that the cost of computation can be reduced by as much as 97%.

The approach described in Sections 3.2-3.3 has been used to derive a simple model for gyrator GB (gyrator of Fig. 3.5 with R_4 connected across terminals 22'). The details of the analysis as well as the arrangement of the model derived can be found in Appendix A.

3.5 Experimental Verification of the Model

In order to verify the validity of the model experimentally, gyrator circuit GA was constructed by using μA741 operational amplifiers. The Q-factor and simulated inductance were then measured by using a series resonance method (see Appendix B). The dc supply voltage and the voltage across the simulated inductance were maintained constant and equal to ±15V and 0.3V, respectively. The responses obtained are shown in Figs. 3.14a and 3.14b.

The dc gains and cut-off frequencies of the two amplifiers were measured (see Appendix C) and found to be

$$A_{01} = 170{,}300$$

$$A_{02} = 159{,}700$$

$$\omega_{01} = 27.82 \text{ rad./sec.}$$

$$\omega_{02} = 26.51 \text{ rad/sec.}$$

giving an average dc gain $A_0 = 165{,}000$ and an average cut-off frequency $\omega_0 = 27.16$ rad./sec. These values together with the data-sheet values of the input and output resistances given in Table 3.1 were used to carry out a model analysis. The variation in the loss of the load

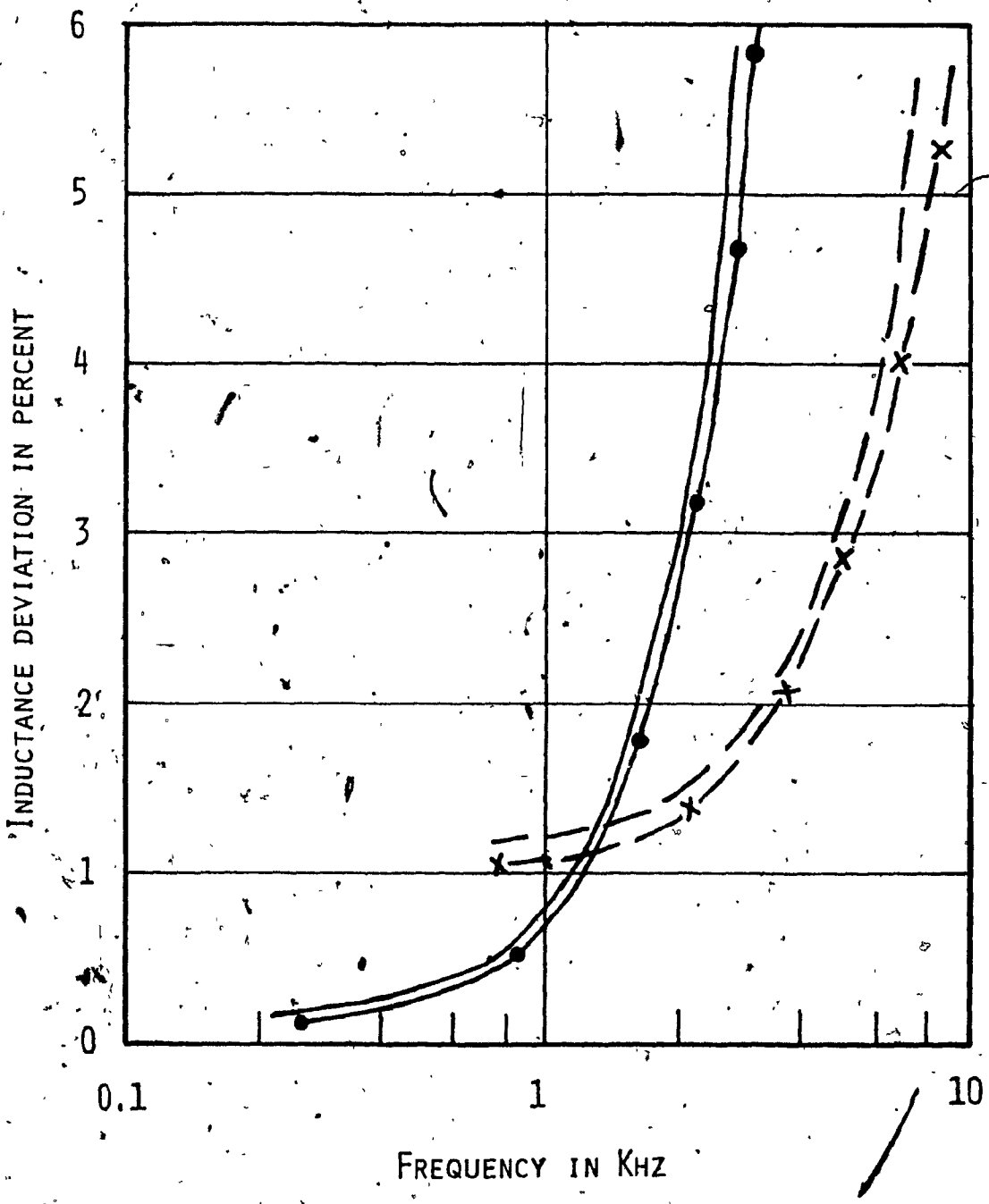

FIG. 3.14A MEASURED VARIATION OF INDUCTANCE DEVIATION WITH FREQUENCY (AMPLIFIER TYPE μA741, R=2.48KΩ, V_i=0.3V, V_S=±15V).

L_O	MODEL ANALYSIS	MEASURED
0.098H	— — — —	×—×—×—×
0.923H	———	●—●—●—●

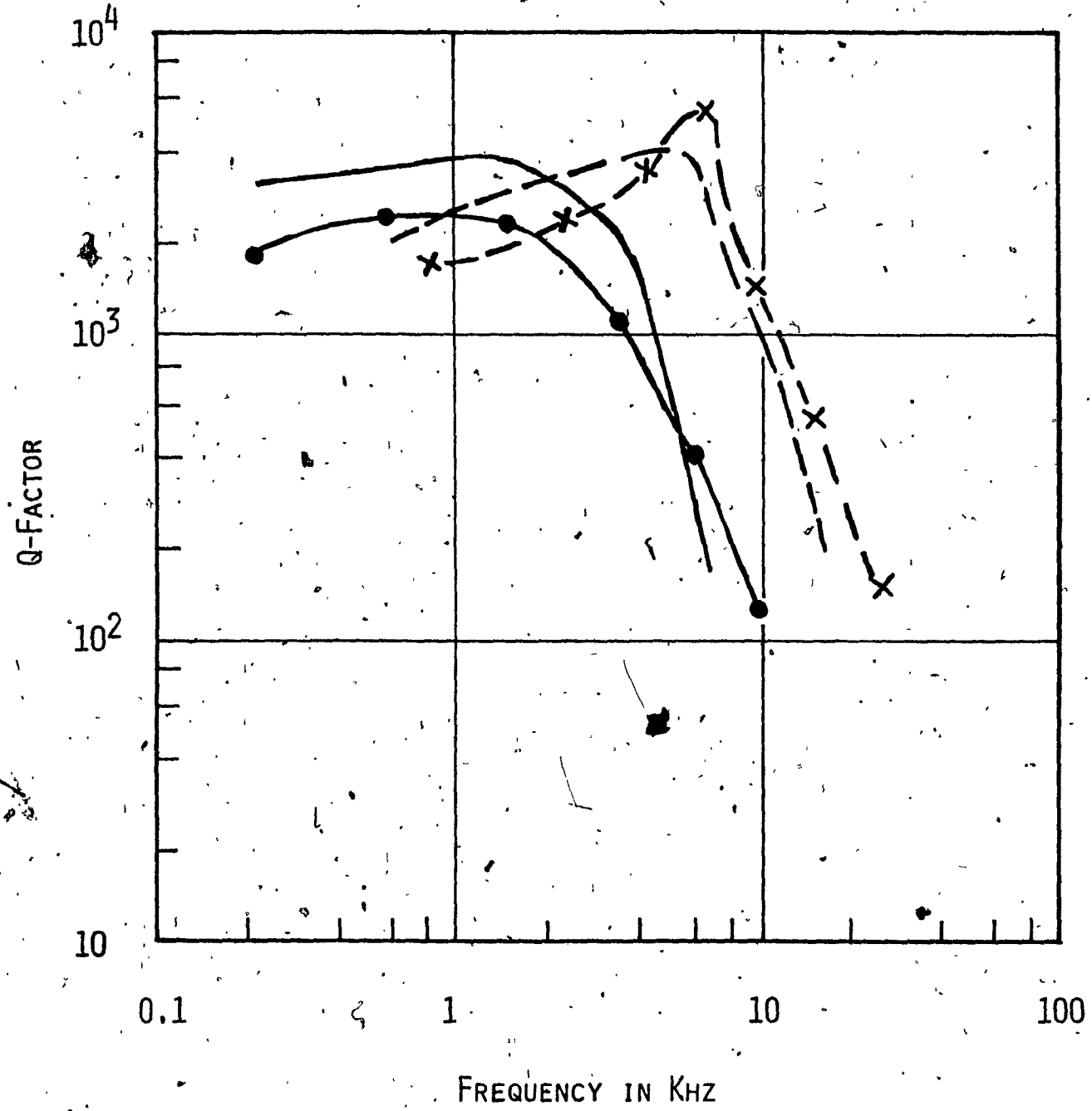

FIG.3.14B . MEASURED VARIATION OF Q-FACTOR WITH FREQUNECY(AMPLIFIER TYPE μA741, $R=2.48K\Omega$, $v_i=0.3v$, $v_s=\pm 15v$).

L_o	MODEL ANALYSIS	MEASURED
0.098H	— — — —	x—x—x—x
0.923H	———	●——●——●——●

capacitor with frequency was also taken into account. Polystyrene capacitors of 0.016 and 0.15μF were used with measured Q-factors of 3,000 and 2,500, respectively. Data sheets show that the Q-factor is approximately independent of frequency and hence the parallel loss resistance of each load capacitor can be computed as $R_L = Q/\omega C$. The predicted responses are compared with the measured responses in Figs. 3.14a and 3.14b. Despite the large tolerances in R_0, R_I, R_P and R_N, a reasonable agreement is evident between theory and practice.

CHAPTER 4

PERFORMANCE OF GYRATOR CIRCUITS

The model developed in Chapter 3 is now used to study the performance of gyrator circuits. The influence of amplifier imperfections on the simulated inductance is examined in Section 4.1. The effects of amplifier mismatch in gyrator circuits is discussed in Section 4.2. The influence of temperature and dc supply voltage variations on the gyrator GA is examined in Sections 4.3 and 4.4. A method for evaluating the voltage handling capabilities of gyrator circuits is proposed in 4.5. This approach is used for the comparison of gyrators GA and GB.

4.1 Influence of Amplifier Imperfections in Gyrator Circuits

For ideal amplifiers and a lossless load capacitor we have

$$\left.\begin{array}{l} A_0,\ A_0\omega_0 \to \infty \\ R_P,\ R_N \to \infty \\ R_I \to R_\infty \\ R_0 \to 0 \\ G_L \to 0 \end{array}\right\} \qquad (4.1)$$

From Eqns. 4.1, 3.71-3.72, 3.74, 3.76, 3.79 and 3.81-3.82 we get

$$\left.\begin{array}{l} G_{p1},\ G_{p2},\ G_{p3} \\ C_p,\ L_p \\ r_{p4},\ r_{p5} \end{array}\right\} \to 0 \qquad (4.2)$$

and from the Fig. 3.9 the simulated inductance is obtained as $L_o = R^2C$, as may be expected. Effectively, the amplifier imperfections introduce a number of series or shunt parasitic elements [78]-[80].

The influence of amplifier imperfections on the gyrator can now be examined by using the model of Fig. 3.9. The loss of the load capacitor introduces a proportional loss in the simulated inductance in the form of series resistance $G_L R^2$. The input resistance R_{P1} at the non-inverting input terminal of the amplifier A_1 introduces a small loss since, in practice, $R_{P1} > 50M\Omega$.

Eqn. 3.72 shows that the input resistance at the inverting input terminals of the amplifiers R_{N1} and R_{N2} introduce a small quantity of enhancement since R_{N1}, $R_{N2} > 50M\Omega$.

The input resistance R_I of the amplifiers gives rise to two sources of loss, a parallel resistance $R_I(2R + 3R_0 + A_0\omega_0 R^2C)/R$ and a frequency dependent parallel resistance $A_0^2\omega_0^2 R_I(2 + A_0\omega_0 RC)/2\omega^2$.

The output resistance R_0 of the amplifiers introduces loss through parallel resistance G_{p1} and G_{p3}, and through series resistances r_{p4} and r_{p5}. At the same time R_0 also gives rise to enhancement through G_{p2}. In addition, R_0 contributes to a certain extent to the parasitic capacitance C_p and to the parasitic inductance L_p.

A finite dc gain gives rise to two sources of loss, a large parallel resistance ($\simeq A_0R/2$) and a small series resistance ($\simeq 2R/A_0$), according to Eqns. 3.71 and 3.81.

Fig. 3.9 shows that the most significant parameter of the operational amplifier is the gain-bandwidth product $A_0\omega_0$. A non-infinite value of $A_0\omega_0$ gives rise to:

and from the Fig. 3.9 the simulated inductance is obtained as $L_o = R^2C$, as may be expected. Effectively, the amplifier imperfections introduce a number of series or shunt parasitic elements [78]-[80].

The influence of amplifier imperfections on the gyrator can now be examined by using the model of Fig. 3.9. The loss of the load capacitor introduces a proportional loss in the simulated inductance in the form of series resistance $G_L R^2$. The input resistance R_{P1} at the non-inverting input terminal of the amplifier A_1 introduces a small loss since, in practice, $R_{P1} > 50M\Omega$.

Eqn. 3.72 shows that the input resistance at the inverting input terminals of the amplifiers R_{N1} and R_{N2} introduce a small quantity of enhancement since R_{N1}, $R_{N2} > 50M\Omega$.

The input resistance R_I of the amplifiers gives rise to two sources of loss, a parallel resistance $R_I(2R + 3R_0 + A_0\omega_0 R^2C)/R$ and a frequency dependent parallel resistance $A_0^2\omega_0^2 R_I(2 + A_0\omega_0 RC)/2\omega^2$.

The output resistance R_0 of the amplifiers introduces loss through parallel resistance G_{p1} and G_{p3}, and through series resistances r_{p4} and r_{p5}. At the same time R_0 also gives rise to enhancement through G_{p2}. In addition, R_0 contributes to a certain extent to the parasitic capacitance C_p and to the parasitic inductance L_p.

A finite dc gain gives rise to two sources of loss, a large parallel resistance ($\simeq A_0R/2$) and a small series resistance ($\simeq 2R/A_0$), according to Eqns. 3.71 and 3.81.

Fig. 3.9 shows that the most significant parameter of the operational amplifier is the gain-bandwidth product $A_0\omega_0$. A non-infinite value of $A_0\omega_0$ gives rise to:

(a) A constant series parasitic inductance L_p.

(b) A constant parallel parasitic capacitance C_p, analogous to the winding capacitance in a real inductor.

(c) A frequency dependent parallel resistant $1/G_{p3}$ which reduces as frequency is increased.

(d) A frequency dependent series resistance r_{p5} which increases as the frequency is increased, analogous to the winding resistance in an inductor which increases due to the skin effect.

(e) Enhancement, for a non-zero R_0.

Note that $G_{p3} > 0$ for the assumed range of amplifier specifications.

At low frequencies, according to Eqn. 3.87, the simulated inductance $L = L_o + L_p$. The parasitic inductance L_p tends to increase the value of the simulated inductance and, in practice, this is not objectionable. However L_p is inversely proportional to gain-bandwidth product $A_0\omega_0$ of the amplifiers and variations in $A_0\omega_0$ will cause variations of similar magnitude in L_p. Since the gain-bandwidth product of the amplifiers is sensitive to temperature and dc supply variations, L_p will also be sensitive to such variations. Thus in order to obtain a stable inductance it is necessary to keep the ratio L_p/L_o small, say less than 0.05. Then a variation of 20% in $A_0\omega_0$ will cause a variation of 20% in L_p but the variation in the simulated inductance $L_o + L_p$ will be less than 1%. For a small value of L_p, a small value of R should be chosen, according to Eqn. 3.79. However, for a fixed value of inductance, the load capacitance has to be increased since $L_o = R^2C$. Clearly, a trade-off exists between the

size of the load capacitance and the stability of the simulated inductance. If $L_p << L_o$ the simulated inductance is independent of the gain-bandwidth product of the amplifiers. It is then possible to obtain an inductance with a prescribed temperature coefficient by matching the temperature coefficient of the four resistors used with that of the load capacitor.

The parasitic capacitance and the frequency dependent resistances tend to limit the useful bandwidth of the gyrator. As $A_0\omega_0$ is increased, C_p, G_{p3} and r_{p5} are reduced and hence the bandwidth of the gyrator is closely related to the gain-bandwidth product of the amplifiers used. It is noted that C_p and G_{p3} can be reduced by increasing R, however, at the same time r_{p5} is increased. It may thus be possible to select R for maximum gyrator bandwidth.

Depending on the relative values of the amplifier parameters and also on the values of R, C and G_L, the enhancement may exceed the total loss and then the simulated inductance will have a negative Q-factor. A negative Q-factor is more likely to occur for small values of R since the enhancement tends to increase faster than the loss as R is reduced, according to Eqn. 3.72. For larger values of gain-bandwidth product $A_0\omega_0$, G_{p3} and r_{p5} are small and hence negative Q-factor is more likely to occur. Note that enhancement in gyrator GA is a secondary spurious effect introduced by amplifier imperfections and it may be undesirable in some applications. Fig. 3.9 shows, however, that enhancement can be readily eliminated by connecting an external parallel resistance equal to $1/|G_{p2}|$ at the input of the gyrator circuit. In other applications, enhancement may be desirable, for example in cases where the loss of the load capacitor is large.

Furthermore it may be desirable to increase the enhancement. This can be easily achieved by connecting a resistance between node 3 and ground in Fig. 3.5. Then the effective value of R_{N1} will be reduced and, consequently, $|G_{p2}|$ will be increased, according to Eqn. 3.72.

The parasitic elements in the model for the gyrator GB are seen to be similar to those of the model for gyrator GA. However, for gyrator GB the negative conductance G'_{p2} is independent of R_{N1} and R_{N2} and hence the input resistances at the inverting input terminals of the operational amplifiers do not introduce enhancement.

From Eqns. 3.72 and A.44 we obtain

$$G_{p2} \approx -\frac{2R_0}{R(2R + A_0\omega_0 R^2 C)} \tag{4.3}$$

$$G'_{p2} \approx -\frac{4R_0}{R(2R + A_0\omega_0 R^2 C)} \tag{4.4}$$

and consequently

$$G'_{p2} = 2G_{p2} \tag{4.5}$$

It follows that a larger amount of enhancement is inherent in the gyrator of Fig. A.1.

4.2 Influence of Amplifier Mismatch in the Gyrator Circuits

The gyrator model of Chapter 3 has been derived on the basis of identical operational amplifiers. This assumption is valid for gyrator circuits using dual operational amplifiers. For discrete operational amplifiers, however, the various amplifier parameters tend to vary significantly from device to device. It is thus of interest to examine the validity of the model in cases where the two amplifiers

are nonidentical. In order to examine the influence of unequal dc gains and cut-off frequencies, gyrator circuit GA in which $A_{02} = 1.2A_{01}$ and $\omega_{02} = 1.2\omega_{01}$ or $A_{02} = 0.8A_{01}$ and $\omega_{02} = 0.8\omega_{01}$ was analyzed, first by using an exact equivalent circuit and then by using the proposed model. In the later case, the parameters A_0 and ω_0 were assumed to be equal to the average values of A_{01}, A_{02}, and ω_{01}, ω_{02} respectively. The gyrator responses predicted by the model are compared with the corresponding exact analysis responses in Figs. 4.1a and 4.1b. Close agreement is observed in Fig. 4.1a. In addition, agreement is evident in Fig. 4.1b for Q-factors less than 4000. Hence the gyrator model can be used to analyze the gyrator circuit in which the dc gains and cut-off frequencies of the two operational amplifiers are unequal.

4.3 The Effect of Temperature Variations on the Performance of Gyrator Circuits

The effective low-frequency inductance can be expressed as

$$L_{EL} = R^2C + \frac{R}{B}\left(2 + \frac{3R_0}{R}\right) \tag{4.5}$$

according to Eqns. 3.87 and 3.78-3.79 where $B = A_0\omega_0$. A variation in temperature will introduce variations in R, C, B, R_0 and, consequently, in L_{EL}. Since

$$R_0 \ll R \tag{4.6}$$

the variation in R_0 can be neglected. The per-unit variation in L_{EL} per ^oC can be obtained from Eqn. 4.5 as

$$\frac{\Delta L_{EL}}{L_{EL}} = \frac{2R^2C}{L_{EL}}\frac{\Delta R}{R} + \frac{R^2C}{L_{EL}}\frac{\Delta C}{C} + \frac{2R}{BL_{EL}}\left(\frac{\Delta R}{R} - \frac{\Delta B}{B}\right) \tag{4.7}$$

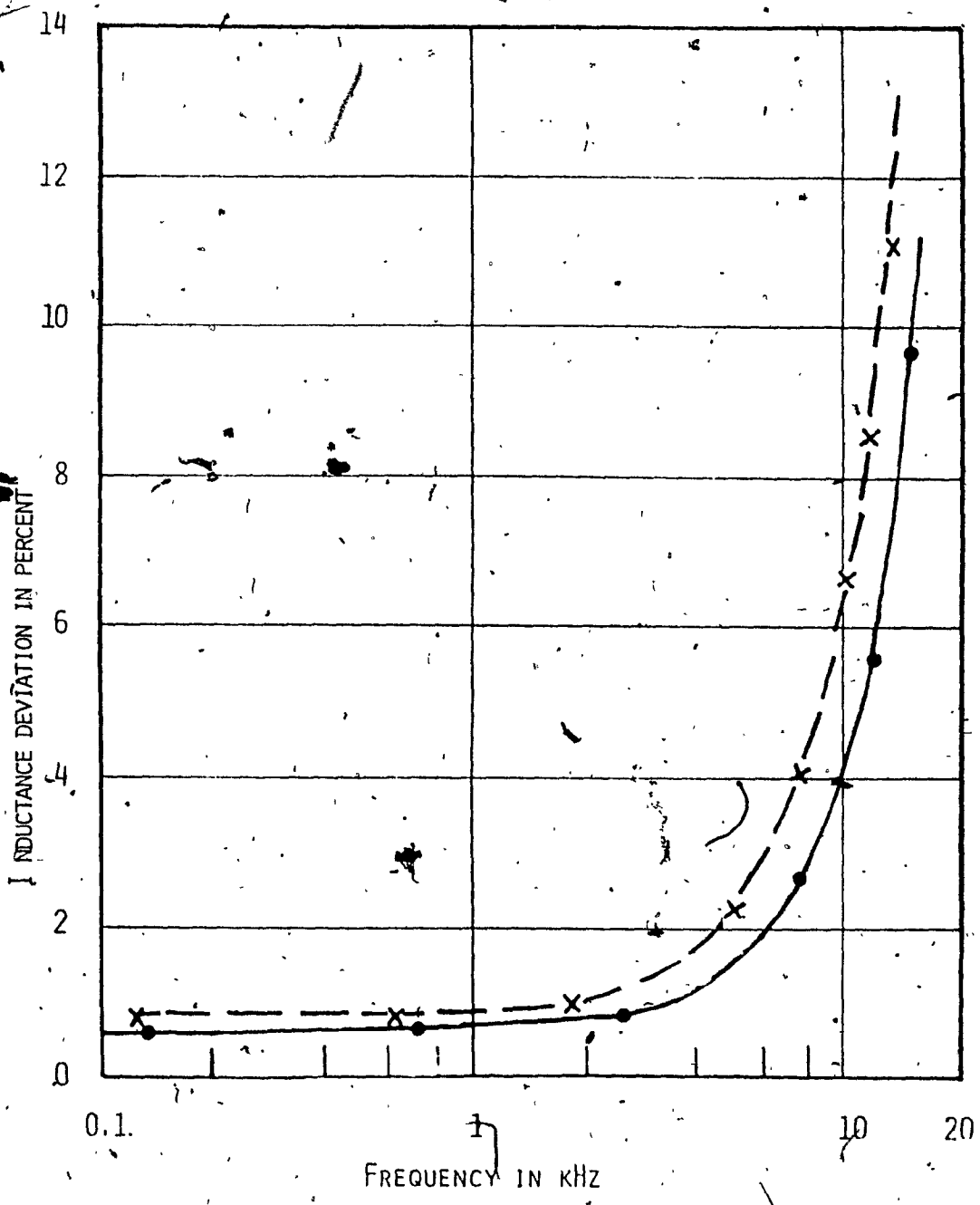

FIG.4.1A VARIATION OF INDUCTANCE DEVIATION WITH FREQUENCY FOR NON-IDENTICAL DC GAINS AND CUT-OFF FREQUENCIES (AMPLIFIER TYPE μA/41C, L = 0.1H, R = 2.5KΩ, $A_{01} = 200 \times 10^3$, $\omega_{01} = 37.6$ RAD. SEC.).

	EXACT ANALYSIS	MODEL ANALYSIS
$A_{02} = 240 \times 10^3$, $\omega_{02} = 44.64$ RAD. SEC.	———	• • •
$A_{02} = 160 \times 10^3$, $\omega_{02} = 29.76$ RAD. SEC.	—·—·—	× × ×

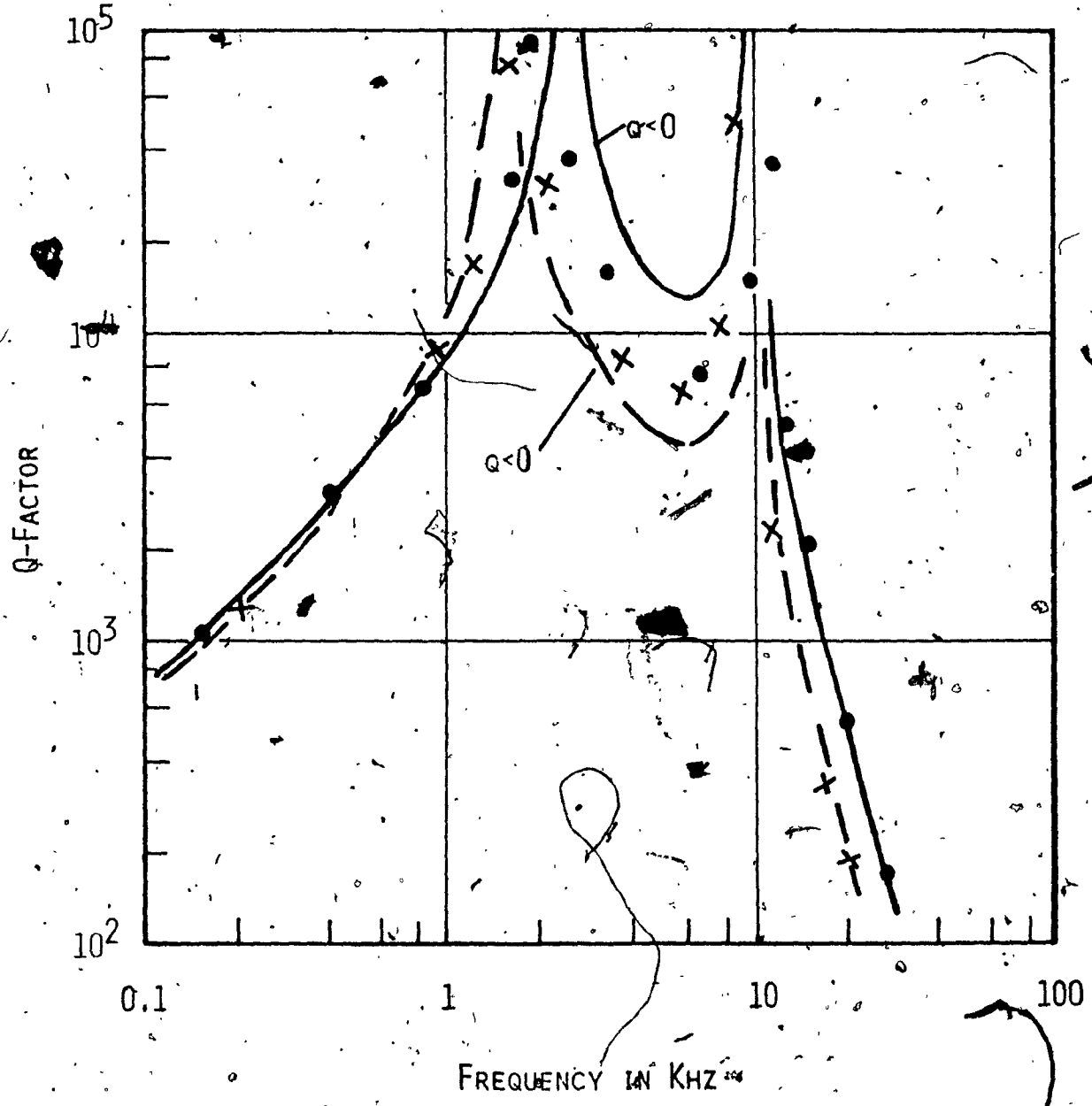

FIG.4.1B VARIATION OF Q-FACTOR WITH FREQUENCY FOR NON-IDENTICAL DC GAINS AND CUT-OFF FREQUENCIES(AMPLIFIER TYPE μA741) L_o=0.1H, R=2.5KΩ, $A_{01}=200\times10^3$, ω_{01}=37.6RAD./SEC.).

	EXACT ANALYSIS	MODEL ANALYSIS
$A_{02}=240\times10^3$, ω_{02}=44.64RAD./SEC.	———	• • •
$A_{02}=160\times10^3$, ω_{02}=29.76RAD./SEC.	— — —	× × ×

If

$$L_o >> L_p \tag{4.8}$$

that is

$$R^2C >> \frac{R}{B}(2 + \frac{3R_o}{R}) \tag{4.9}$$

Eqn. 4.7 can be expressed as

$$\frac{\Delta L_{EL}}{L_{EL}} = \frac{2\Delta R}{R} + \frac{\Delta C}{C} + \frac{2R}{BL_o}(\frac{\Delta R}{R} - \frac{\Delta B}{B}) \tag{4.10}$$

Hence

$$T_L \simeq 2T_R + T_C + \frac{2R}{BL_o}(T_R - T_B) \tag{4.11}$$

where T_L, T_R, T_C and T_B are the temperature coefficients of L_{EL}, R, C and B, respectively, in ppm per ^oc. In practice, T_B is negative and also

$$|T_B| > T_R \tag{4.12}$$

Therefore, an increase in gyration resistance R will tend to increase the temperature coefficient of the simulated inductance.

To examine the effect of temperature variation experimentally, gyrator GA was constructed using μA741 operational amplifiers, film nickel-chromium resistors (T_R = +100 ppm per ^oc) and polystyrene capacitors (T_C = -100±50 ppm per ^oc). A nominal inductance of L_o = 88mH was simulated using gyration resistances of 1, 2, 4 and 10 kΩ. The effective inductance and the Q-factor were measured at a frequency of 1kHz and over a temperature range -10^{o}c to +70^{o}c. The dc supply voltage to the operational amplifiers and the input voltage to the gyrator were maintained constant and equal to ±15V and 0.3V, respectively.

The inductance deviation due to variations in temperature is defined as

$$LD_T = \frac{(L_t - L_{20})}{L_{20}} 100\% \qquad (4.13)$$

where L_t and L_{20} are the effective inductances for temperatures t °c and 20 °c, respectively. The variation of LD_T with temperature for R = 1, 2, 4 and 10kΩ is illustrated in Fig. 4.2a. As expected, a reduction in gyration resistances improves the stability of the simulated inductance.

The Q-factor deviation due to variations in temperatures is defined as

$$QD_T = \frac{(Q_t - Q_{20})}{Q_{20}} 100\% \qquad (4.14)$$

where Q_t and Q_{20} are the Q-factors at temperatures t °c and 20 °c, respectively. The variation of QD_T with temperature for R = 1, 2, 4 and 10kΩ is illustrated in Fig. 4.2b. The Q-factor deviation for the temperature range of -10 °c to +70 °c is in the range -11% to +3%. Except for R = 10kΩ, the Q-factor is maximum at the room temperature. This is probably due to the fact that the optimum performance of the operational amplifiers occurs at room temperature.

4.4 The Effect of dc Supply Variations on the Performance of Gyrator Circuits

A variation in the dc supply voltage tends to change the gain bandwidth product B of the operational amplifiers and, consequently, the simulated inductance L_{EL} will also change. The per-unit variation in L_{EL} per volt change in the dc supply voltage can be obtained from Eqn. 4.5 as

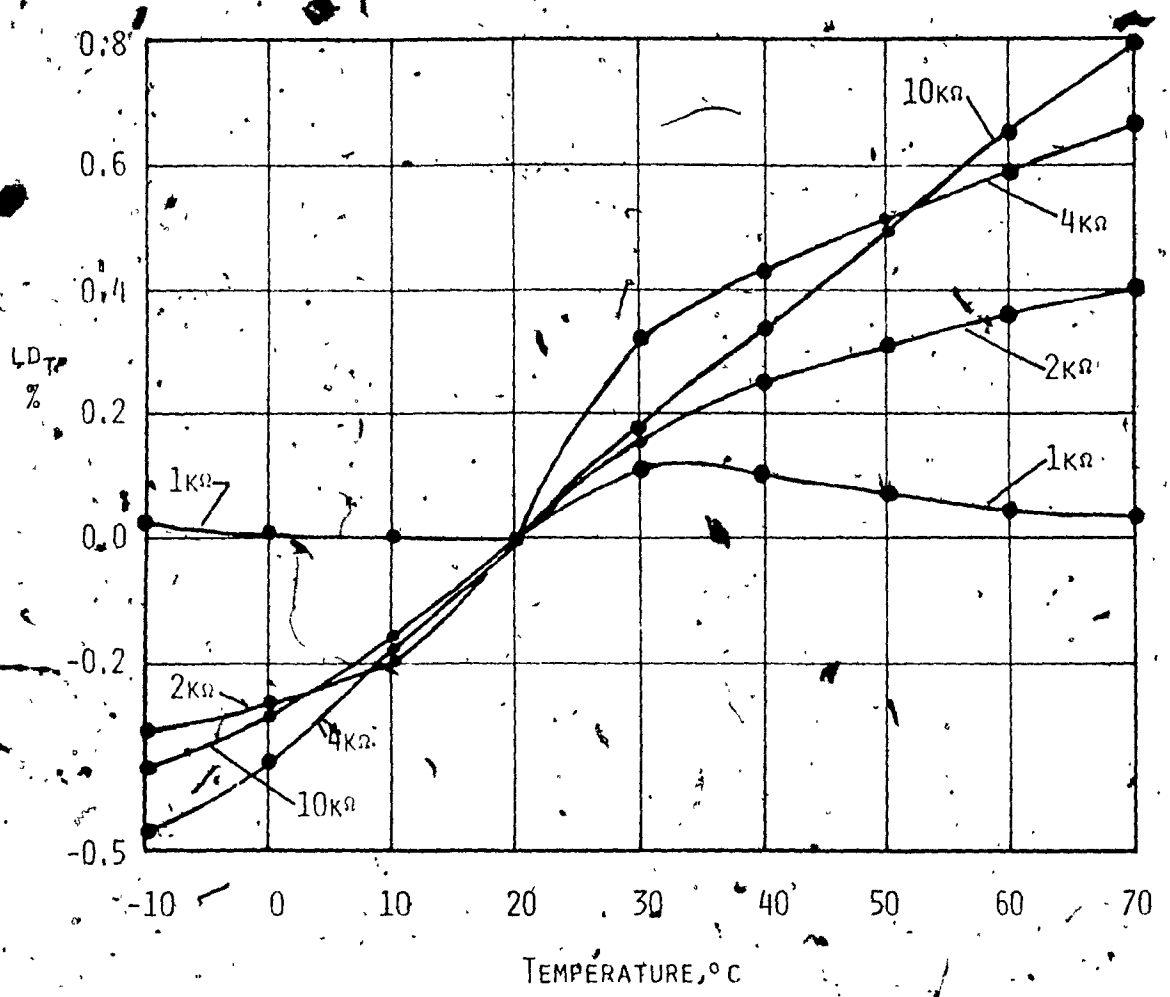

FIG.4.2A MEASURED VARIATION OF INDUCTANCE DEVIATION WITH TEMPERATURE (AMPLIFIER TYPE μA741, L_0=88MH, V_1=0.3V, V_S=±15V, F=1KHz).

R	L_{20}
1KΩ	88.8MH
2KΩ	87.93MH
4KΩ	89.08MH
10KΩ	92.19MH

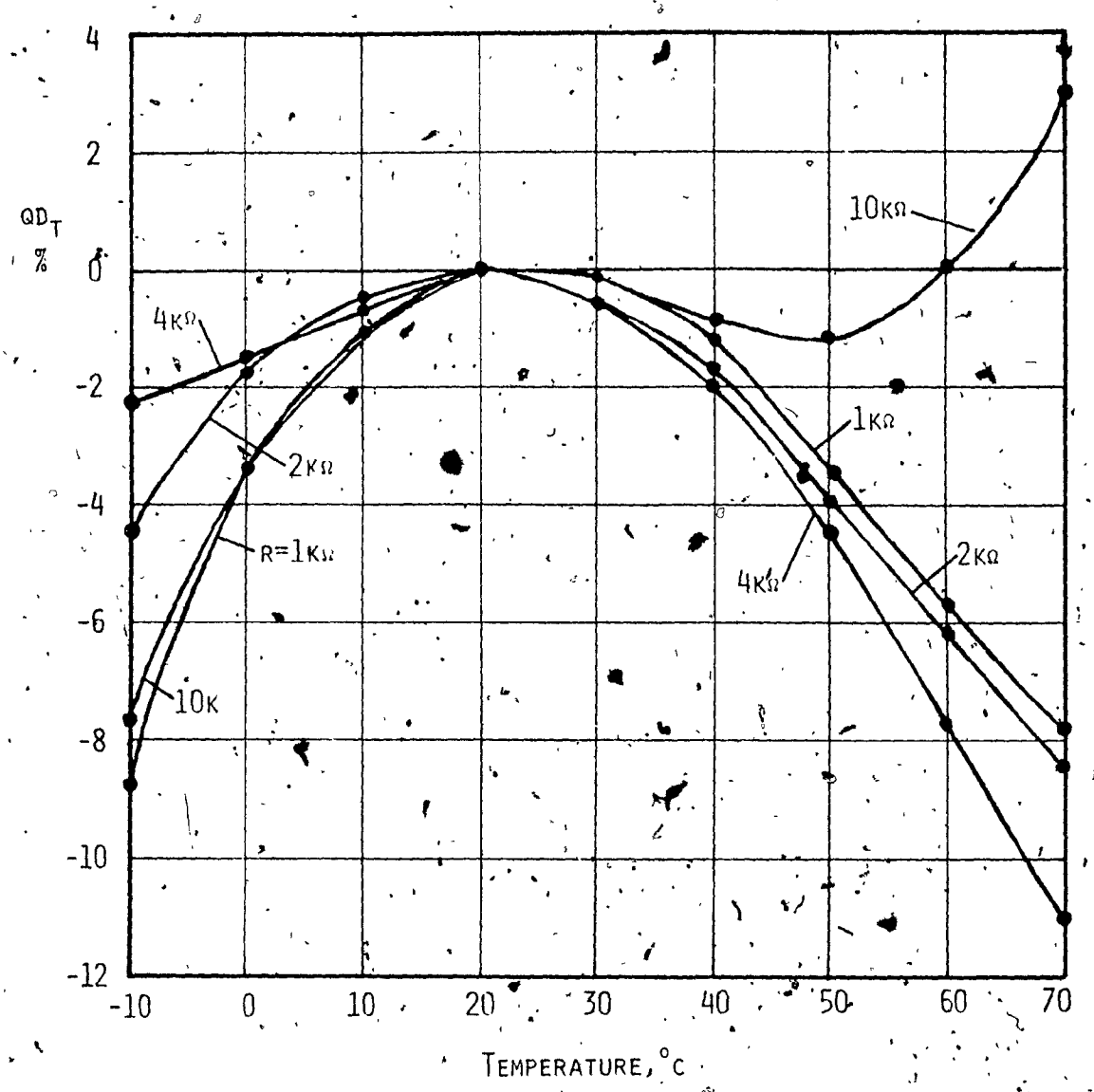

FIG.4.2B MEASURED VARIATION OF Q-FACTOR WITH TEMPERATURE (AMPLIFIER TYPE μA741, L_0=88MH, V_i=0.3V, V_S=±15V, F=1KHz).

R	Q20
1KΩ	2690.0
2KΩ	2028.0
4KΩ	1444.0
10KΩ	850.0

$$\frac{\Delta L_{EL}}{L_{EL}} = -\frac{R}{BL_{EL}}\left(2 + \frac{3R_0}{R}\right)\frac{\Delta B}{B} \qquad (4.15)$$

Using Eqns. 4.5 and 4.9 we can write Eqn. 4.15 as

$$\frac{\Delta L_{EL}}{L_{EL}} \simeq -\frac{R}{BL_0}\left(2 + \frac{3R_0}{R}\right)\frac{\Delta B}{B} \qquad (4.16)$$

The per-unit variation in B is positive and thus the per-unit variation in L_{EL} is negative. Furthermore, the per-unit variation in L_{EL} is proportional to R and, therefore, the gyration resistance should be as small as possible.

To examine the effect of dc supply variations experimentally, gyrator GA, constructed as described in Section 4.3, was tested for dc supply voltages in the range ±8V to ±18V. The measurements were carried out at room temperature for gyration resistances of 1, 2, 4 and 10kΩ and a nominal inductance of 88mH. The frequency and level of the input signal were maintained at 1kHz and 0.3V, respectively.

The inductance deviation due to dc supply variations is defined as

$$LD_V = \frac{L_V - L_{12}}{L_{12}}\,100\% \qquad (4.17)$$

where L_V and L_{12} are the effective inductances for dc supply voltages ±V volts and ±12 volts, respectively. The variation of LD_V with dc supply voltage for R = 1, 2, 4 and 10kΩ is illustrated in Fig. 4.3a. As anticipated earlier, a reduction in the gyration resistance tends to improve the stability of the simulated inductance.

The Q-factor deviation due to dc supply variations is defined as

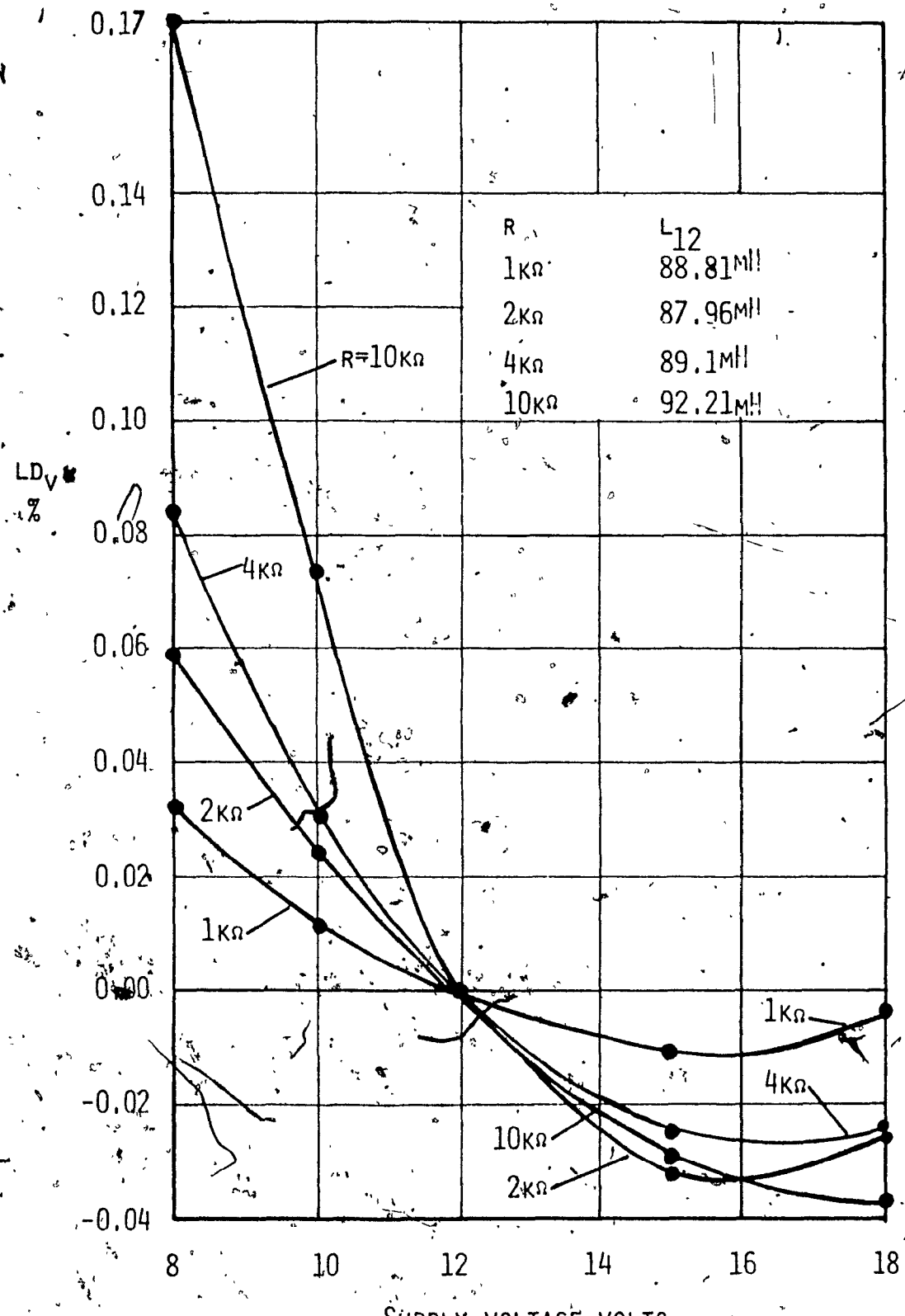

FIG.4.3A MEASURED VARIATION OF INDUCTANCE DEVIATION WITH SUPPLY VOLTAGE (AMPLIFIER TYPE μA741, L_0=88mH, V_i=0.3V, T=20°C, F=1KHz).

$$QD_V = \frac{Q_V - Q_{12}}{Q_{12}} 100\% \qquad (4.18)$$

where Q_V and Q_{12} are the Q-factors for dc supply voltages of $\pm V$ volts and $\pm 12V$, respectively. The variation of QD_V with dc supply voltage for R = 1, 2, 4 and 10kΩ is illustrated in Fig. 4.3b. In contrast with the stability of the simulated inductance, the stability of the Q-factor is worsened if the gyration resistance R is reduced.

4.5 Voltage Handling Capacity of Gyrator Circuits

The maximum undistorted input voltage of a gyrator circuit is closely related to the voltage handling capabilities of the operational amplifiers employed. A method will now be developed for evaluating the voltage handling capacity of gyrators.

Consider a capacitively terminated gyrator GA. Let V_{im} be the maximum undistorted voltage across the simulated inductance. Also let $\hat{V}_{01}$ and $\hat{V}_{02}$ be the maximum undistorted voltages at the outputs of amplifiers A_1 and A_2, respectively. The transfer functions between the input of the gyrator and the output of amplifiers A_1 and A_2 are denoted as $T_1(s)$ and $T_2(s)$, respectively. For linear operation the voltages at the outputs of the two amplifiers should not exceed $\hat{V}_{01}$ and $\hat{V}_{02}$, and, therefore, the maximum input voltage can be obtained as

$$V_{im} = \text{Min}\left[\frac{\hat{V}_{01}}{|T_1(j\omega)|}, \frac{\hat{V}_{02}}{|T_2(j\omega)|}\right] \qquad (4.19)$$

For identical amplifier with

$$R_0 = 0$$
$$R_I = R_P = R_N = \infty \qquad (4.20)$$

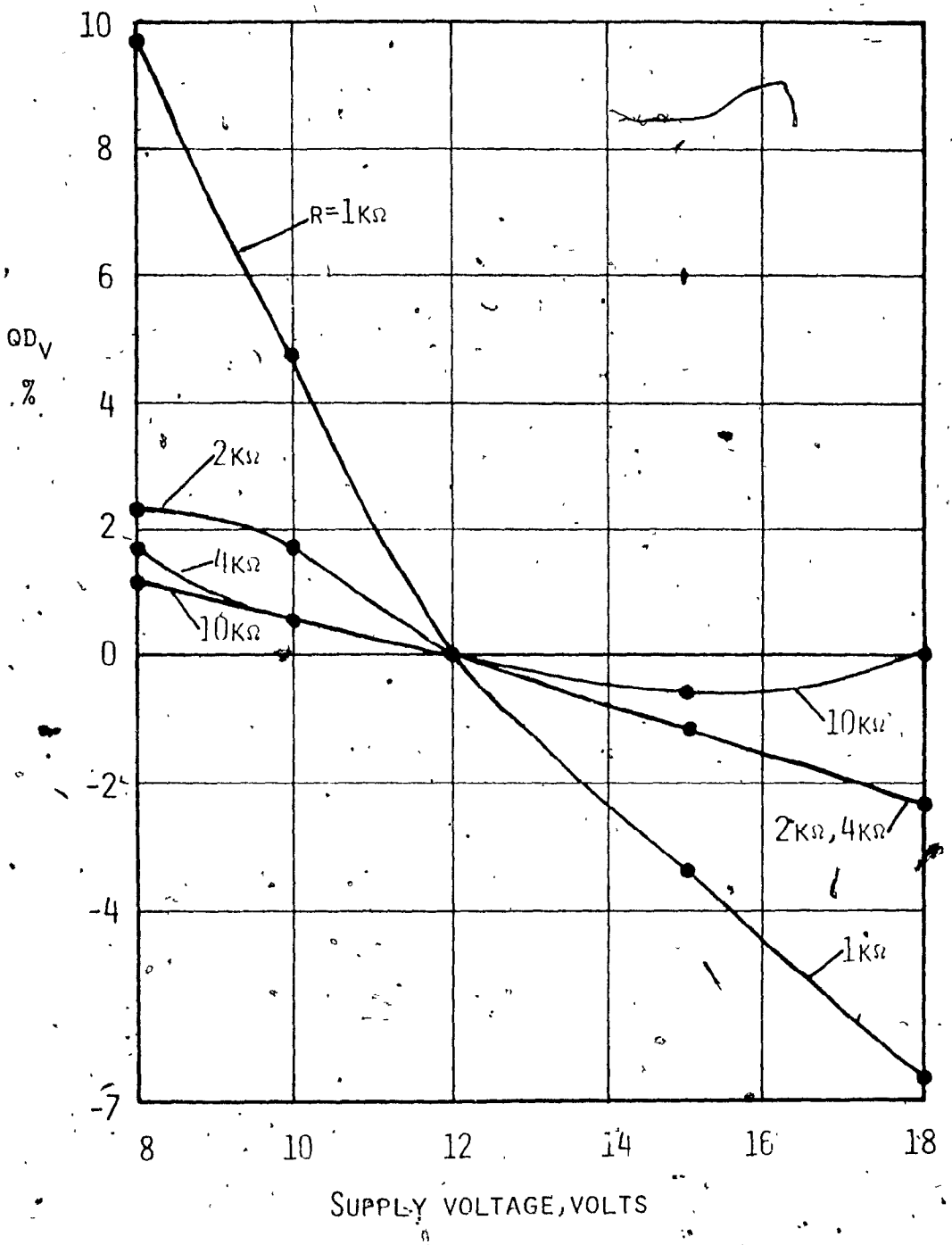

FIG.4.3B MEASURED VARIATION OF Q-FACTOR WITH SUPPLY VOLTAGE - (AMPLIFIER TYPE μA741, L_0=88MH, V_i=0.3V, T=20°C, F=1KHz).

R	Q_{12}
1KΩ	2784.0
2KΩ	2050.0
4KΩ	1460.0
10KΩ	845.0

Fig. 3.5 gives

$$T_1(s) = \frac{A(A+2)}{\frac{A^2 R}{R + Z_L} + 2A + 2} \tag{4.21}$$

where

$$Z_L = \frac{1}{sC} \tag{4.22}$$

and C is the load capacitance. For compensated amplifiers and frequencies such that $\omega << A_0\omega_0$ and $|A| >> 1$, Eqns. 3.14 and 4.22 give

$$T_1(j\omega) = \frac{A_0\omega_0(1 + j\omega RC)}{2\omega_0 - 2\omega^2 RC + j\omega(A_0\omega_0 RC + 2 + 2\omega_0 RC)} \tag{4.23}$$

Hence

$$|T_1(j\omega)| \simeq A_0\omega_0 \left\{ \frac{1 + \omega^2 R^2 C^2}{4\omega_0^2 + \omega^2(2 + A_0\omega_0 RC)^2} \right\}^{(1/2)} \tag{4.24}$$

Similarly,

$$T_2(s) = \frac{A^2(R - Z_L)}{A^2 R + 2(R + Z_L)A + 2(R + Z_L)} \tag{4.25}$$

and

$$|T_2(j\omega)| \simeq A_0\omega_0 \left\{ \frac{1 + \omega^2 R^2 C^2}{4\omega_0^2 + \omega^2(2 + A_0\omega_0 RC)^2} \right\}^{(1/2)} \tag{4.26}$$

$$= |T_1(j\omega)| \tag{4.27}$$

By letting $\hat{V}_{01} = \hat{V}_{02} = V_s$, Eqn. 4.27 shows that the two operational amplifiers will saturate simultaneously and hence from Eqn. 4.19

$$V_{im} = \frac{V_s}{|T_1(j\omega)|} \tag{4.28}$$

From Eqn. 4.24 and 4.28 we obtain

$$V_{im} = \frac{V_S}{A_0\omega_0}\left[\frac{4\omega_0^2R^2 + \omega^2(2R + A_0\omega_0L_o)^2}{R^2 + \omega^2L_o^2}\right]^{(1/2)} \qquad (4.29)$$

where $L_o = R^2C$ is the nominal inductance. Effectively the maximum input voltage is proportional to the saturation output voltage of the operational amplifiers and also it is a function of the frequency, gyration resistance and the nominal inductance.

Eqn. 4.29 has been used to evaluate V_{im} for R = 2.5kΩ and a variable value of L_o as shown in Fig. 4.4. Also for L_o = 0.1H and a varying value of R as shown in Fig. 4.5. The data for the operational amplifier type μA741 has been used and V_s was assumed constant and equal to 10V for the frequency range 0 - 10kHz. Figs. 4.4-4.5 show that the voltage handling capacity of gyrator GA tends to be reduced significantly at low frequency. An increase in the nominal inductance tends to increase the voltage handling capacity as shown in Fig. 4.4, whereas an increase in the gyration resistance tends to reduce it as shown in Fig. 4.5.

The maximum undistorted voltage at the input of gyrator GA has been determined experimentally. The signal was taken to be distorted when the percentage of distortion was in excess of 5%. The results are shown in Fig. 4.6-4.7. Agreement between experimental and theoretical results is restricted to low frequencies only. At higher frequencies the internal loading to the amplifiers tends to reduce the effective values of $\hat{V}_{01}$ and $\hat{V}_{02}$ and hence a corresponding reduction in V_{im} is introduced. The theoretical approach neglects the loading effect on the operational amplifiers and an optimistic value for V_{im} is thus predicted.

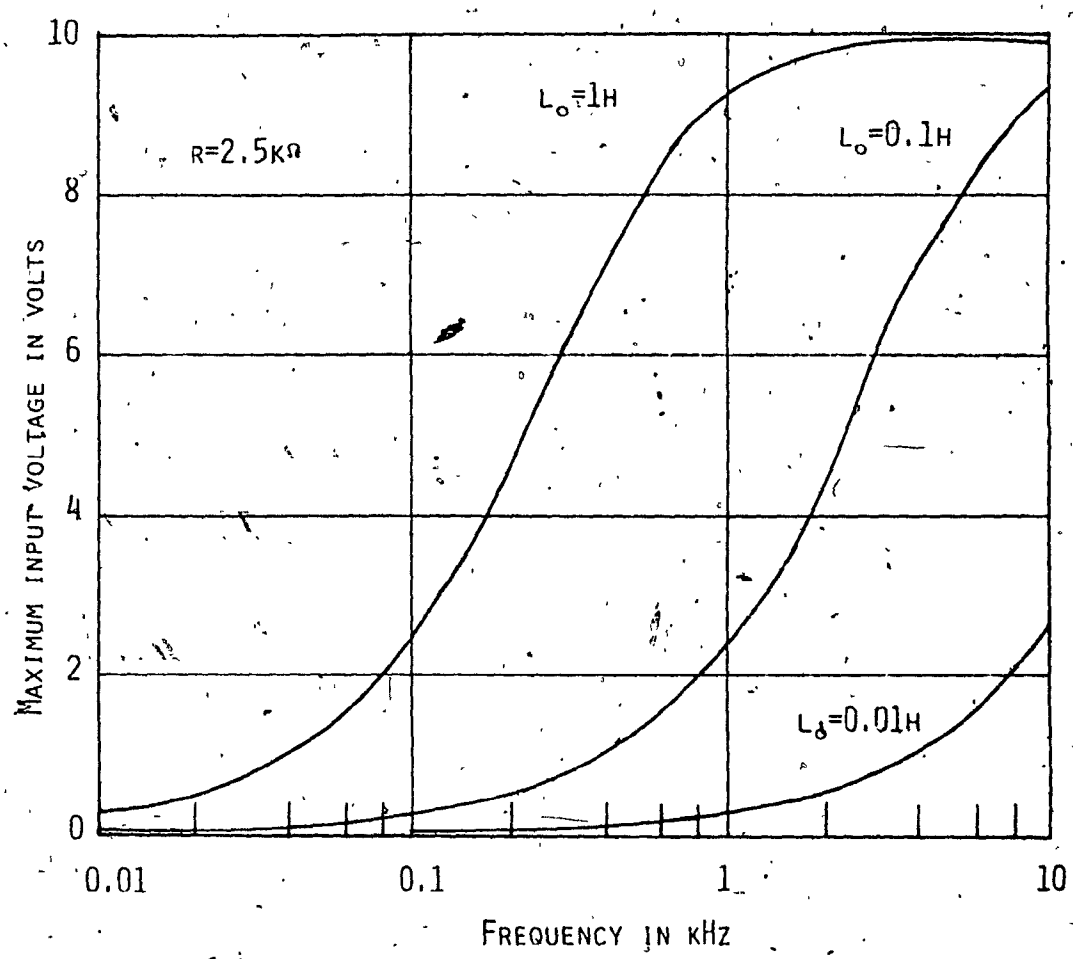

FIG.4.4 THEORETICAL MAXIMUM INPUT VOLTAGE AGAINST FREQUENCY, FOR DIFFERENT NOMINAL INDUCTANCES (AMPLIFIER TYPE μA741C).

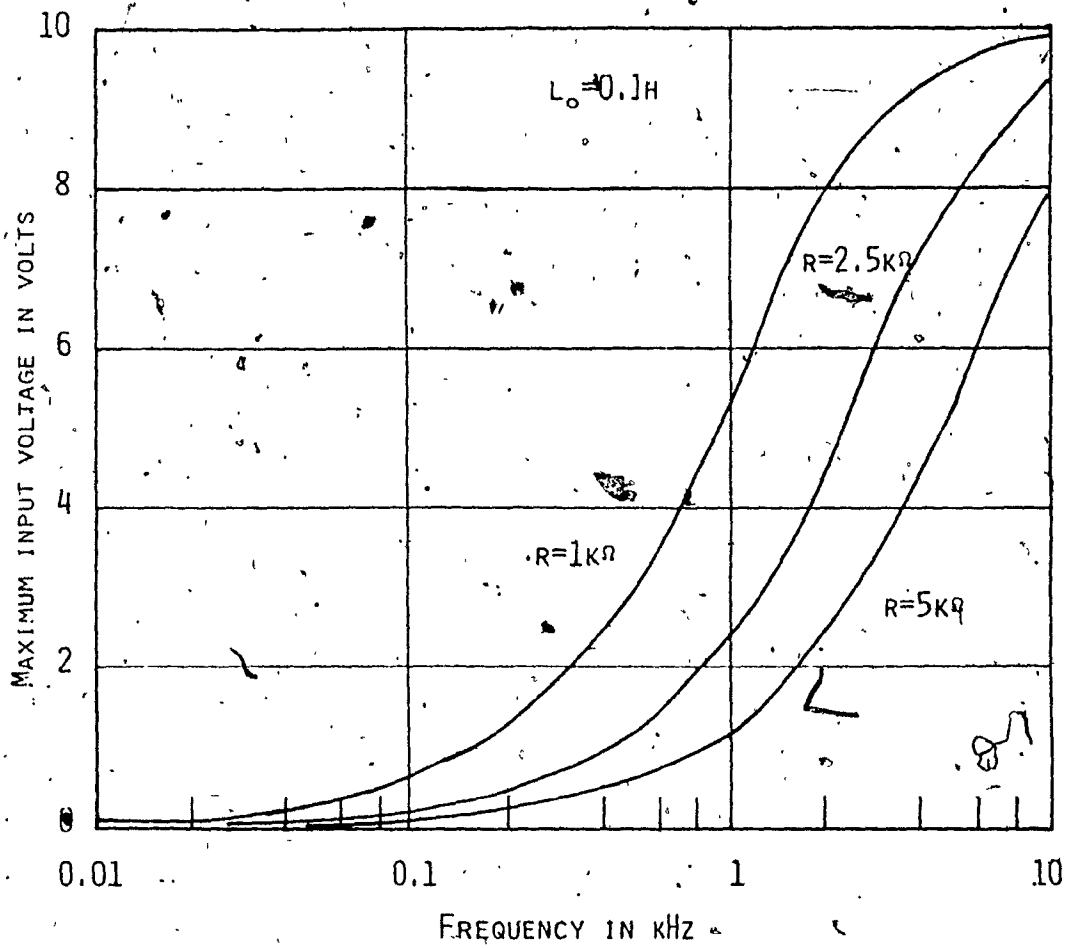

FIG.4.5 THEORETICAL MAXIMUM INPUT VOLTAGE AGAINST FREQUENCY FOR DIFFERENT GYRATION RESISTANCES (AMPLIFIER TYPE μA741C).

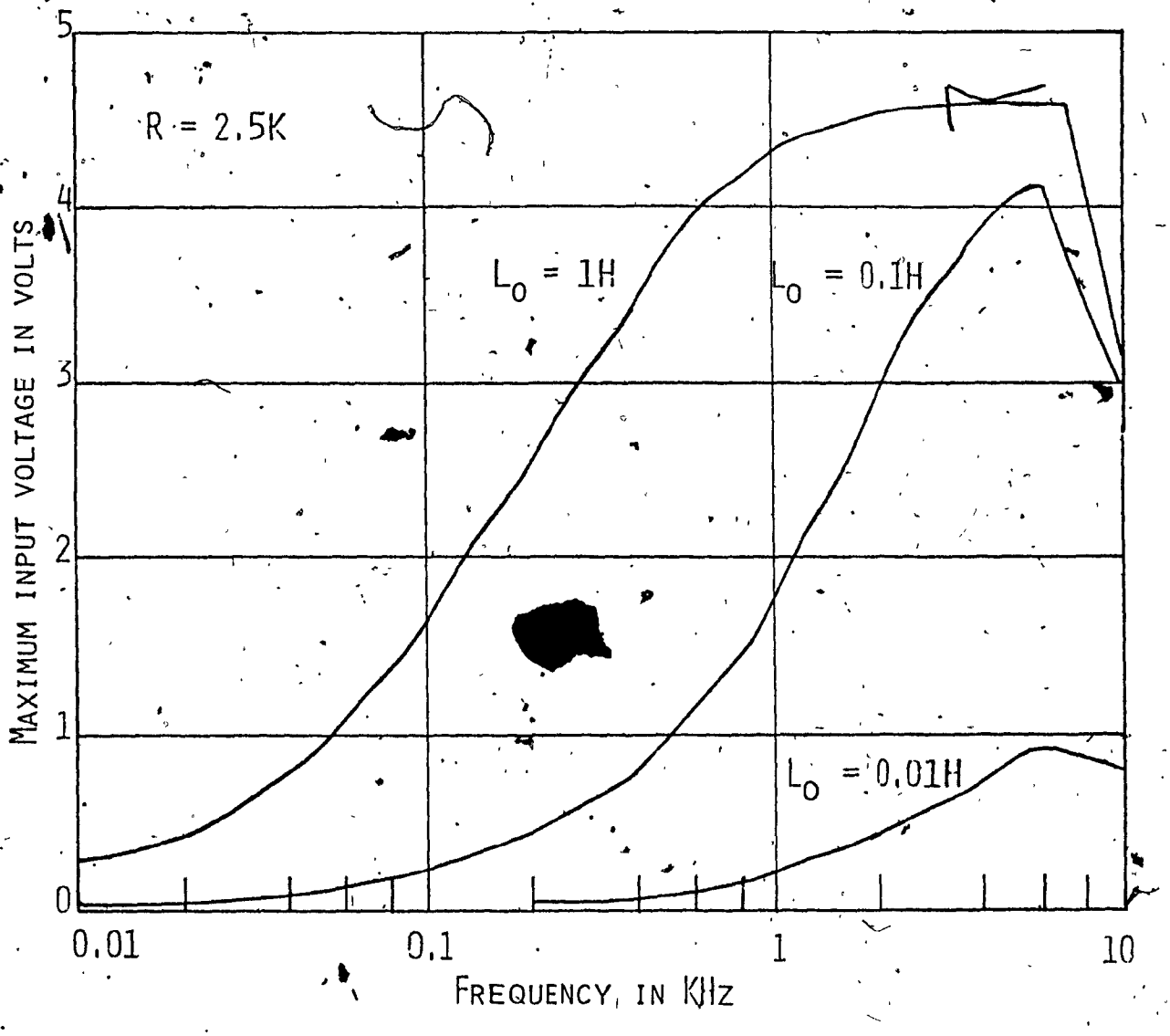

FIG. 4.6 MEASURED MAXIMUM INPUT VOLTAGE AGAINST FREQUENCY FOR DIFFERENT NOMINAL INDUCTANCES. (GYRATOR GA, AMPLIFIER TYPE μA741C).

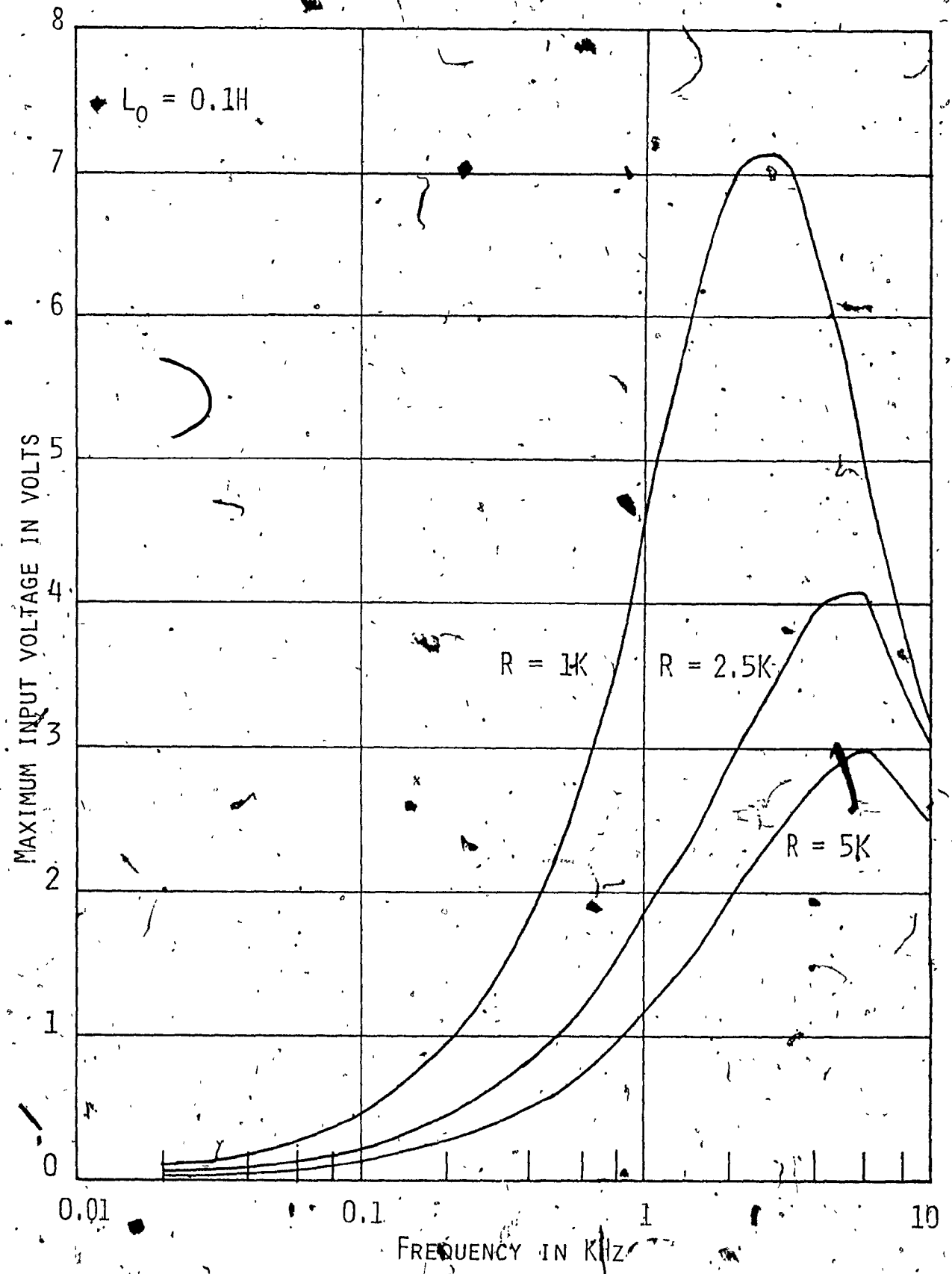

FIG. 4.7 MEASURED MAXIMUM INPUT VOLTAGE AGAINST FREQUENCY FOR DIFFERENT GYRATION RESISTANCES (GYRATOR GA, AMPLIFIER TYPE μA741C).

The voltage handling capacity of gyrator GB is examined in Appendix D.

4.6 Comparison of Gyrators GA and GB

The performance of gyrator GA is very similar to that of gyrator GB. The two circuits differ in two respects:

(a) Enhancement in gyrator GA is less pronounced.

(b) The voltage handling capacity of gyrator GA is larger.

In gyrator GB the voltage at the output of amplifier A_1 is proportional to the voltage at the input of the gyrator, according to Eqn. D.5. This property is useful for the design of second-order filter sections with low output resistance. Two possibilities are illustrated in Figs. 4.8a and 4.8b. The transfer function in Fig. 4.8a is obtained as

$$\frac{V_0}{V_i} = \frac{s^2}{s^2 + \frac{R_x}{L_o} s + \frac{1}{L_o C_x}} \tag{4.30}$$

From Eqn. D.5, $V_0' = 2V_0$ and hence

$$\frac{V_0'}{V_i} = \frac{2s^2}{s^2 + \frac{R_x}{L_o} + \frac{1}{L_o C_x}} \tag{4.31}$$

Similarly, from Fig. 4.8b

$$\frac{V_0}{V_i} = \frac{s/R_x C_x}{s^2 + \frac{1}{R_x C_x} s + \frac{1}{L_o C_x}} \tag{4.32}$$

and hence

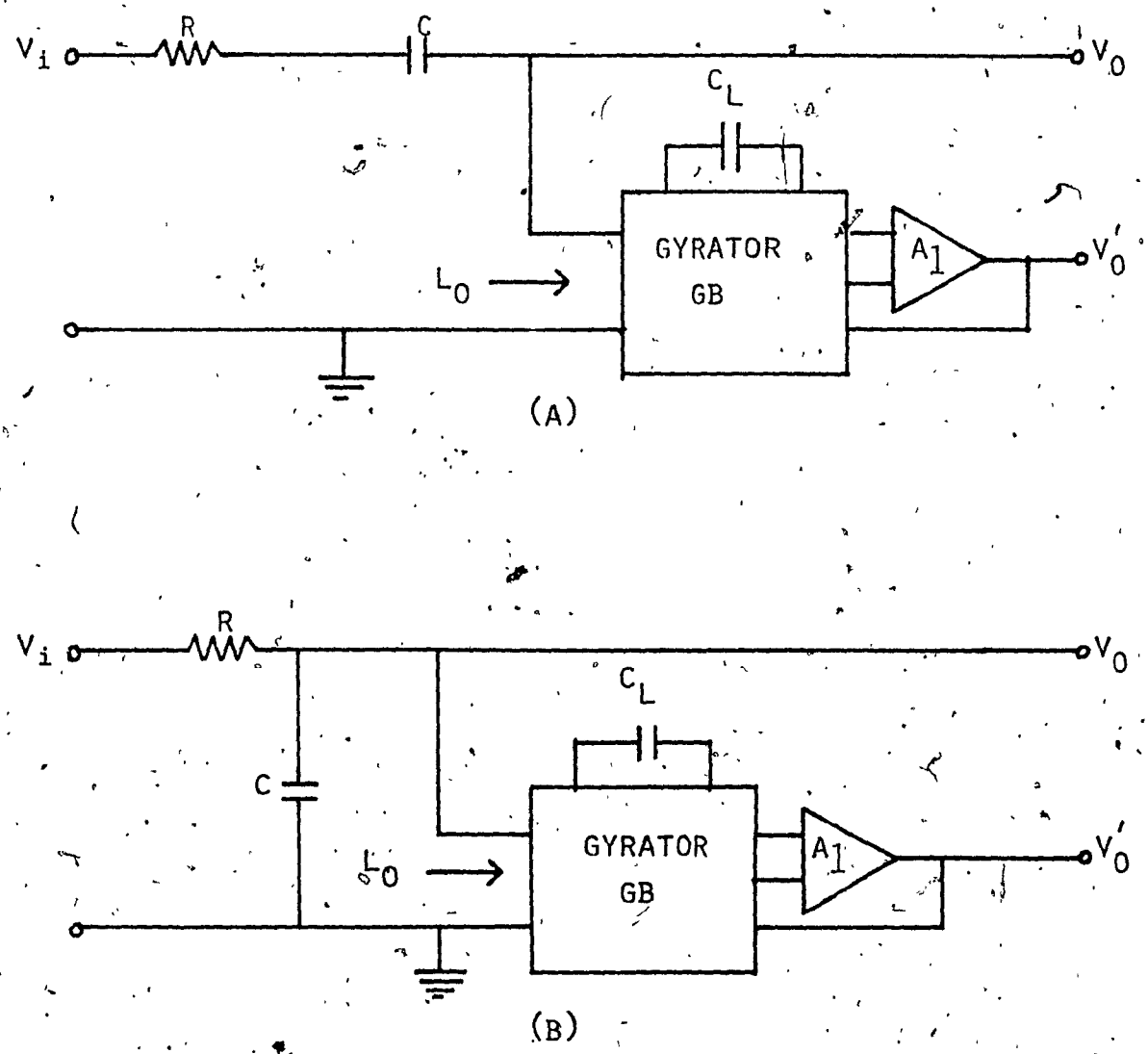

FIG. 4.8 SECOND ORDER FILTER SECTIONS USING GYRATOR GB.
(A) HIGH-PASS FILTER SECTION.
(B) BAND-PASS FILTER SECTION.

$$\frac{V_0'}{V_i} = \frac{2s/R_x C_x}{s^2 + \frac{1}{R_x C_x} s + \frac{1}{L_o C_x}} \qquad (4.33)$$

Owing to the low output resistance of the operational amplifier A_1, the filter sections of Fig. 4.8 have a low output resistance. Consequently, a number of such sections can be cascaded without isolation amplifiers.

Eqns. 4.24 and 4.27 show that in gyrator GA neither $T_1(s)$ nor $T_2(s)$ is a constant and hence the isolation property of Fig. 4.8 can not be achieved.

CHAPTER 5

COMPENSATION TECHNIQUE

As was shown in section 4.1, the finite gain-bandwidth product of the amplifiers gives rise to a parasitic inductance and a parasitic capacitance in the gyrator model. The parasitic inductance causes no problems since this can be used as part of the required inductance. The parasitic capacitance, however, tends to limit the useful bandwidth of the gyrator circuit. This chapter describes a compensation technique whereby the parasitic capacitance can be eliminated. In this way the useful bandwidth of the gyrator circuit can be increased significantly. The compensation technique is verified first by a computer-aided analysis and then by experiment.

5.1 Simplified Models

The relative magnitudes of the various parasitic impedances in the model of Fig. 3.9 tend to change with frequency. At low frequencies, say less than 100Hz,

$$r_{p4} \gg r_{p5} \tag{5.1}$$

$$|G_{p1} + G_{p2}| \gg G_{p3} \tag{5.2}$$

$$\omega C_p \ll \frac{1}{\omega(L_p + L_o)} \tag{5.3}$$

and hence the gyrator model can be simplified as shown in Fig. 5.1.

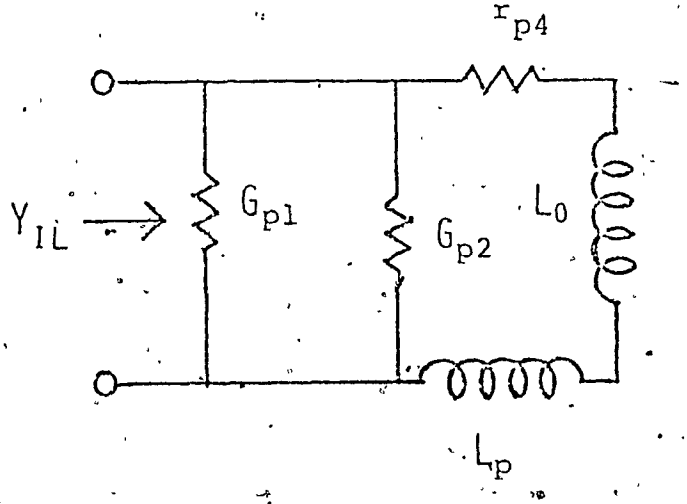

FIG. 5.1 SIMPLIFIED LOW-FREQUENCY GYRATOR MODEL

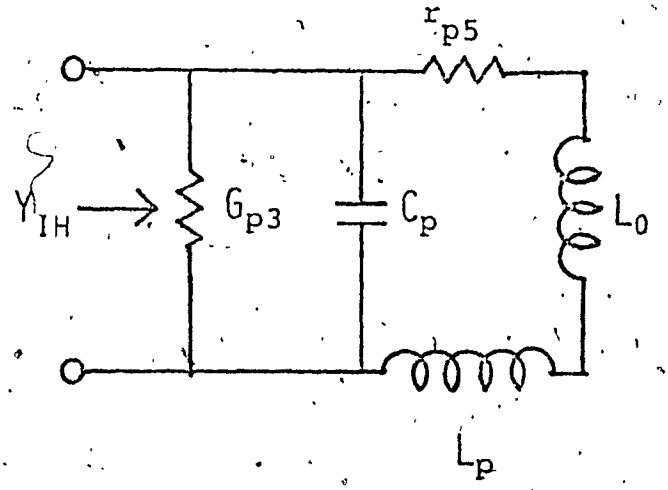

FIG. 5.2 SIMPLIFIED HIGH-FREQUENCY GYRATOR MODEL

The low frequency input admittance can be obtained as

$$Y_{IL} = G_{p1} + G_{p2} + \frac{1}{r_{p4} + j\omega(L_o + L_p)} \tag{5.4}$$

$$= G_{EL} + \frac{1}{j\omega L_{EL}} \tag{5.5}$$

where

$$G_{EL} = G_{p1} + \frac{r_{p4}}{r_{p4}^2 + \omega^2 (L_o + L_p)^2} \tag{5.6}$$

and

$$L_{EL} = \frac{r_{p4}^2 + \omega^2 (L_o + L_p)^2}{\omega^2 (L_o + L_p)} \tag{5.7}$$

are the effective input conductance and effective input inductance respectively. Even for very low frequencies

$$r_{p4} << \omega(L_o + L_p) \tag{5.8}$$

according to Eqns. 3.78 - 3.79, and 3.81. From Eqn. 5.7,

$$L_{EL} \simeq L_o + L_p \tag{5.9}$$

Eqn. 3.79 shows that the parasitic inductance L_p is inversely proportional to the gain-bandwidth product of the amplifiers. Therefore, its tolerance and temperature coefficient can be large. In practice, however, R and C can be chosen to give $L_p << L_o$, so that the tolerance and temperature coefficient of L_{EL} can be kept small. Consequently, L_p can be used as part of the required inductance.

The low frequency Q-factor is given by

$$Q_{LF} = \frac{-\text{Im } Y_{IL}}{\text{Re } Y_{IL}} = \frac{1}{\omega L_{EL} G_{EL}} \tag{5.10}$$

and from Eqns. 5.6, 5.7 and 5.10.

$$Q_{LF} = \frac{\omega(L_o + L_p)}{(G_{p1} + G_{p2})\left\{r_{p4}^2 + \omega^2 (L_o + L_p)^2\right\} + r_{p4}} \tag{5.11}$$

$$= \frac{\omega(L_o + L_p)}{r_{p4}\left\{1 + r_{p4}(G_{p1} + G_{p2})\right\} + \omega^2 (L_o + L_p)^2 (G_{p1} + G_{p2})} \tag{5.12}$$

Q_{LF} is zero when $\omega = 0$. If $G_{p1} + G_{p2}$ is positive, Q_{LF} will increase and then decrease after reaching a maximum as frequency is increased from zero. Q_{LF} is always positive. If $G_{p1} + G_{p2}$ is negative, Q_{LF} will increase from zero to infinity and then become negative as the frequency is increased from zero, since

$$r_{p4}(G_{p1} + G_{p2}) << 1 \tag{5.13}$$

according to Eqns. 3.71, 3.72 and 3.81. The conductance G_{p1} can be increased by using a shunt resistance across the input of the gyrator circuit. Similarly, Eqn. 3.72 shows that $-G_{p2}$ can be increased by using a shunt resistance between node 3 and ground in Fig. 3.5 and hence Q_{LF} can be easily increased or reduced as necessary.

For high frequencies, say in excess of 10kHz,

$$\left.\begin{aligned} r_{p5} &>> r_{p4} \\ G_{p3} &>> \left| G_{p1} + G_{p2} \right| \end{aligned}\right\} \tag{5.14}$$

and hence the model of Fig. 3.9 can now be simplified as shown in Fig. 5.2. If the required inductance appears in parallel with a filter capacitance C_f, the parasitic capacitance C_p can be used as part of C_f. Otherwise, C_p is an undesirable capacitance. The high-frequency input admittance can be obtained from Fig. 5.2 as

$$Y_{IH} = G_{p3} + j\omega C_p + \frac{1}{r_{p5} + j\omega(L_o + L_p)} \tag{5.15}$$

$$= G_{EH} + \frac{1}{j\omega L_{EH}} \tag{5.16}$$

where the effective input conductance and input inductance are now given by

$$G_{EH} = G_{p3} + \frac{r_{p5}}{r_{p5}^2 + \omega^2 (L_o + L_p)^2} \tag{5.17}$$

and

$$L_{EH} = \frac{(L_o + L_p)^2 + \frac{r_{p5}^2}{\omega^2}}{(L_o + L_p) - C_p\left\{r_{p5}^2 + \omega^2 (L_o + L_p)^2\right\}} \tag{5.18}$$

Clearly, C_p tends to increase the effective inductance by an amount which increases with frequency. Since the simulated inductance is required to be constant with frequency, C_p imposes a limit on the useful bandwidth of the gyrator circuit. The high frequency Q-factor is obtained from Eqns. 5.17 and 5.18 as

$$Q_{HF} = \frac{-\text{Im } Y_{IH}}{\text{Re } Y_{IH}} = \frac{1}{\omega L_{EH} G_{EH}} \tag{5.19}$$

$$= \frac{\omega\left[(L_o + L_p) - C_p\left\{r_{p5}^2 + \omega^2(L_o + L_p)^2\right\}\right]}{G_{p3}\left\{r_{p5}^2 + \omega^2(L_o + L_p)^2\right\} + r_{p5}}$$

$$\simeq \frac{\omega(L_o + L_p)}{G_{p3}\left\{r_{p5}^2 + \omega^2(L_o + L_p)^2\right\} + r_{p5}} \qquad (5.20)$$

Since G_{p3} and r_{p5} are positive, Q_{HF} is positive. Also the high frequency Q-factor Q_{HF}, is smaller for larger values of L_o.

5.2 Compensation Technique

It was shown, in section 4.1, that the finite gain-bandwidth product of the amplifiers gives rise to a parasitic inductance and a parasitic capacitance. The parasitic inductance causes no problems since this can be used as part of the required inductance, as explained in section 5.1. The parasitic capacitance, however, tends to limit the useful bandwidth of the gyrator circuit. This section describes a compensation technique whereby the useful bandwidth of the gyrator circuit can be increased [81]. Trimmel and Heinlein [75] have also considered the problem of gyrator broadbanding. However, their technique is applicable only to gyrator circuits constructed with floating transconductance amplifiers. Their emphasis is to maximize the bandwidth over which the Q-factor remains high. Here, the emphasis is to maximize the bandwidth over which the simulated inductance remains constant.

The useful bandwidth of the gyrator circuit of Fig. 3.5 can be extended if the parasitic capacitance C_p can be eliminated. Eqn. 3.72 shows that R_{N1}, which can be considered as an external resistance between

node 3 and ground, gives rise to a negative resistance $-R_{N1}$ across the input terminals of the gyrator circuit. It is, therefore, expected that a positive capacitance C_c between node 3 and ground will give rise to a negative capacitance in parallel with the positive parasitic capacitance C_p so that C_p may be eliminated. This possibility is now examined.

The use of a compensating capacitance between node 3 and ground in Fig. 3.5 will modify the model of Fig. 3.9. The modified model can be derived by repeating the analysis presented in section 3.2. For the sake of brevity, however, only the changes will be indicated. The input resistances R_{N1}, R_{N2} and R_{p1} have been assumed to be infinite since these are very large in practice, of the order of 500MΩ.

The parameter y_{11} for the gyrator circuit as given by Eqn. 3.39 is now obtained as

$$y_{11} = G_f + G_h + \frac{j\omega}{A_0\omega_0 R}\left(2 + \frac{R_0}{R} - A_0\omega_0 RC_c\right) \qquad (5.21)$$

where

$$G_f = \frac{1}{A_0 R}\left(2 + \frac{R_0}{R}\right) \qquad (5.22)$$

and

$$G_h = \frac{\omega^2}{A_0\omega_0}\left\{\frac{2}{A_0\omega_0 R} + \frac{8R_0}{A_0\omega_0 R^2} - C_c\left(2 + \frac{3R_0}{R}\right)\right\} \qquad (5.23)$$

The parameters y_{12}, y_{21}, and y_{22}, however, remain the same as for the uncompensated gyrator circuit. For a lossy load capacitor in which

$$Y_L = G_L + sC \tag{5.24}$$

the input admittance of the gyrator circuit is given by

$$Y_i = y_{11} - \frac{y_{12}\, y_{21}}{y_{22} + G_L + sC} \tag{5.25}$$

By using Eqns. 3.26, 3.27, 3.40 - 3.42, 5.21 - 5.24 and 5.25, the input admittance can be expressed as

$$Y_i = G_{p1} + G_{p2} + G_{p3} + j\omega C_p + \frac{1}{r_{p4} + r_{p5} + j\omega(L_o + L_p)} \tag{5.26}$$

where G_{p1}, G_{p2}, r_{p4}, r_{p5}, L_p and L_o are still given by Eqns. 3.71, 3.72, 3.81, 3.82, 3.78 and 3.79, respectively.

Now

$$G_{p3} = \frac{\omega^2}{A_0^2\omega_0^2 R}\left\{2 + \frac{8R_0}{R} + \frac{2R}{R_I(2+A_0\omega_0 RC)} - \frac{2R_0}{R(2+A_0\omega_0 RC)} - A_0\omega_0 RC_c\left(2 + \frac{3R_0}{R}\right)\right\} \tag{5.27}$$

and

$$C_p = \frac{1}{A_0\omega_0 R}\left(2 + \frac{R_0}{R} - A_0\omega_0 RC_c\right) \tag{5.28}$$

The new model for the gyrator circuit is still given by Fig. 3.9 except that the values for G_{p3} and C_p are now modified by C_c. As anticipated earlier, C_c reduces C_p, and if

$$C_c = \frac{2R + R_0}{A_0 \omega_0 R^2} \tag{5.29}$$

$C_p = 0$, that is, the parasitic capacitance is completely eliminated. The compensating capacitance C_c has another effect on the performance of the gyrator circuit. It introduces a negative term in G_{p3} which represents Q-factor enhancement, according to Eqn. 5.27. For a sufficiently large value of C_c, G_{p3} can actually become negative, and then Q_{HF} can also become negative. Negative Q-factors are sometimes undesirable, since they tend to cause peaking in the filter response.

5.3 Validity of the Compensated Model

The modified model has been used for the analysis of a compensated gyrator circuit. An exact computer-aided analysis has also been carried out in order to test

(a) the validity of the modified model,

(b) the validity of the compensation technique.

The percentage inductance deviation, as defined by Eqn. 3.83, and the Q-factor have been computed for a range of frequencies. The specifications of amplifier type ML748C (Microsystems International Ltd.) given in Table 5.1 were used for the analysis. The gyration resistance R and load capacitance C were assumed to be 2kΩ and 22nF, respectively.

The Q-factor for the load capacitor was assumed constant and equal to 3000. The results for various values of C_c in the range 0 - 360pF are illustrated in Figs. 5.3a and 5.3b where close agreement is evident between model-analysis and exact-analysis curves. The validity of the modified model is thus confirmed.

TABLE 5.1

Parameter	ML748C	μA741	Units
A_0	150	200	k
ω_0	18.8	37.6	rad./Sec.
R_0	75	75	Ω
R_I	2	2	MΩ
R_p	500	500	MΩ
R_N	500	500	MΩ

Fig. 5.3a illustrates the influence of C_p on the effective inductance. As may be expected from Eqn. 5.18, the high-frequency inductance deviation tends to increase rapidly with frequency and thus the useful bandwidth of the gyrator circuit is limited. As C_c is increased, C_p is reduced according to Eqn. 5.28 and, therefore, the high-frequency inductance deviation is reduced. As a consequence, the useful gyrator bandwidth is increased. Fig. 5.3b shows that the low-frequency Q-factor is independent of C_p, as can be expected from Eqn. 5.11.

The high-frequency Q-factor is positive for small values of C_c, but as C_c is increased, Q-factor enhancement is introduced and eventually the

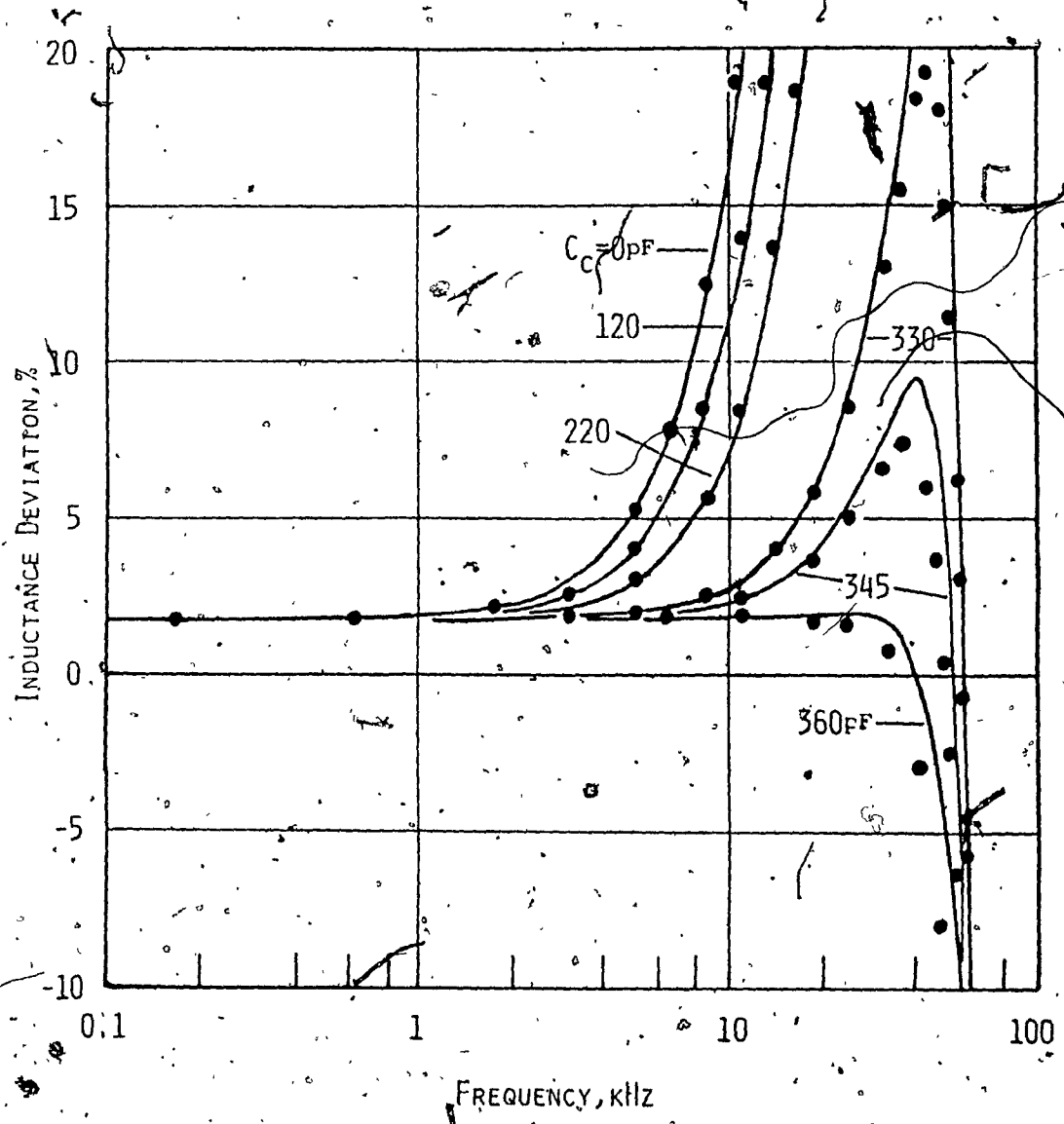

FIG. 5.3A VARIATION OF INDUCTANCE DEVIATION WITH FREQUENCY FOR VARIOUS COMPENSATING CAPACITANCES (AMPLIFIER TYPE ML748C, R = 2KΩ, L_0 = .88MH).
EXACT ANALYSIS ————————
MODEL ANALYSIS • • • •

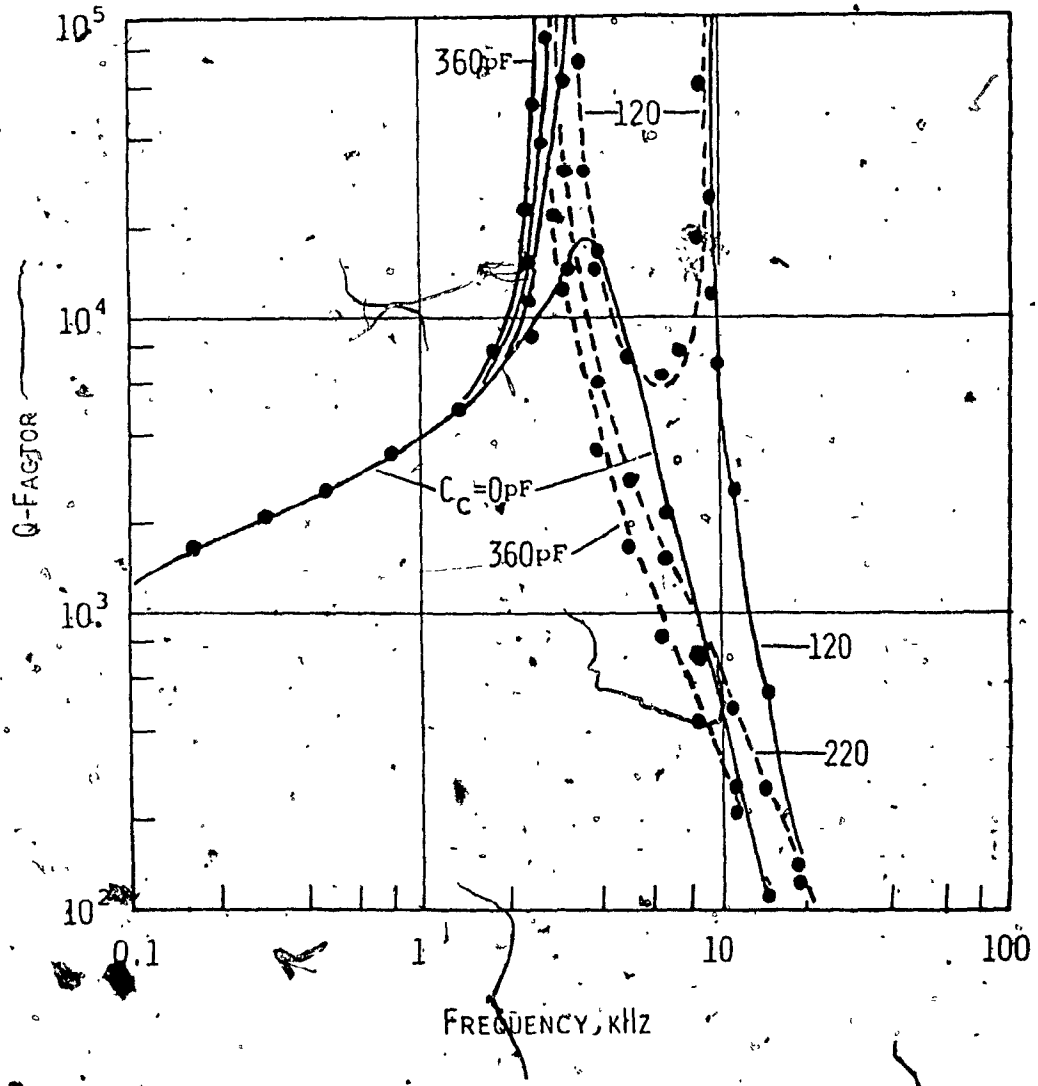

FIG. 5.5B VARIATION OF Q-FACTOR WITH FREQUENCY FOR VARIOUS COMPENSATING CAPACITANCES (AMPLIFIER TYPE ML748C, R = 2kΩ, L_0 = 88mH).
EXACT ANALYSIS ——————
MODEL ANALYSIS • • • •

Q-factor becomes negative, as anticipated earlier.

5.4 Experimental Verification of the Compensated Model

In order to test the feasibility of the proposed compensation technique experimentally, a gyrator circuit was built using ML748C type amplifiers. The gyration resistance and load capacitance used were 2kΩ and 22nF (L_o = 88mH), respectively, and the external amplifier compensating capacitance was 30pF. The effective inductance and Q-factor were measured, maintaining a constant voltage of 0.3Vrms across the inductance and using a dc supply voltage of ±15V. The measured responses are shown in Figs. 5.4a and 5.4b. Some differences are evident between experimental and theoretical responses which are mainly due to the large tolerances on the amplifier parameters. In general, however, the predicted pattern is maintained.

The effective inductance with C_c = 0 and with C_c = 330pF remains constant to within ±1% over the frequency range 0-2kHz and 0-10.3kHz, respectively. Therefore, the compensation technique introduces a five-fold increase in the useful bandwidth of the gyrator circuit.

The tolerance and temperature coefficient of C_p, like those of L_p, can be large, since C_p is inversely proportional to the gain-bandwidth product of the amplifiers. Consequently, exact compensation of C_p is difficult to achieve and maintain in practice. However, even if only 80-90% of C_p is cancelled, or even if C_p is over-compensated by 10-20%, the resulting increase in the gyrator bandwidth may be adequate for many applications. Precise compensation can be achieved by trimming C_c for each gyrator circuit individually and by choosing the temperature coefficient of C_c to be equal and opposite to that of $A_0\omega_0R_0$.

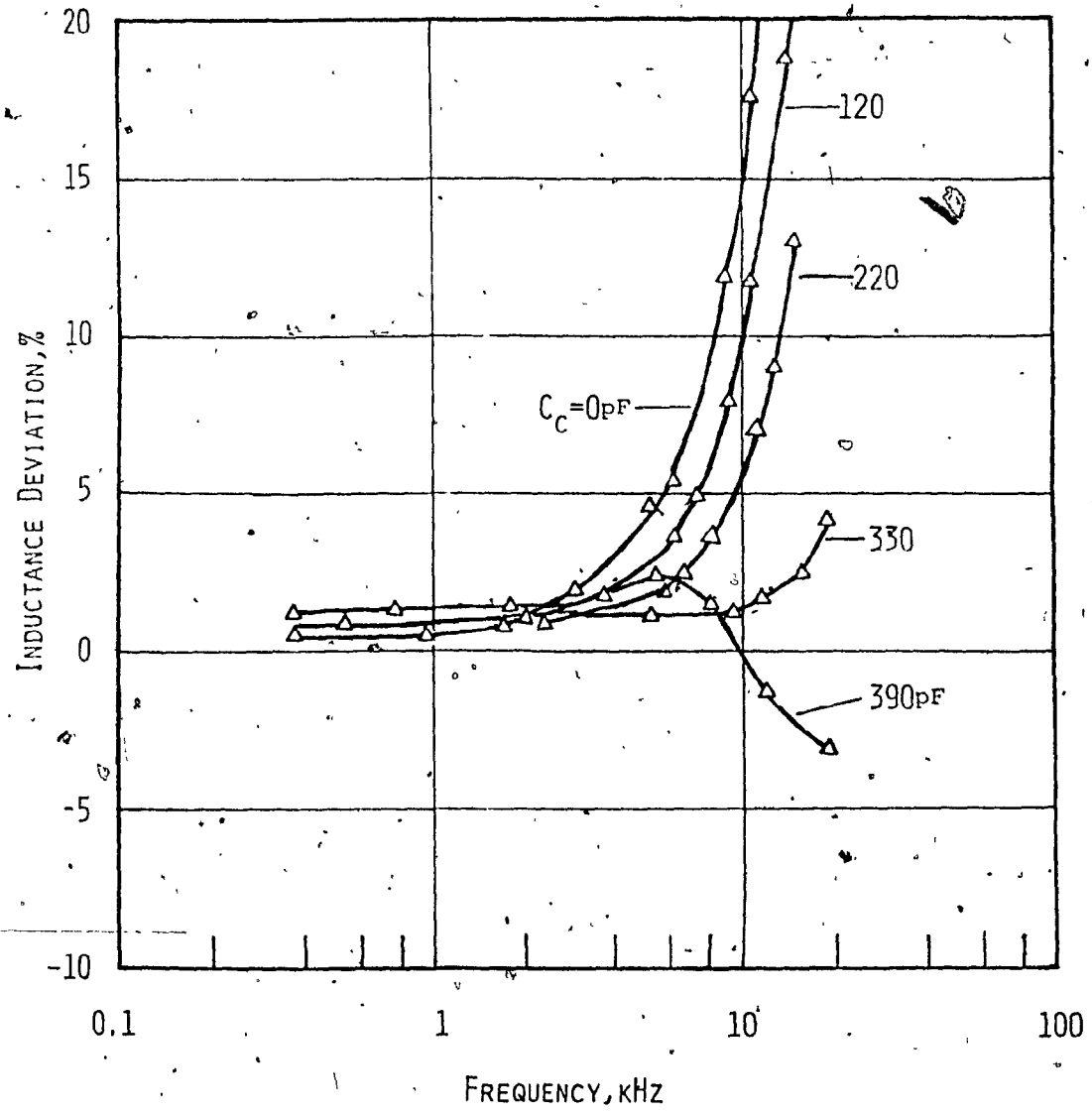

FIG. 5.4A. MEASURED VARIATION OF INDUCTANCE DEVIATION WITH FREQUENCY FOR VARIOUS COMPENSATING CAPACITANCES (AMPLIFIER TYPE ML748C, R = 2kΩ, L_0 = 88mH, V_I = 0.3V, V_S = ±15V).

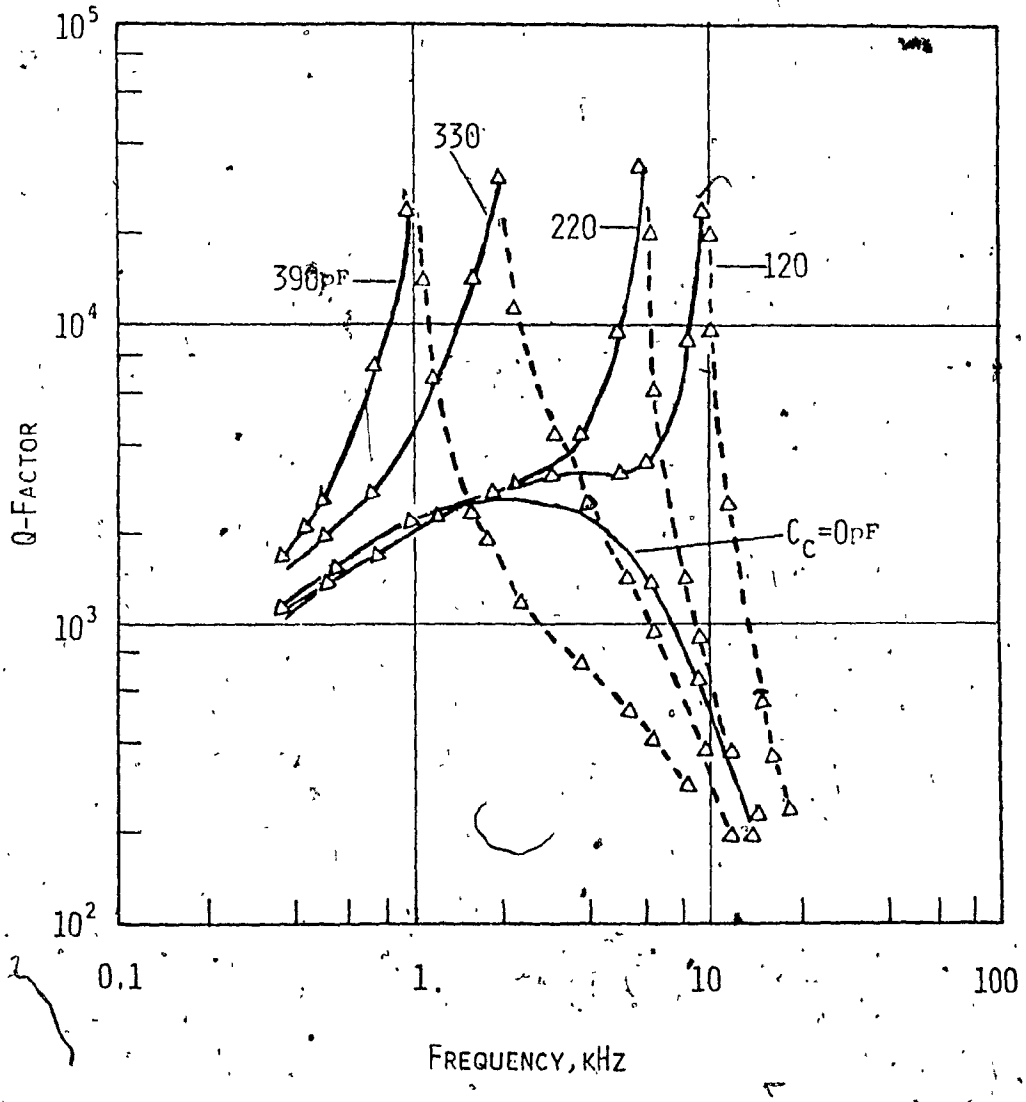

FIG. 5.4B MEASURED VARIATION OF Q-FACTOR WITH FREQUENCY FOR VARIOUS COMPENSATING CAPACITANCES (AMPLIFIER TYPE ML748C, R = 2kΩ, L_0 = 88mH, V_I = 0.3V, V_S = ±15V).

CHAPTER 6

DESIGN OF GYRATOR-C CHANNEL BANDPASS FILTER

Frequency division multiplexing relies on the selection of one sideband of an amplitude modulated signal by analog filtering. By successive modulation and filtering a large number of voice channels are "stacked" for transmission over a single communication link. A typical method of obtaining the basic 12-channel group band is shown in Fig. 6.1 where two stages of modulation are used. The 12-channel group in the range 60-108kHz is internationally standardized.

The two step modulation method of Fig. 6.1 has been successfully implemented using LC predistorted filters [76] in the MA-5A multiplex system which is currently in production. This chapter deals with the design of the most critical filter in the system, which is the 20-24kHz channel bandpass filter, using gyrators to replace inductors [81]. The modelling considerations of chapter 3 and the compensation technique of chapter 5 have been used in the design.

6.1 Design

The filter specifications require a bandpass ripple of ± .3dB over the frequency range of 20.6kHz to 22.4kHz with a controlled response from 20.3kHz to 23.9kHz. The prototype RLC filter employed is described by Valihora and Lim in [77]. The schematic and element values for this filter are given in Fig. 6.2 and Table 6.1, respectively.

The filter was first analyzed assuming ideal inductors and lossy capacitors. The variation in the loss of the capacitors with frequency

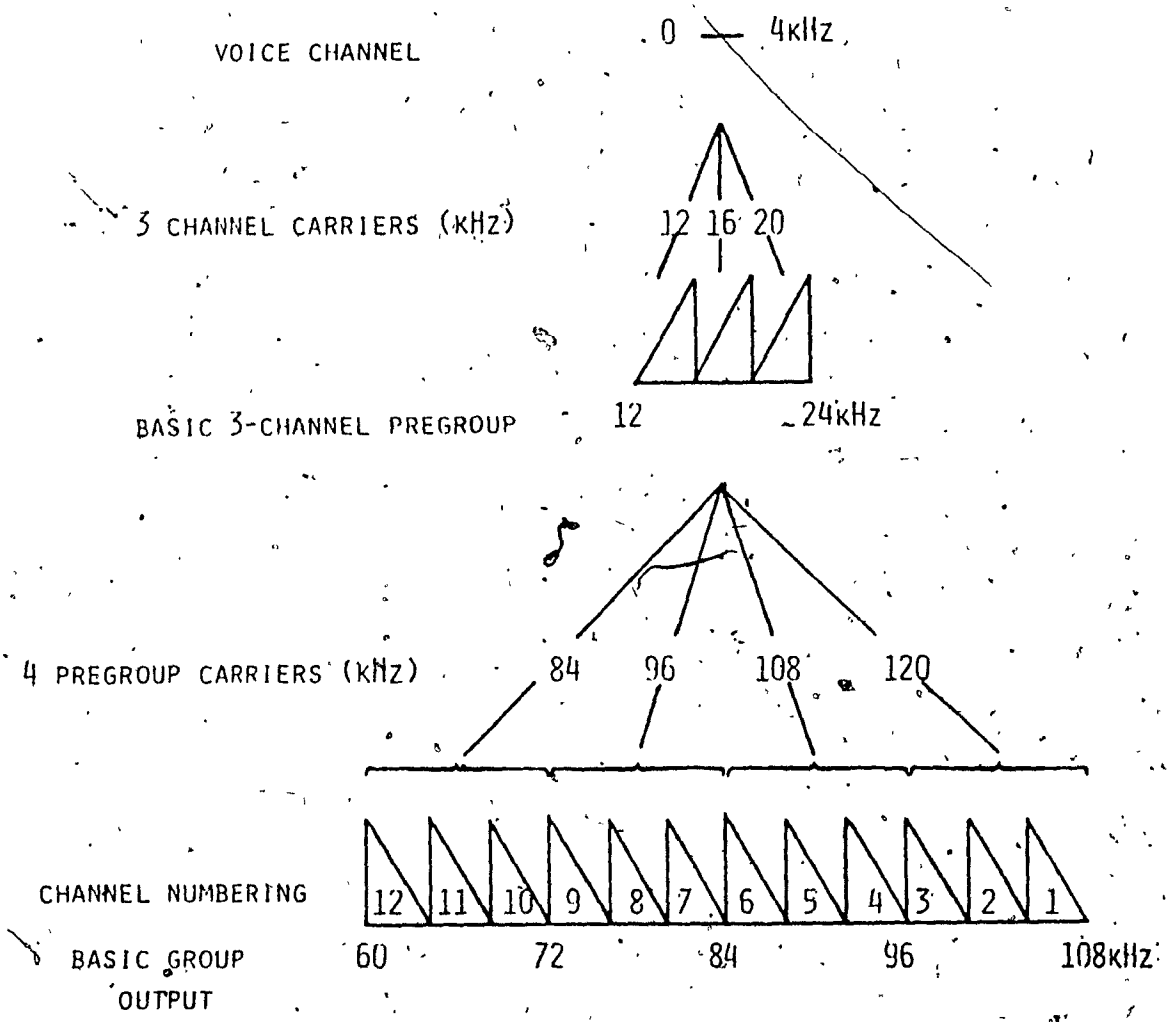

FIG. 6.1 A MULTIPLEXING SCHEME

THE CHANNEL BANK TRANSLATES TWELVE 0 TO 4kHz VOICE CHANNELS THROUGH TWO STAGES OF MULTIPLEXING TO THE 60 TO 180kHz GROUP FREQUENCY BAND.

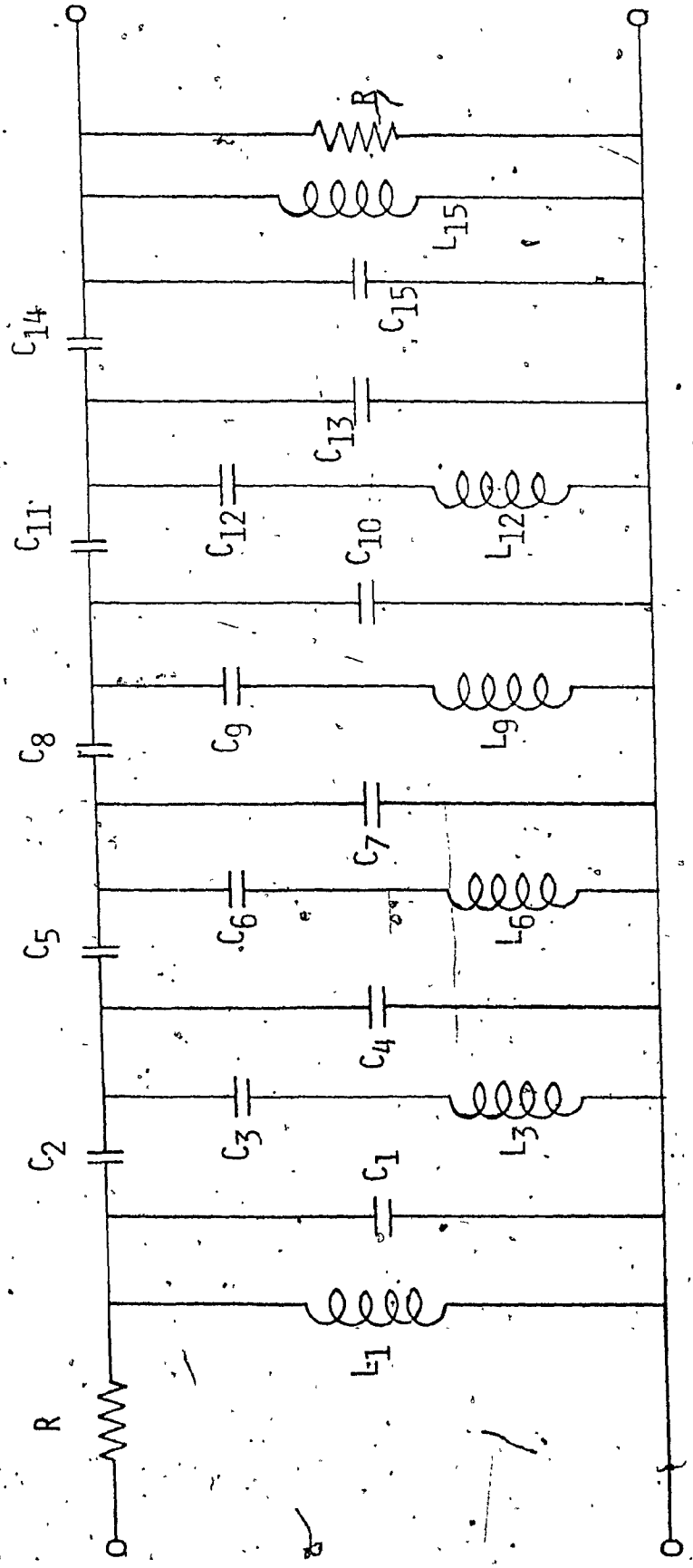

FIG. 6.2 PROTOTYPE CHANNEL BANDPASS FILTER

TABLE 6.1

n	L_n, mH	C_n, nF
1	6.9417	6.6464
2	-	1.3293
3	50.0	1.6355
4	-	0.7467
5	-	1.7152
6	50.0	1.4033
7	-	1.9090
8	-	3.5273
9	50.0	1.3378
10	-	0.1105
11	-	8.1488
12	50.0	1.2922
13	-	9.0199
14	-	4.5935
15	6.9417	4.2480

were also taken into account. The parallel loss resistance of each load capacitor was computed as $R = Q/\omega C$. The response obtained is shown as curve A in Figs. 6.3 - 6.5.

Each inductor was then simulated using gyrator circuit of Fig. 3.5. A gyration resistance of 2kΩ was used throughout. The gyrator load capacitors were obtained by assuming that the required inductances are equal to the nominal inductances R^2C. Each gyrator circuit was then replaced by the model of Fig. 3.9. The resulting filter was then analyzed for μA741 operational amplifiers and lossy capacitors (Q=2000). The frequency response obtained is illustrated as curve B in Fig. 6.3. Fig. 6.3 shows that the gyrator imperfections introduce a significant lateral shift in the response of the filter. If no corrections were possible for the gyrator imperfections, amplifier μA741 would clearly be unsuitable for this application because of its relatively low gain-bandwidth product.

In order to eliminate errors due to the parasitic inductance L_p, the gyrator-C filter was redesigned using L_p as part of each filter inductance. The gyrator load capacitors were calculated as follows:

$$\text{Required inductance} = \text{Nominal inductance} + L_p$$

$$= L_o + L_p$$

$$= R^2 C + L_p$$

or

$$C = \frac{(\text{Required inductance} - L_p)}{R^2} \qquad (6.1)$$

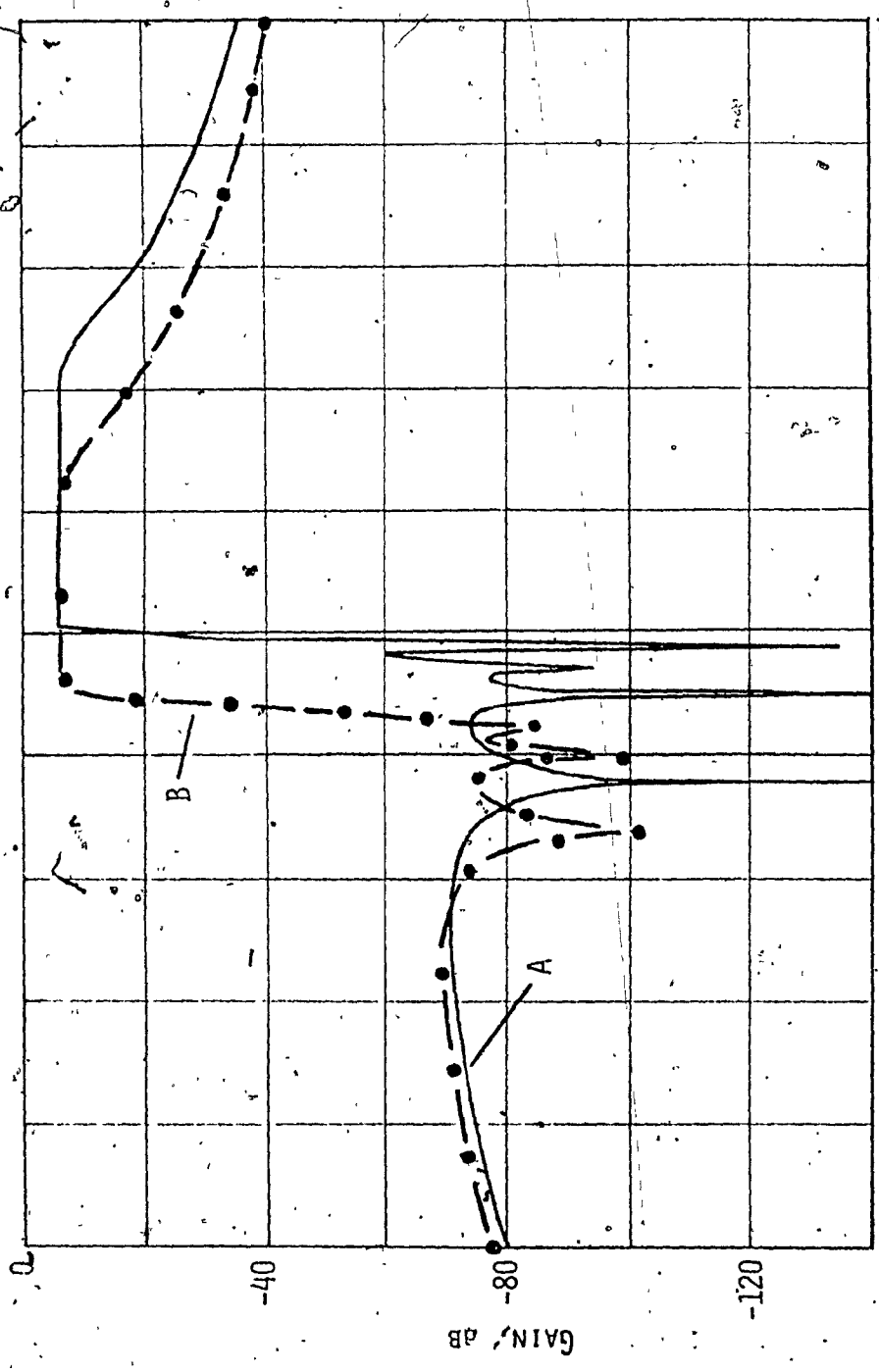

FIG. 6.3: COMPUTED FREQUENCY RESPONSES OF GYRATOR-C FILTER WITH NO CORRECTIONS
—CURVE A: FILTER RESPONSE WITH IDEAL INDUCTORS
CURVE B: FILTER RESPONSE WITH NONIDEAL GYRATORS

where R is the gyration resistance and C is the gyrator load capacitor. L_p was obtained from Eqn. 3.79, using μA741 operational amplifier specifications. The response obtained, illustrated as curve B in Fig. 6.4, shows that lateral shift is eliminated for frequencies up to 14kHz.

The lateral shift in the filter response for frequencies above 14kHz is due to C_p. The compensation technique developed in chapter 5 was used to eliminate C_p. The gyrator compensating capacitances were calculated using Eqn. 5.29. The channel bandpass filter was analyzed using the modified model for the compensated gyrator circuits. The frequency response obtained, illustrated as curve B in Fig. 6.5, shows that the lateral shift is completely eliminated. However, peaking is introduced near the cut-off frequency of the filter caused by negative Q-factors of the simulated inductances.

The high-frequency Q-factor of the simulated inductance can be made large, and positive by using a shunt resistance R_{Sh} at the input of the compensated gyrator circuit. The frequency response for four values of shunt resistance is shown in Fig. 6.6. Peaking can be eliminated by using a shunt resistance $R_{Sh} = 3.8M\Omega$ at the input of each gyrator circuit.

The procedure for the design of gyrator-C filters can be summarized as follows:

(i) Design an LC filter satisfying the required specifications with all grounded inductors.

(ii) For each grounded inductance desigh a gyrator circuit after predistorting the nominal inductance by L_p.

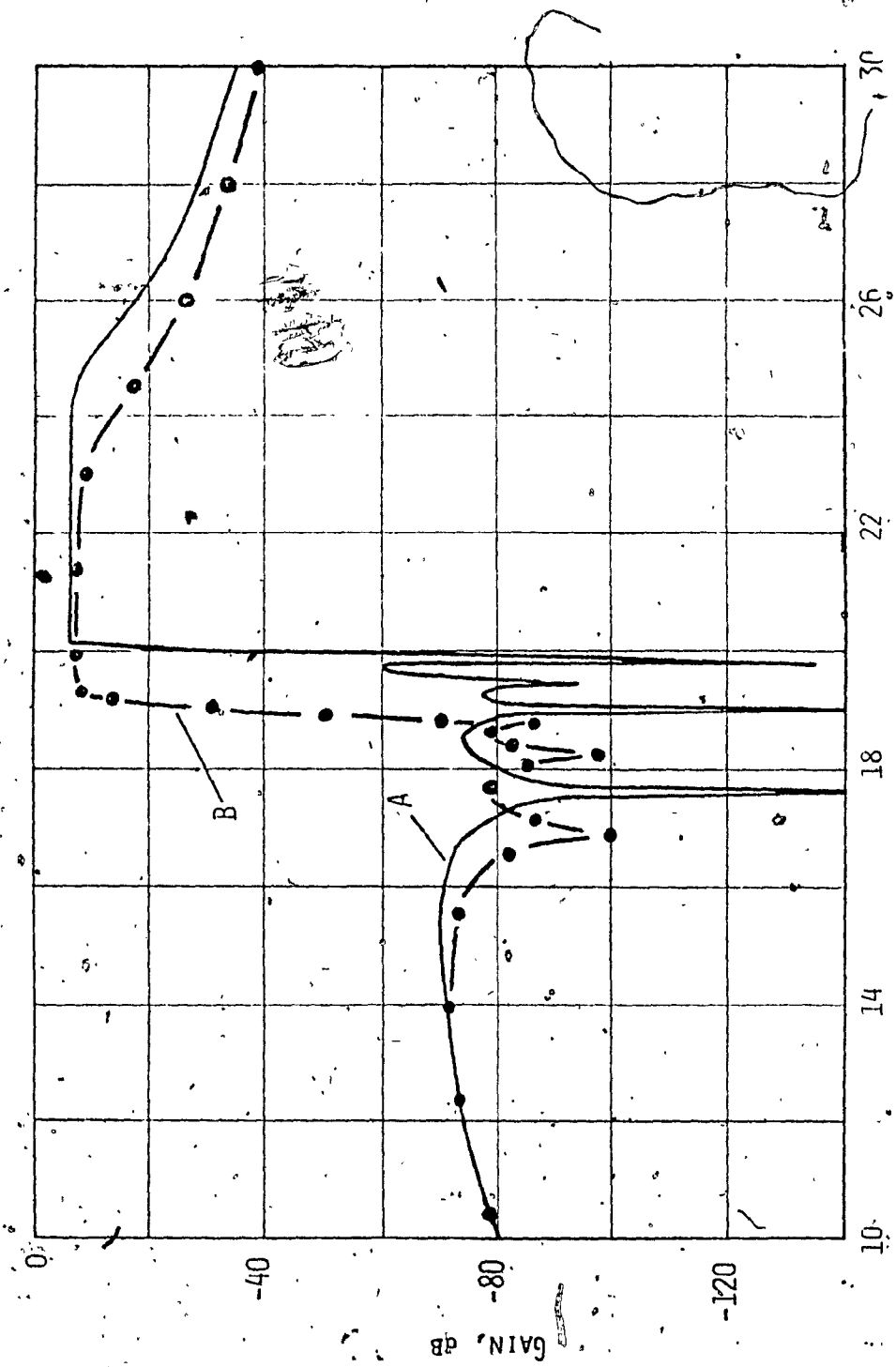

FIG. 6.4 COMPUTED FREQUENCY RESPONSE OF GYRATOR-C FILTER WITH CORRECTIONS FOR L_p
CURVE A: FILTER RESPONSE WITH IDEAL INDUCTORS
CURVE B: FILTER RESPONSE WITH NONIDEAL GYRATORS

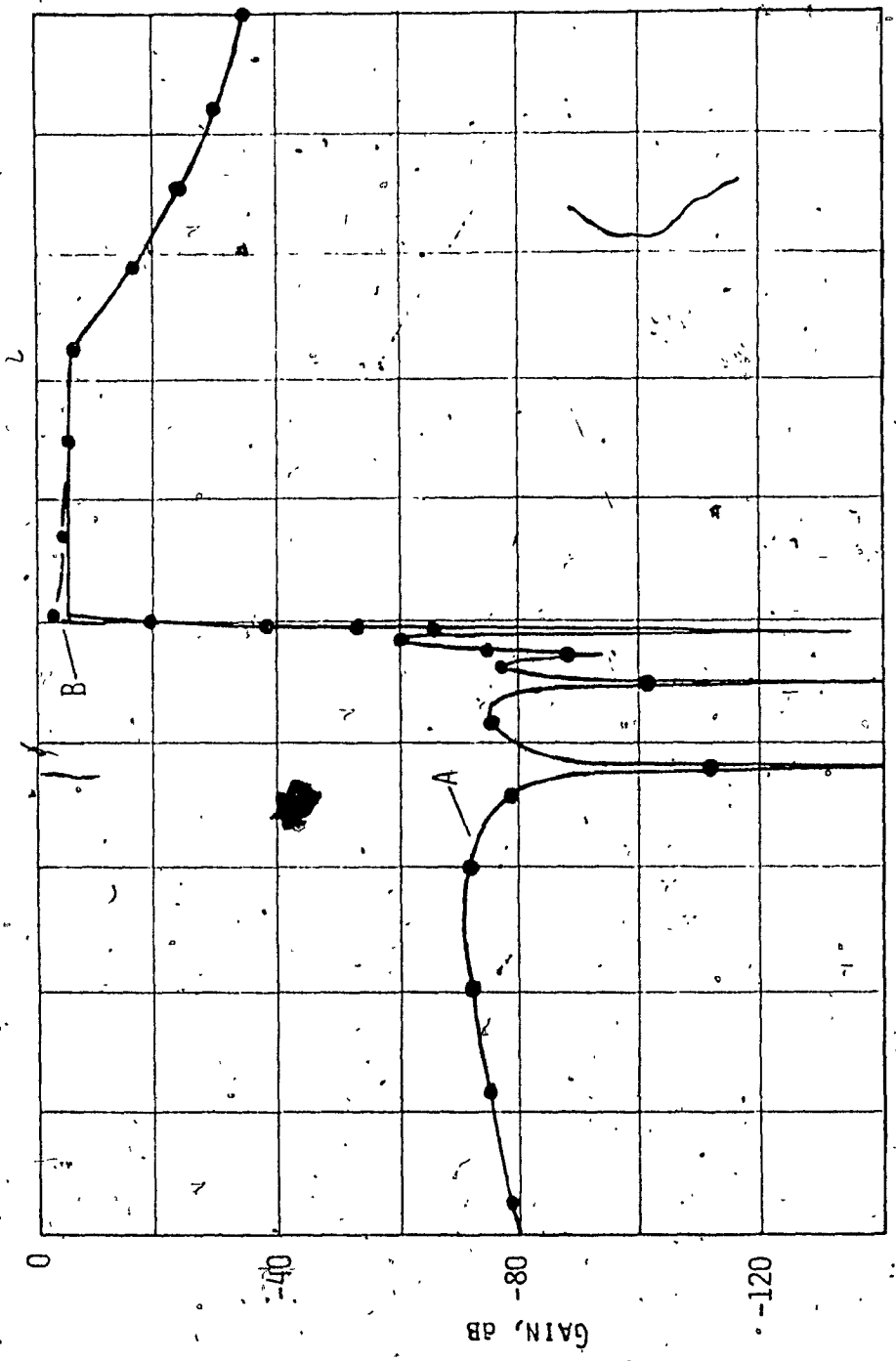

FIG. 6.5 COMPUTED FREQUENCY RESPONSE OF GYRATOR-C FILTER WITH CORRECTIONS FOR L_p AND C_p
CURVE A: FILTER RESPONSE WITH IDEAL INDUCTORS
CURVE B: FILTER RESPONSE WITH NONIDEAL GYRATORS

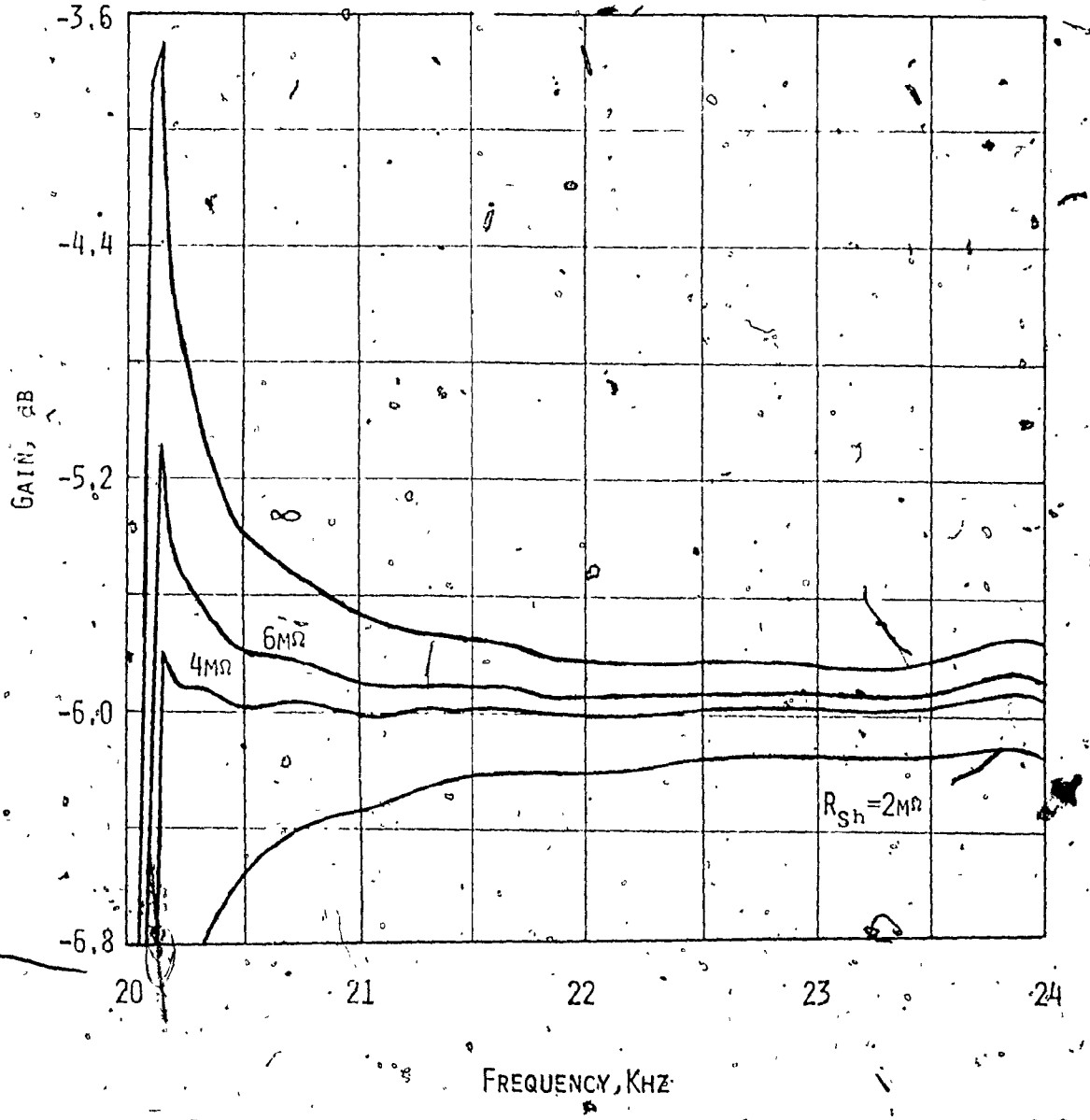

FIG. 6.6 COMPUTED PASSBAND RESPONSES FOR R_{Sh} = 2, 4, 6 AND ∞ MΩ.

(iii) Calculate the gyrator compensating capacitance.

(iv) Choose an input shunt resistance R_{Sh} for the gyrator circuits to avoid peaking in the filter response. R_{Sh} can be obtained in two ways. (a) The effective negative input resistance of the compensated gyrator circuit can be calculated at the cut-off frequency of the filter by using the modified model. R_{Sh} can then be taken as the magnitude of the calculated negative input resistance. (b) The filter can be analyzed using different values for R_{Sh}. The optimum R_{Sh} can then be choosen by examining the frequency responses of the filter.

6.2 Experimental Results

The low cost, commercial grade operational amplifier μA741 was selected to construct the channel bandpass filter. A gyration resistance 2kΩ was used throughout. By using the data sheet specifications for the amplifiers, the parasitic inductance L_p was calculated as 0.561mH. By using Eqn. 6.1 the gyrator load capacitances were obtained as 1.595nF and 12.359nF for the required inductances of 6.9417mH and 30.0mH, respectively.

The channel bandpass filter of Fig. 6.2 was constructed using metal-film resistors (tolerance ≤ 1% and temperature coefficient +100ppm/°C) and polystyrene capacitors (tolerance ≤ 1% and temperature coefficient -100±50ppm/°C).

First the simulated inductances were set to the required filter inductances at 1kHz by adjusting the gyrator load capacitances. Then

each simulated inductance was adjusted by varying C_c so as to obtain a constant inductance in the range 20-24kHz. Shunt resistances of 2.9MΩ were then used at the inputs of the gyrator circuits to reduce peaking in the filter response. The filter was tested with an input signal level of 0.4V. The experimental response for an ambient temperature of 20°C and a dc supply voltage of ±15V, illustrated as curve B in Figs. 6.7 and 6.8, agrees with the theoretical response.

The influence of dc supply voltage variations on the performance of the filter is illustrated in Fig. 6.7. A change in the supply voltage introduces lateral shift in the response of the filter which is mainly due to variations in C_p produced by variations in $A_0\omega_0$. Note that a similar shift would result even if the gyrator circuits were uncompensated. The improvement brought about by the compensation is that any shift in the response occurs about the nominal response of the filter.

The influence of ambient temperature variations is illustrated in Fig. 6.8. Again, lateral shift is introduced which, in this case, is due to the combined effects of variations in $A_0\omega_0$ and in the RC products.

The stability of the filter can be improved by optimising the gyration resistances as shown in section 6.3. Further improvements can be brought about by employing filter and gyrator load capacitors with temperature coefficient equal and opposite to that of gyrator resistors and by employing compensating capacitors with temperature coefficient equal and opposite to that of $A_0\omega_0 R$. Since the temperature coefficient of $A_0\omega_0$ is usually large and negative (about - 200ppm/°C for the μA741), the temperature coefficient of the compensating capacitors should be large and positive.

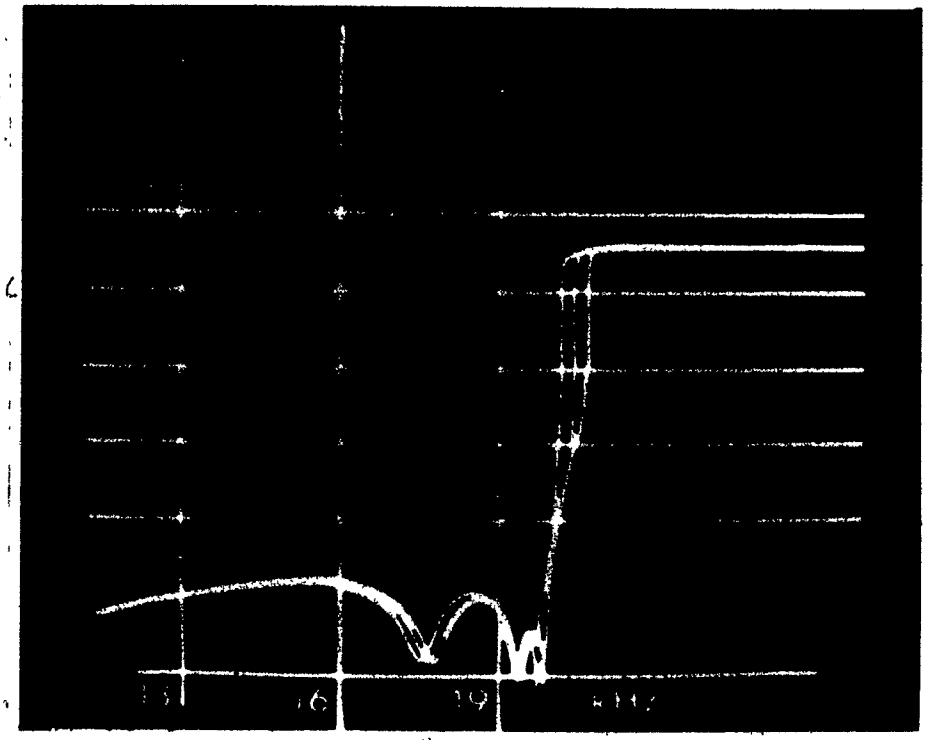

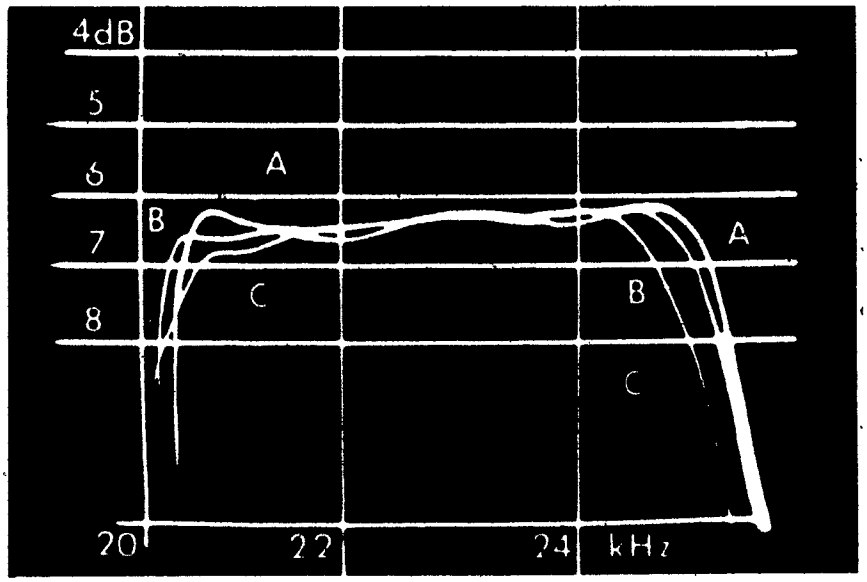

FIG. 6.7 EXPERIMENTAL FREQUENCY RESPONSE FOR VARIOUS DC SUPPLY VOLTAGES
CURVE A: ±11V;
CURVE B: ±15V;
CURVE C: ±17V.

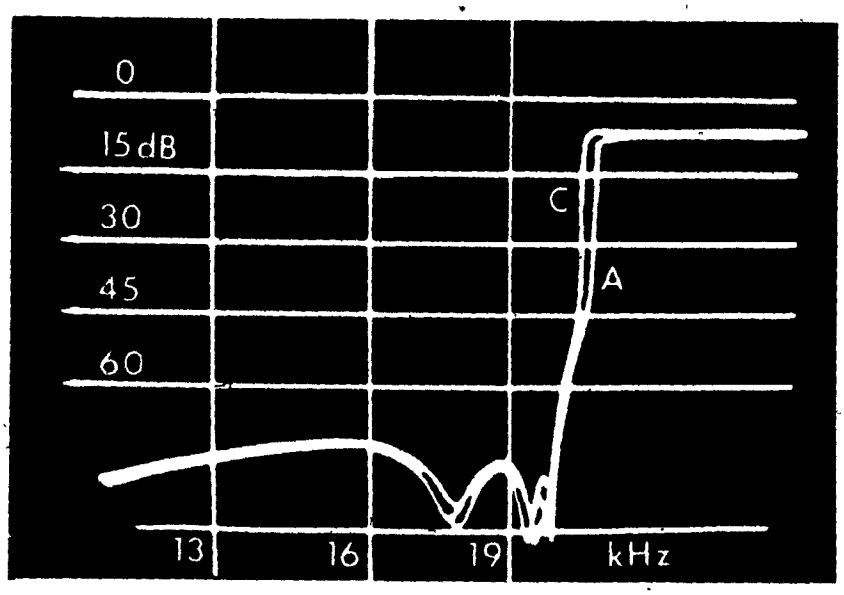

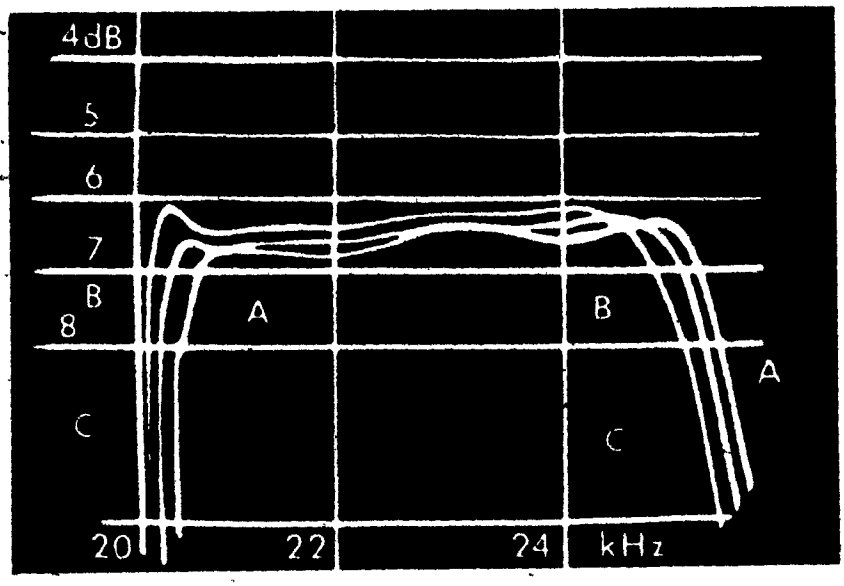

FIG. 6.8 EXPERIMENTAL FREQUENCY RESPONSES FOR VARIOUS AMBIENT TEMPERATURES.
CURVE A: 0°C;
CURVE B: 20°C;
CURVE C: 70°C.

6.3 Optimum Gyration Resistance

The effective input inductance of a compensated gyrator for the frequency range $0 \leq \omega << B\ (= A_0\omega_0)$ can be readily obtained as

$$L = \frac{\omega^2(L_o + L_p)^2 + (r_{p4} + r_{p5})^2}{\omega^2\left[(L_o + L_p) - C_p\left\{(r_{p4} + r_{p5})^2 + \omega^2(L_o + L_p)^2\right\}\right]} \tag{6.2}$$

by using the modified gyrator model. In practice,

$$\omega^2(L_o + L_p)^2 >> (r_{p4} + r_{p5})^2 \tag{6.3}$$

and thus

$$L \simeq \frac{(L_o + L_p)}{1 - \omega^2 C_p(L_o + L_p)} \tag{6.4}$$

Also, $R >> R_0$ and hence Eqns. 3.79 and 5.28 give

$$L_p \simeq \frac{2R}{B} \tag{6.5}$$

$$C_p \simeq \frac{2}{BR} = C_c \tag{6.6}$$

In effect, both L_p and C_p are small quantities and thus Eqn. 6.4 can be simplified as

$$L \simeq L_o + L_p + \omega^2 C_p (L_o + L_p)^2 \tag{6.7}$$

$$\approx L_o + L_p + \omega^2 C_p L_o^2 \tag{6.8}$$

From Eqns. 6.5 - 6.8 we can now write

$$L = L_o (1-\omega^2 L_o C_c) + \frac{2}{B}\left(R + \frac{\omega^2 L_o^2}{R}\right) \tag{6.9}$$

and, consequently

$$\frac{\partial L}{\partial B} = -\frac{2}{B^2}\left(R + \frac{\omega^2 L_o^2}{R}\right) \tag{6.10}$$

For a given frequency $\omega=\omega_c$ and constant L_o, $\partial L/\partial B$ is minimum when

$$R=\omega_c L_o \tag{6.11}$$

that is, the rate of change in the effective inductance with respect to variations in the gain-bandwidth-product can be minimized by choosing the gyration resistance to be equal to the reactance of L_o at ω_c. This value of R is also optimum in the case of an uncompensated gyrator circuit, as was shown by Valihora and Lim in [77]. Since, in practice, variations in L are most objectionable for frequencies in the transition region of a filter, ω_c should be chosen to be the cut-off frequency of the filter.

With $C_p \simeq 0$, Eqns. 6.5, 6.8 and 6.11 give

$$L \simeq \frac{R}{\omega_c} + \frac{2R}{B} \tag{6.12}$$

and hence the optimum value of R is obtained as

$$R \simeq \frac{\omega_c L}{1 + \frac{\omega_c L}{B}} \tag{6.13}$$

The optimum gyration resistance for the filter of Fig. 6.2 can be calculated as 844Ω for L_1 and L_{15} and 6080Ω for L_3 - L_{12}.

CHAPTER 7

CONCLUSIONS AND SUGGESTIONS FOR FURTHER WORK

A new approach for the analysis and modelling of operational amplifier gyrator circuits has been proposed. Two gyrator circuits were considered (Gyrators GA and GB). For the sake of simplicity, the amplifiers were taken to be identical. Assuming a typical range of amplifier specifications, a model was derived for each gyrator circuit comprising resistances, capacitances and inductances. The validity of the derived models was established using an exact computer-aided analysis. The simplicity of the models by comparison with an exact equivalent circuit leads to a large saving in the cost of computation. The models have been found to give gyrator frequency responses which are in close agreement with those obtained by an experiment.

The derived models indicate clearly the influence of each amplifier imperfection on the performance of the gyrator circuits. It has been established that the most significant parameter of the amplifier is the gain-bandwidth product. A noninfinite gain-bandwidth product of the amplifiers introduces a parasitic inductance L_p and a parasitic capacitance C_p. Effectively the useful bandwidth of the gyrator circuit and the stability of the simulated inductance are closely related to the gain-bandwidth product of the amplifiers. The output resistance of the amplifiers tends to introduce enhancement and sometimes the Q-factor of the simulated inductance may become negative. Nevertheless, for the gyrator GA, enhancement can be easily eliminated or increased by using an additional resistor. A small value of gyration resistance leads to a very stable inductance but at the same time a large load

capacitance is required to simulate a given inductance. The choice of gyration resistance also influences the useful bandwidth and the Q-factor of the simulated inductance. A computer analysis has shown that the gyration models can be used for the analysis of gyrator circuits employing nonidentical amplifiers with unequal dc gains and cut-off frequencies.

The influence of temperature and dc supply voltage variations on the gyrator circuit have been examined. The choice of gyration resistance was shown to influence the sensitivity of the simulated inductance to temperature and dc supply voltage variations. A low gyration resistance tends to give a more stable simulated inductance.

A theoretical study has shown that the voltage-handling capabilities of gyrator circuits tends to be reduced significantly at low frequencies. An increase in the simulated inductance or a decrease in the gyration resistance tends to increase the voltage-handling capacity. These aspects were also confirmed by experimental results.

A comparison of the two gyration circuits has shown that the enhancement in gyrator GA is less pronounced; also the voltage handling capacity of the gyrator GA is larger. On the other hand, gyrator GB can be used for the design of filter sections with low output impedances.

The derived model was used to study the low and high frequency operation of the gyrator GA. The parasitic inductance L_p tends to degrade the stability of the simulated inductance at low frequencies. The parasitic capacitance C_p increases the effective inductance by an amount which increases with frequency. Consequently, C_p limits the useful bandwidth of the gyrator circuit.

A compensation technique has been developed whereby the useful bandwidth of the gyrator can be increased. The compensation technique was verified first by computer-aided analysis and then by experiment. It was shown that a significant increase in the useful gyrator bandwidth can be achieved by using an inexpensive capacitor.

The compensation technique has been applied successfully in the design of a critical twelfth order channel bandpass filter. Peaking in the filter response caused by negative Q-factors can be eliminated using a shunt resistance at the input of each gyrator circuit. A design procedure was given for gyrator-C filters which can be used for filters with grounded inductors.

The compensated gyrator-C filter was constructed using cheap commercial grade amplifiers. Despite the relatively low gain-bandwidth product of the amplifiers the nominal frequency response was achieved. Dc voltage and ambient temperature variations tend to introduce lateral shift in the response of the filter. This however can be reduced by optimizing the gyration resistances and by choosing the temperature coefficients of the elements employed. In effect it was shown that highly selective gyrator-C filters can be designed using low cost commercial operational amplifiers.

Since the most significant parameter of the amplifier is the gain-bandwidth product, the author, therefore, feels that it is worthwhile to investigate an optimum compensation for operational amplifiers (such as ML748) to maximize the gyrator bandwidth.

As shown in Chapter 5 useful bandwidth of the simulated inductance depends on C_p. The tolerance and temperature coefficient of C_p can be

large, since C_p is inversely proportional to the gain-bandwidth product of the amplifiers. It is also desirable, in the author's opinion, to investigate the high frequency stability of the simulated inductance to temperature and supply voltage variations.

The noise produced by the filter depends on the noise present in the gyrator. The noise and dynamic range properties of the gyrator circuits should also be studied. It is very useful to develop design procedure to optimize the voltage handling capacity of gyrator circuits with nonideal amplifiers taking into account the internal loading on the amplifiers.

Floating inductances can be designed using the techniques proposed by Holt and Taylor [12] or Gorski-Popiel [50] where identical gyrators are required. The method of modelling should be extended to these circuits.

Also in view of the suitability of FDNR elements for the design of highly selective low-pass filters, modelling of these elements should also be considered.

In conclusion, the author hopes that in view of the rapid advances, and considerable interest in hybrid integrated circuit technology, and the need for inexpensive gyrator-C filters in many areas, such as data communications, the results obtained in this thesis would advance the state-of-the-art in the design of highly selective filters.

REFERENCES

1. E.A. Guillemin, Synthesis of Passive Networks, Wiley, New York, 1957.

2. D.F. Tuttle, Jr., Network Synthesis, vol.1, Wiley, New York, 1958.

3. L. Weinberg, Network Analysis and Synthesis, McGraw-Hill, New York, 1962.

4. H.H. Scott, "A New Type of Selective Circuit and Some Applications," Proc. IRE, vol.26, pp. 226-235, Feb. 1938.

5. A.E. Lessor, L.I. Maissel, and R.E. Thein, "Thin-film Circuit Technology: Part I - Thin Film RC Networks," IEEE Spectrum, vol.1 pp. 72-80, April 1964.

6. R.W. Newcomb, Active Integrated Circuit Synthesis, Prentice-Hall, Englewood Cliffs, New Jersey, 1968.

7. S.K. Mitra, Analysis and Synthesis of Linear Active Networks, Wiley, New York, 1969.

8. W.E. Newell, "The Frustrating Problem of Inductors in Integrated Circuits," Electronics, vol.37, pp. 50-52, March 13, 1964.

9. Burr-Brown: 1975 Catalog.

10. B.D.H. Tellegen, "The Gyrator, a new Electric Element", Phillips Res. Rept., vol.3, no.2, pp. 81-101, 1948.

11. L.T. Bruton, "Network Transfer Functions using the Concept of Frequency-Dependent Negative Resistances," IEEE Trans. Circuit Theory, vol.CT-16, pp. 406-408, Aug. 1969.

12. A.G.J. Holt and J. Taylor, "Method of Replacing Ungrounded Inductors by Grounded Gyrators," Electron. Letters, vol.1, pp. 105, June 1965.

13. W.F. Lovering, "Analog Simulation of Transfer Functions," Proc. IEEE, vol.53, pp. 306, 1965.

14. B.B. Bhattacharya and M.N.S. Swamy, "Active Synthesis using Operational Amplifiers," Int. J. Electron., vol.23, pp. 401-412, Nov. 1967.

15. S.K. Mitra, "Transfer Function Synthesis using a Single Operational Amplifier," Electron. Letters, vol.3, pp. 333-334, July 1967.

16. K.S. Rao and V.G.K. Murti, "Synthesis of Transfer Functions using Differential Input Amplifiers," Proc. 7th Annual Allerton Conf. Circuit and Systems Theory, pp. 782-791, Oct. 1969.

17. R.P. Sallen and E.L. Key, "A Practical Method of Designing RC Active Filters," IRE Trans. Circuit Theory, vol.CT-2, no.1, pp.74-85, March 1955.

18. A. Antoniou, "Synthesis of Active Filters with Optimum Sensitivity," Radio Electron. Eng., vol.36, pp. 135-147, Sept. 1968.

19. T.R. Narasimhan and V. Ramachandran, "Synthesis of Arbitrary Driving Point and Transfer Functions using Controlled Sources," Alta Freq., vol.37, pp. 1102-1103, Nov. 1968.

20. J.G. Linvill, "RC Active Filters," Proc. IRE, vol.42, pp. 555-564, March 1954.

21. T. Yanagisawa, "RC Active Networks using Current Inversion Type Negative Impedance Converters," IRE Trans. on Circuit Theory, vol.CT-4, pp. 140-144, Sept. 1957.

22. B.K. Kinariwala, "Synthesis of Active RC Networks," Bell Systems Tech. J., vol.38, pp. 1269-1316, Sept. 1959.

23. A. Antoniou, "New RC-Active Network Synthesis Procedures using Negative-Impedance Converter," Proc. Inst. Elect. Eng., vol.114, pp. 894-902, July 1967.

24. A. Antoniou, "Improved Negative-Impedance Converters and Related Synthesis Procedures," Ph.D. Thesis, University of London, England, May 1966.

25. A. Antoniou, "Novel RC-Active Network Synthesis using Generalized-Immittance Converters," IEEE Trans. Circuit Theory, vol.CT-17, pp. 212-217, May 1970.

26. L.T. Bruton, "Biquadratic Sections using Generalized Impedance Converters," The Radio and Electronic Engineer, vol.41, pp. 510-512, Nov. 1971.

27. L.T. Bruton, "Frequency Selectivity using Positive Impedance Converter-Type Networks," Proc. IEEE, vol.56, pp. 1378-1379, Aug. 1968.

28. B.B. Bhattacharya, W.B. Mikhael and A. Antoniou, "Design of RC-Active Networks using Generalized-Immittance Converters," Journal of the Franklin Institute, vol.297, No.1, Jan. 1974.

29. J.C. Giguere, B.B. Bhattacharyya and M.N.S. Swamy, "A class of Generalized Impedance Converters," Int. J. Electron., Vol.26, pp. 1-4, Jan. 1969.

30. I.M. Horowitz, "Optimization of Negative Impedance Conversion Methods of Active RC Synthesis," IRE Trans. on Circuit Theory, Vol. CT-6, pp. 296-303, Sept. 1959.

31. P.T. McVey, "Sensitivity in Some Simple RC-Active Networks," Proc. IEE (London), vol.112, pp. 1263-1269, July 1965.

32. H.J. Orchard, "Inductorless Filters," Electron. Letters, vol. 2, pp. 224-225, June 1966.

33. J. Woodward and R.W. Newcomb, "Sensitivity Improvement of Inductorless Filters," Electron. Letters, vol.2, pp. 349-350, Sept. 1966.

34. W.E. Newell, "Tuned Integrated Circuits - A State-of-the-Art Survey," Proc. IEEE, vol.52, pp. 1603-1608, Dec. 1964.

35. W.J. Kerwin, L.P. Huelsman, and R.W. Newcomb, "State Variable Synthesis for Insensitive Integrated Circuit Transfer Functions," IEEE J. Solid-State Circuits, vol.SC-2, pp. 87-92, Sept. 1967.

36. S.S. Hakin, "Synthesis of RC Active Filters with Prescribed Pole Sensitivity," Proc. IEE, vol.112, no.12, pp. 2235-2242, Dec. 1965.

37. R. Tarmy and M.S. Ghausi, "Very High-Q Insensitive Active RC Networks," IEEE Trans. Circuit Theory, vol.CT-17, pp. 358-366, Aug. 1970.

38. H.J. Orchard and D.F. Sheahan, "Inductorless Bandpass Filters," IEEE J. Solid-State Circuits, vol.SC-5, pp. 108-118, June 1970.

39. D.F. Sheahan, "Inductorless Filters," Tech. Rept. 6560-15, SEL-67-086, Stanford Electronics Lab., Stanford University, Calif., Sept. 1967.

40. A. Antoniou, "Realization of Gyrators using Operational Amplifiers and Their use in RC-Active Network Synthesis," Proc. Inst. Elec. Eng., vol.116, pp. 1838-1850, Nov. 1969.

41. R.H.S. Riordan, "Simulated Inductance using Differential Amplifiers," Electron. Letters, vol.3, pp. 50-51, Feb. 1967.

42. W.H. Holmes, S. Gruetzman and W.E. Heinlein, "High Quality Active C Filters using Gyrators," Int. Solid-State Circuits Conf. Dig., 1967.

43. G.K. Skwirzynski, Design Theory and Data for Electrical Filters, Van Nostrand, 1965.

44. White Electromagnetics, Inc., A Handbook on Electrical Filters, Maryland: WEI, 1963.

45. M.P. Beddoes and K.R. Morin, "Bibliography on Inductance Simulation using Gyrator Methods," IEEE Trans. Circuit Theory, vol.CT-14, pp. 107-111, March, 1967.

46. L. DePian, "Active Filters: Part 2 - Using the Gyrator," Electronics, vol.41, pp. 114-120, June 10, 1968.

47. T.N. Rao, P. Gary, and R.W. Newcomb, "Equivalent Inductance and Q of a Capacitor-Loaded Gyrator," IEEE J. Solid-State Circuits, vol.SC-2, pp. 32-33, March 1967.

48. C. Fromberg, "Gyrator for Simulating Inductance in Microelectronic Low Frequency Circuits," Electron. Eng., vol.40, pp. 12-15, Jan. 1968.

49. L.T. Bruton, "Worst-Case Sensitivities of Simulated-Inductance and FDNR Ladder Filters," Proc. of Nat. Inst. Conf. Sept. 1972.

50. J. Gorski-Popiel, "RC-Active Synthesis using Positive Immittance Converters," Electron. Letters, vol.3, pp. 381-382, Aug. 1967.

51. T.N. Rao, "Gyrator-Capacitor Filters," presented at NEREN, Boston, Mass., Nov. 7, 1969.

52. D.F. Sheahan and H.J. Orchard, "Bandpass Filter Realization using Gyrators," Electron. Letters, vol.3, pp. 40-42, Jan. 1967.

53. W.H. Holmes, S. Gruetzmann, and W.E. Heinlein, "High Quality Active C Filters using Gyrators," Int. Solid-State Circuits Conf. Dig., 1967.

54. W.H. Holmes, W.E. Heinlein, and S. Gruetzmann, "Sharp-Cutoff Low-Pass Filters using Floating Gyrators," IEEE J. Solid-State Circuits, vol.SC-4, pp. 38-50, Feb. 1969.

55. S.S. Hakim, "RC-Gyrator Low-Pass Filter," Proc. Inst. Elec. Eng., vol.113, pp. 1504-1506, Sept. 1966.

56. B.A. Shenoi, "Practical Realization of a Gyrator Circuit and RC Gyrator Filters," IEEE Trans. Circuit Theory, vol.CT-12, pp. 374-380, Sept. 1965.

57. L.T. Bruton, "Nonideal Performance of Two-Amplifier Positive Impedance Converters," IEEE Trans. on Circuit Theory, vol.CT-16, pp.572-574, Nov. 1969.

58. W.H. Holmes, S. Gruetzmann and W.E. Heinlein, "High Performance Direct-Coupled Gyrators," Electron. Letters, vol.3, pp. 46-47, Feb. 1967.

59. S.S. Haykim, S. Karmer, J. Schewchum, and D.H. Treleaven, "Integrated-Circuit Implementation of Direct-Coupled Gyrator," IEEE J. Solid-State Circuits, vol.SC-4, pp. 164-166, June 1969.

60. T.N. Rao and R.W. Newcomb, "A Direct-Coupled Gyrator Suitable for Integrated Circuits and Time Variations," Electron. Letters, vol.2, pp. 250-251, July 1966.

61. D.F. Sheahan and H.J. Orchard, "Integrable Gyrator using m.o.s. and Bi-Polar Transistors," Electron. Letters, vol.3, pp. 390-391, Oct. 1966.

62. L.P. Huelsman, Active Filters: Lumped, Distributed, Integrated, Digital, and Parametric, McGraw-Hill, New York, Chapter 3, (1970).

63. A. Antoniou, "New Gyrator Circuits Obtained using Nullors," Electron. Letters, vol.4, pp. 87-89, March 8, 1968.

64. A. Antoniou, "Gyrators using Operational Amplifiers," Electron. Letters, vol.3, pp. 350-352, Aug. 1967.

65. A. Antoniou, "Stability Properties of Some Gyrator Circuits," Electron. Letters, vol.4, pp. 510-512, Nov. 15, 1968.

66. H.W. Bode, Network Analysis and Feedback Amplifier Design, Von Nostrand, 1945.

67. R.H.S. Riordan, "Simulated Inductors using Differential Amplifiers," Electron. Letters, vol.3, pp. 50-51, Feb. 1967.

68. A.S. Morse and L.P. Huelsman, "A Gyrator Realization using Operational Amplifiers," IEEE Trans. Circuit Theory, vol.CT-11, pp. 277-278, June 1964.

69. G.J. Deboo, "Application of a Gyrator Type Circuit to Realize Ungrounded Inductors," IEEE Trans. Circuit Theory, vol.CT-14, pp. 101-102, March 1967.

70. A. Antoniou, "Three Terminal Gyrator Circuits using Operational Amplifiers," Electron. Letters, vol.4, pp. 591-592, Dec. 27, 1968.

71. J. Valihora, "Modern Technology Applied to Network Implementation," Proc. 1972 Int. Symposium on Circuit Theory, pp. 169-173, April 1972.

72. L.T. Bruton, "Non-ideal Performance of a Class of Positive Impedance Converters," IEEE Trans. Circuit Theory, vol.16, pp. 572-574, Nov. 1969.

73. H.R. Trimmel, "Realization of Canonical Bandpass Filters with Frequency-Dependent and Frequency-Independent Negative Resistances," Proc. 1973 Int. Symposium on Circuit Theory, pp. 134-137, April 1973.

74. L.T. Bruton and R.T. Pederson, "Tunable RC-Active Filters using Periodically Switched Conductances," IEEE Trans. Circuit Theory, vol.CT-20, May 1973.

75. H.R. Trimmel and H.E. Heinlein, "Fully Floating Chain-Type Gyrator Circuit using Operational Transconductance Amplifiers," IEEE Trans. Circuit Theory (corresp.), vol.CT-18, pp. 719-721, Nov. 1971.

76. J. Valihora, "Filter Networks for the MA-5A Multiplex System," Telesis, vol.1, No.7, Jan. 1970, pp. 223-225.

77. J. Valihora and J.T. Lim, "The Feasibility of Active Filtering in Frequency Division Multiplex Systems," Proc. Int. Symposium on Circuit Theory, pp. 121-125, April 1974.

78. A. Antoniou and K.S. Naidu, "Modelling of a Gyrator Circuit," IEEE Trans. Circuit Theory, vol.CT-20, pp. 533-540, Sept. 1973.

79. A. Antoniou and K.S. Naidu, "The Influence of Amplifier Imperfections in Gyrators," Report No. EE1, Sir George Williams University, April 1972.

80. A. Antoniou and K.S. Naidu, "The Influence of Amplifier Imperfections in Gyrators - Part II," Report No. EE2, Sir George Williams University, June 1973.

81. A. Antoniou and K.S. Naidu, "A Compensation Technique for a Gyrator and its use in the Design of a Channel-Bank Filter," IEEE Trans. Circuits and Systems, April 1975.

82. V. Ramachandran and M.N.S. Swamy, "Generalized Gyrator and Driving Point Function Synthesis," Int. J. Electron., Vol.23, pp. 333-341, 1967.

APPENDICES

APPENDIX A

ANALYSIS AND MODELLING OF GYRATOR GB

In this appendix the more exact method of analysing gyrator circuits, presented in Section 3.2, is used to analyze gyrator GB. A simple model is developed for the capacitively terminated gyrator circuit in Section A.2. The validity of the model is justified in Section A.3.

A.1 Analysis of Gyrator GB

Gyrator GB is shown in Fig. A.1. By using the model of Fig.3.6b for each operational amplifier, the equivalent circuit obtained for the gyrator GB is shown in Fig.A.2. After a star-delta transformation at node M, a signal flow graph analysis gives the y parameters as

$$y'_{11} = \frac{1}{R_{P1}} + \frac{1}{D'R_j}\left\{1 + \frac{R_{02}}{R_i} + \frac{R_k}{R_i} + \frac{R_{02}}{R_e} + \frac{R_k}{R_b+R_i} + A_2 + \frac{A_2R_k}{R_b+R_i} + \frac{R_{02}}{R_e}\left(\frac{R_k}{R_i} + \frac{R_k}{R_b+R_i}\right) + \frac{R_{02}R_k}{R_i(R_b+R_i)} + \frac{A_2R_k}{(R_b+R_i)}\right\} \quad (A.1)$$

$$y'_{12} = \frac{1}{D'}\left[\frac{A_1A_2R_b}{R(R_b+R_i)} + \frac{A_1R_{02}}{RR_i} + \frac{R_{02}}{R_eR}\left(1 + \frac{R_k}{R_i} + \frac{R_k}{R_b+R_i}\right) + \frac{R_{02}}{RR_i}\left(1 + \frac{R_k}{R_b+R_i}\right) + \frac{A_2}{R}\left(1 + \frac{2R_k}{R_b+R_i}\right) - \frac{1}{R_{I1}}\left\{1 + \frac{R_k}{R_i} + \frac{R_k}{R_b+R_i}\right\}\right] \quad (A.2)$$

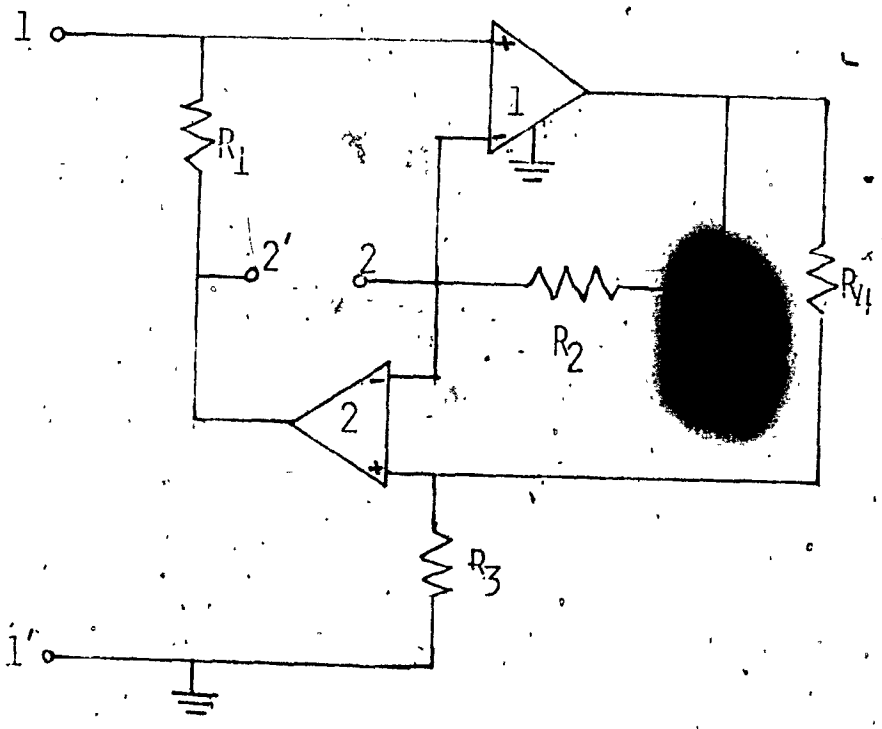

FIG. A.1 GYRATOR GB

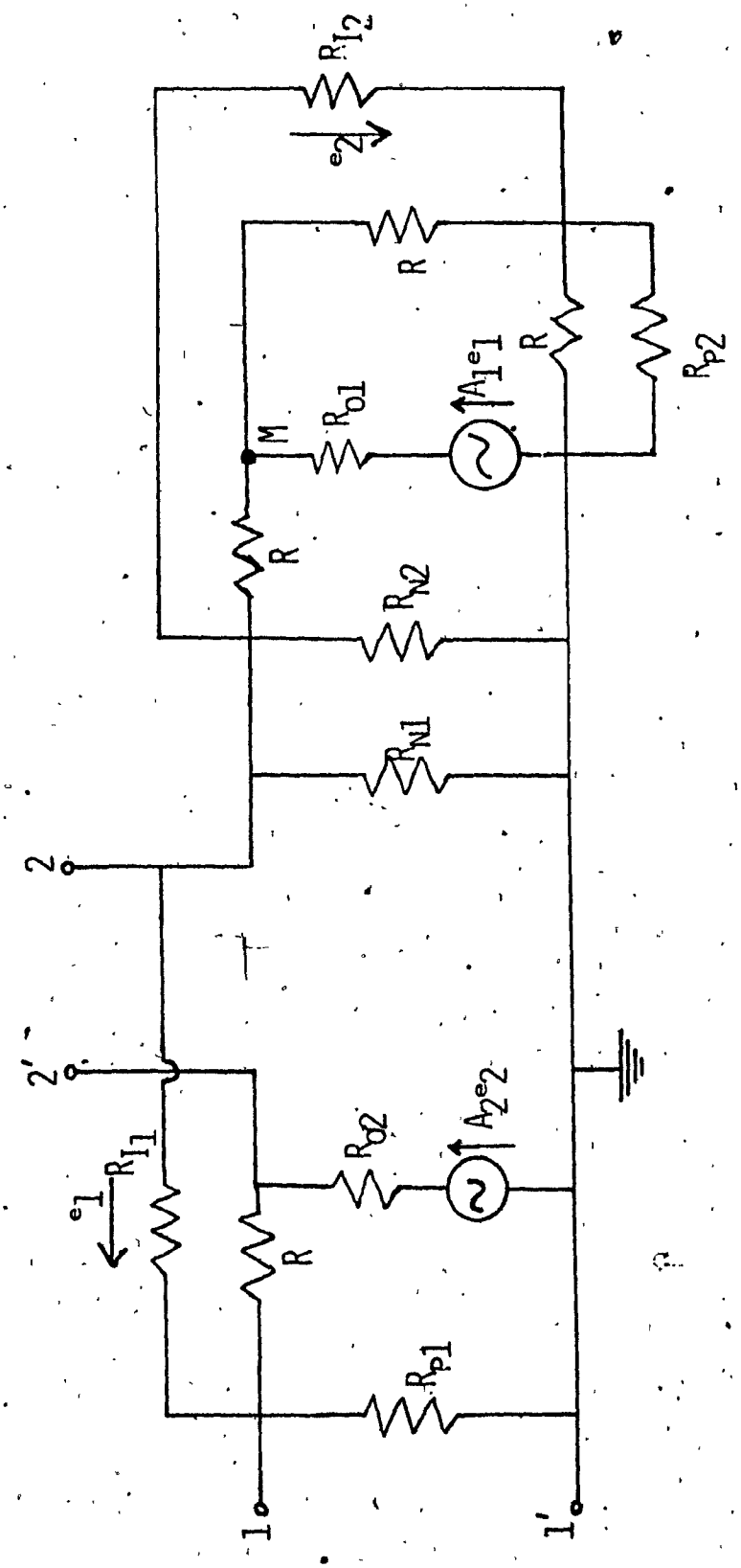

FIG. A.2 EQUIVALENT CIRCUIT FOR GYRATOR GB

$$y'_{21} = \frac{1}{D'}\left[\frac{R_{02}}{RR_e}\left(1 + \frac{R_k}{R_i} + \frac{R_k}{R_b + R_i}\right) + \frac{R_{02}}{RR_i}\left(1 + \frac{R_k}{R_b + R_i}\right)\right.$$

$$+ \frac{A_1A_2R}{R_e(R_b + R_i)} - \frac{A_2}{R_i} - \frac{A_1A_2}{R_b + R_i}$$

$$\left. - \frac{1}{R_{I1}}\left\{1 + \frac{R_k}{R_i} + \frac{R_k}{(R_b + R_i)} + A_2 + \frac{A_2R_k}{R_b + R_i}\right\}\right] \qquad (A.3)$$

$$y'_{22} = \frac{1}{D'}\left[\frac{1}{R_i}\left\{1 + \frac{R_{02}}{R} + \frac{R_k}{R_b + R_i} + \frac{R_{02}R_k}{R(R_b + R_i)} + A_1 + \frac{A_1R_{02}}{R}\right\}\right.$$

$$+ \frac{1}{R_{I1}}\left\{1 + \frac{R_{02}}{R} + \frac{R_k}{R_i} + \frac{R_k}{R_b + R_i} + \frac{R_{02}}{R}\left(\frac{R_k}{R_i} + \frac{R_k}{R_b + R_i}\right)\right\}$$

$$\left. + \frac{1}{R_e}\left\{1 + \frac{R_{02}}{R} + \frac{R_k}{R_i} + \frac{R_k}{R_b + R_i} + \frac{R_{02}}{R}\left(\frac{R_k}{R_i} + \frac{R_k}{R_b + R_i}\right)\right\}\right] \qquad (A.4)$$

where

$$R_b = \frac{RR_{p2}}{R + R_{p2}} \qquad (A.5)$$

$$R_i = \frac{RR_{I2}}{2R + R_{I2}} \qquad (A.6)$$

$$R_j = \frac{RR_{I1}}{R + R_{I1}} \qquad (A.7)$$

$$R_k = R_{01} + \frac{R^2}{2R + R_{I2}} \qquad (A.8)$$

and

$$D' = 1 + A_2 + \frac{R_k}{R_i} + \frac{(1 + A_1)R_{02}}{R_i} + \frac{R_{02}}{R_j}\left(1 + \frac{R_k}{R_i} + \frac{R_k}{R_b + R_i}\right)$$

$$+ \frac{R_{02}}{R_e}\left(1 + \frac{R_k}{R_i} + \frac{R_k}{R_b + R_i}\right)$$

$$+ \frac{I}{(R_b + R_i)}\left(R_k + 2A_2R_k + A_1A_2R_b + \frac{R_{02}R_k}{R_i}\right) \qquad (A.9)$$

For identical amplifiers Eqns. A.5 - A.8, 3.27 and 3.28 give

$$\left.\begin{aligned} R_b &\simeq R_i \simeq R_j' \simeq R \\ R_k &\simeq R_0 \end{aligned}\right\} \qquad (A.10)$$

By using Eqns. 3.27 - 3.28 and A.10, the y parameters can be approximated as

$$y_{11}' \simeq \frac{1}{R_{P1}} + \frac{1}{D'R}\left(1 + A + \frac{AR_0}{R} + \frac{5R_0}{2}\right) \qquad (A.11)$$

$$y_{12}' \simeq \frac{1}{D'}\left(\frac{A^2}{2R} + \frac{A}{R} + \frac{2AR_0}{R^2} + \frac{R_0}{R^2}\right) \qquad (A.12)$$

$$y_{21}' \simeq -\frac{1}{D'}\left(\frac{A^2}{2R} + \frac{A}{R} + \frac{A}{R_I} + \frac{AR_0}{RR_I} + \frac{1}{R_I} - \frac{R_0}{R^2}\right) \qquad (A.13)$$

$$y_{22}' \simeq \frac{1}{D'}\left(\frac{A}{R} + \frac{AR_0}{R^2} + \frac{1}{R} + \frac{3R_0}{R^2}\right) \qquad (A.14)$$

where

$$D' \simeq \frac{A^2}{2} + A + \frac{2AR_0}{R} + 1 \qquad (A.15)$$

Now from Eqns. 3.27 and A.15 the y parameters can be written as

$$y_{11}' \simeq \frac{1}{R_{P1}} + \frac{2}{AR} + \frac{2R_0}{AR^2} - \frac{2}{A^2R} - \frac{7R_0}{A^2R^2} \qquad (A.16)$$

$$y'_{12} \simeq \frac{1}{R} - \frac{2}{A^2R} - \frac{4}{A^3R} \qquad (A.17)$$

$$y'_{21} \simeq -\frac{1}{R} + \frac{4R_0}{AR^2} - \frac{2}{AR_I} \qquad (A.18)$$

$$y'_{22} \simeq \frac{2}{AR} + \frac{2R_0}{AR^2} - \frac{2}{A^2R} - \frac{9}{A^2R^2} \qquad (A.19)$$

If $s = j\omega$ in the Eqn. 3.14, the use of Eqns. 3.14, 3.26 and 3.27 further simplifies the y parameters as

$$y'_{11} \simeq G'_f + G'_g + \frac{2j\omega}{A_0\omega_0 R}\left(1 + \frac{R_0}{R}\right) \qquad (A.20)$$

$$y'_{12} \simeq \frac{1}{R} - \frac{(4A_0\omega_0^2 + 4\omega^2)}{A_0^3\omega_0^3 R}\, j\omega \qquad (A.21)$$

$$y'_{21} \simeq -\frac{1}{R} + \frac{2j\omega}{A_0\omega_0}\left(\frac{2R_0R_I - R^2}{R^2R_I}\right) \qquad (A.22)$$

$$y'_{22} \simeq \frac{2}{A_0R} + \frac{2R_0}{A_0R^2} + \frac{2\omega^2}{A_0^2\omega_0^2 R} + \frac{9R_0\omega^2}{A_0^2\omega_0^2R^2} + \frac{2j\omega}{A_0\omega_0}\left(\frac{1}{R} + \frac{R_0}{R^2}\right) \qquad (A.23)$$

where

$$G'_f = \frac{1}{R_{Pl}} + \frac{2}{A_0R} + \frac{2R_0}{A_0R^2} \qquad (A.24)$$

$$G'_g = \frac{\omega^2}{A_0^2\omega_0^2}\left(\frac{2}{R} + \frac{7R_0}{R^2}\right) \qquad (A.25)$$

A.2 New Model for Gyrator GB

Analysis of Section A.1 can be used for deriving a model for the gyrator GB. From the Eqns. 3.48, A.21, A.22 and A.23, the input admittance for the capacitively loaded gyrator GB can be expressed as

$$Y_i'(j\omega) = y_{11}'(j\omega) + \frac{H'(j\omega + k_1')\ (j\omega + k_2')}{j\omega + k_3'} \qquad (A.26)$$

where

$$H' = 8\,\frac{(A_0\omega_0^2 + \omega^2)\ (2R_0R_I - R^2)}{A_0^3\omega_0^3RR_I(2R + 2R_0 + A_0\omega_0R^2C)} \qquad (A.27)$$

$$k_1' = \frac{-A_0^3\omega_0^3}{4(A_0\omega_0^2 + \omega^2)} \qquad (A.28)$$

$$k_2' = \frac{A_0\omega_0RR_I}{2(R^2 - 2R_0R_I)} \qquad (A.29)$$

and

$$k_3' = \frac{2A_0\omega_0^2R + 2A_0\omega_0^2R_0 + A_0^2\omega_0^2R^2G_L + \omega^2(2R + 9R_0)}{A_0\omega_0(2R + 2R_0 + A_0\omega_0R^2C)} \qquad (A.30)$$

The input admittance of Eqn. A.26 can now be expressed as

$$Y_i'(j\omega) = y_{11}'(j\omega) + H'j\omega + H'k_4' + \frac{H'k_5'}{j\omega + k_3'} \qquad (A.31)$$

where

$$k_4' = k_1' + k_2' - k_3' \qquad (A.32)$$

$$k_5' = k_1'k_2' - k_3'k_4' \qquad (A.33)$$

Eqns. A.32, A.28, A.29 and A.30 give

$$k_4' = \frac{A_0^3\omega_0^3}{4(A_0\omega_0^2 + \omega^2)} - \frac{A_0\omega_0 RR_I}{2(2R_0R_I - R^2)}$$

$$- \frac{2A_0\omega_0^2R + 2A_0\omega_0^2R_0 + A_0^2\omega_0^2R^2G_L + \omega^2(2R + 9R_0)}{(2R + 2R_0 + A_0\omega_0R^2C)A_0\omega_0} \qquad (A.34)$$

and by using Eqns. 3.26 and 3.27 we obtain

$$k_4' \simeq -\frac{A_0^3\omega_0^3}{4(A_0\omega_0^2 + \omega^2)} - \frac{A_0\omega_0 RR_I}{2(2R_0R_I - R^2)} \qquad (A.35)$$

Also from Eqns. A.33, A.28-A.30 and A.35

$$k_5' = \frac{A_0^4\omega_0^4RR_I}{8(A_0\omega_0^2 + \omega^2)(2R_0R_I - R^2)} + \frac{1}{(2R + 2R_0 + A_0\omega_0R^2C)}$$

$$\times \left(\frac{2A_0\omega_0^2R + 2A_0\omega_0^2R_0 + A_0^2\omega_0^2R^2G_L + \omega^2(2R + 9R_0)}{A_0\omega_0} \right)$$

$$\times \left(\frac{2A_0^3\omega_0^3(2R_0R_I - R^2) + 4A_0\omega_0RR_I(A_0\omega_0^2 + \omega^2)}{8(A_0\omega_0^2 + \omega^2)(2R_0R_I - R^2)} \right) \qquad (A.36)$$

and by using Eqns. 3.26-3.27, k_5' reduces to

$$k_5' \simeq \frac{A_0^4\omega_0^4RR_I}{8(A_0\omega_0^2 + \omega^2)(2R_0R_I - R^2)} \qquad (A.37)$$

The input admittance of Eqn. A.31 can now be expressed as

$$Y_i'' = Y_A' + \frac{1}{Z_B' + Z_C'} \qquad (A.38)$$

where

$$Y_A' = y_{11}' + H'k_4' + H'j\omega \qquad (A.39)$$

$$Z'_B = \frac{j\omega}{H'k'_5} \tag{A.40}$$

$$Z'_C = \frac{k'_3}{H'k'_5} \tag{A.41}$$

From Eqns. A.39, A.20, A.24-A.25, A.27 and A.35 we can write

$$Y'_A = G'_{p1} + G'_{p2} + G'_{p3} + j\omega C'_p \tag{A.42}$$

where

$$G'_{p1} = \frac{1}{R_{P1}} + \frac{2}{A_0 R} + \frac{2R_0}{A_0 R^2} + \frac{2R}{R_I(2R + 2R_0 + A_0\omega_0 R^2 C)} \tag{A.43}$$

$$G'_{p2} = \frac{-4}{(2R + 2R_0 + A_0\omega_0 R^2 C)}\left(\frac{1}{A_0} + \frac{R_0}{R}\right) \tag{A.44}$$

$$G'_{p3} = \frac{\omega^2}{A_0^2\omega_0^2 R}\left(2 + \frac{7R_0}{R} - \frac{4R}{(2R + 2R_0 + A_0\omega_0 R^2 C)}\right) \tag{A.45}$$

$$C'_p = \frac{2}{A_0\omega_0 R}\left(1 + \frac{R_0}{R}\right) + 8\,\frac{(A_0\omega_0^2 + \omega^2)\,(2R_0R_I - R^2)}{A_0^3\omega_0^3 RR_I(2R + 2R_0 + A_0\omega_0 R^2 C)} \tag{A.46}$$

By using eqns. 3.26-3.27, C'_p reduces to

$$C'_p = \frac{2}{A_0\omega_0 R}\,(1 + \frac{R_o}{R}) \tag{A.47}$$

Hence from Eqns. A.40, A.27 and A.37

$$Z'_B = L'_o j\omega + L'_p j\omega \tag{A.48}$$

where

$$L_o = R^2 C \tag{A.49}$$

$$L'_p = \frac{2R}{A_0\omega_0} + \frac{2R_0}{A_0\omega_0} \qquad (A.50)$$

Similarly, from Eqns. A.41, A.27, A.30, and A.37

$$Z'_C = r'_{p4} + r'_{p5} \qquad (A.51)$$

where

$$r'_{p4} = G_L R^2 + \frac{2R}{A_0} + \frac{2R_0}{A_0} \qquad (A.52)$$

$$r'_{p5} = \frac{2\omega^2}{A_0^2\omega_0^2}(R + R_0) \qquad (A.53)$$

A model for a capacitively terminated gyrator GB can now be obtained by connecting the components of Y'_A, Z'_B and Z'_C as shown in Fig. A.3.

A.3 Validity of the Model

The model of Fig. A.3 has been used to obtain the performance curves of the gyrator GB. An exact computer-aided analysis has also been carried out using the network analysis program NASAP. The performance curves for different sets of parameters are shown in Figs. A.4-A.7.

Figs. A.4-A.7 show that the gyrator responses predicted by the model agree closely with those obtained by exact analysis and, therefore, the validity of the model is justified.

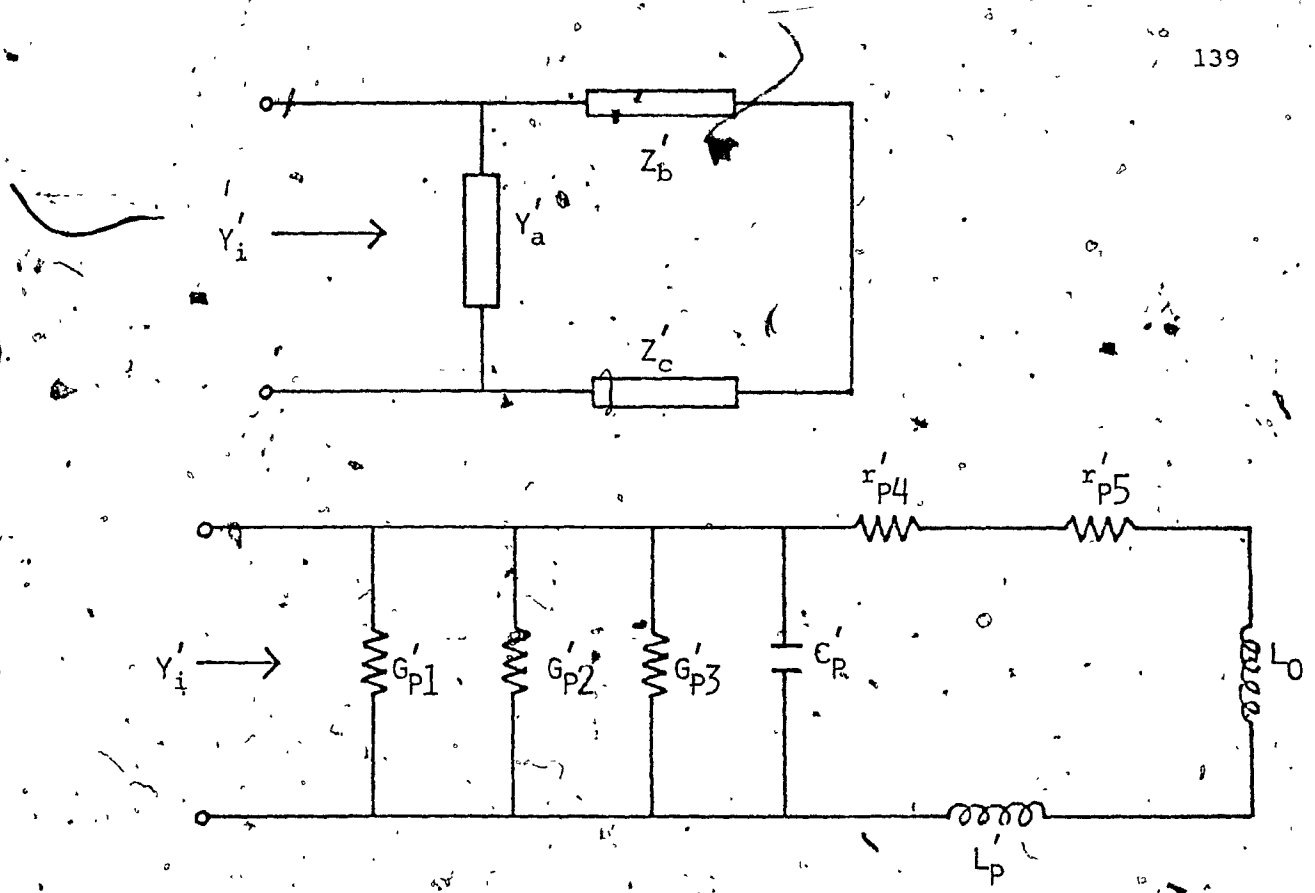

FIG. A.3 MODEL FOR THE CAPACITIVELY TERMINATED GYRATOR GB.

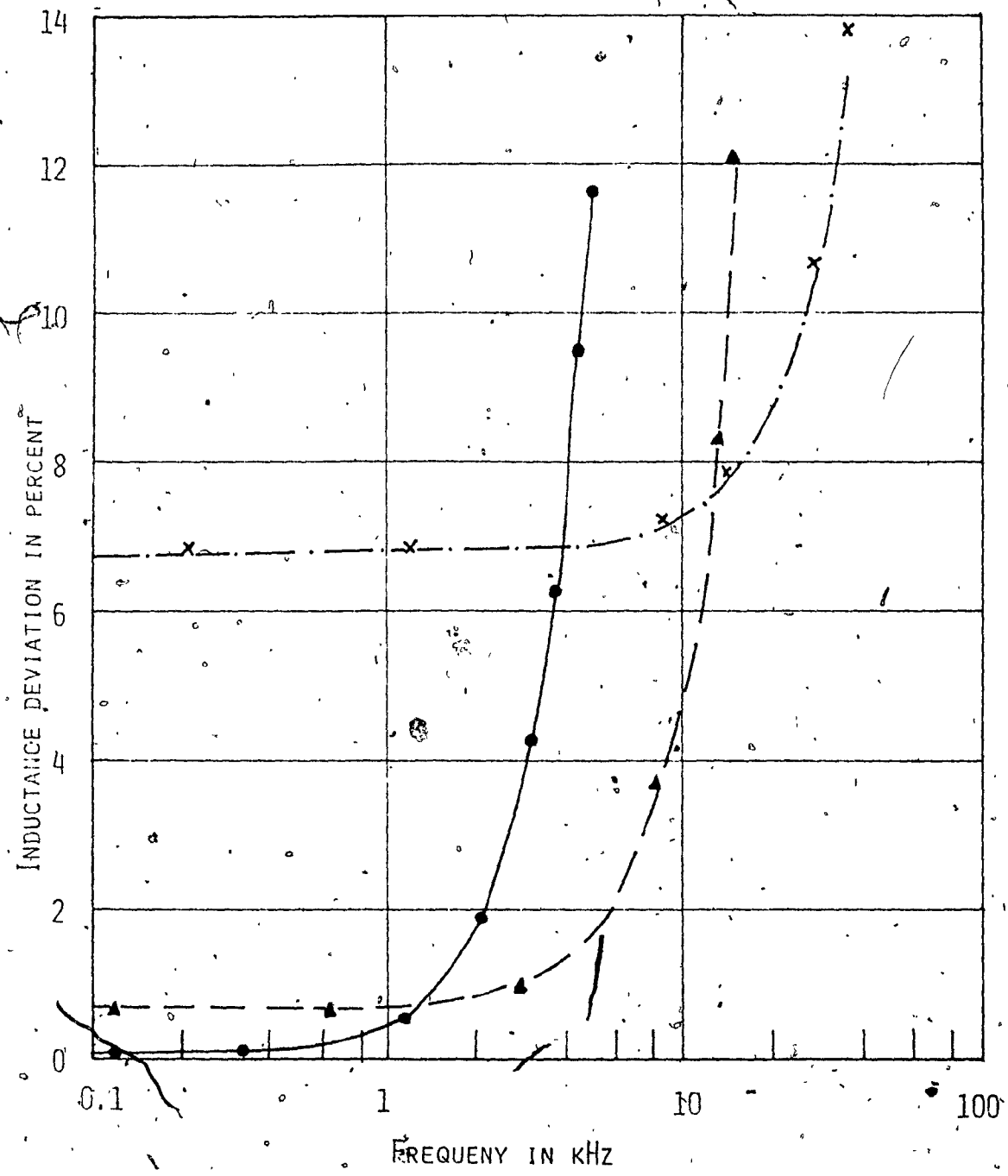

FIG.A.4A VARIATION OF INDUCTANCE DEVIATION WITH FREQUENCY FOR DIFFERENT NOMINAL INDUCTANCES (AMPLIFIER TYPE μA741C).

$R=2.5K\Omega, L_o$ EXACT ANALYSIS , MODEL ANALYSIS

1.0H ——— • • • •

0.1H — — — — ▲ ▲ ▲ ▲

0.01 — · — · — × × × ×

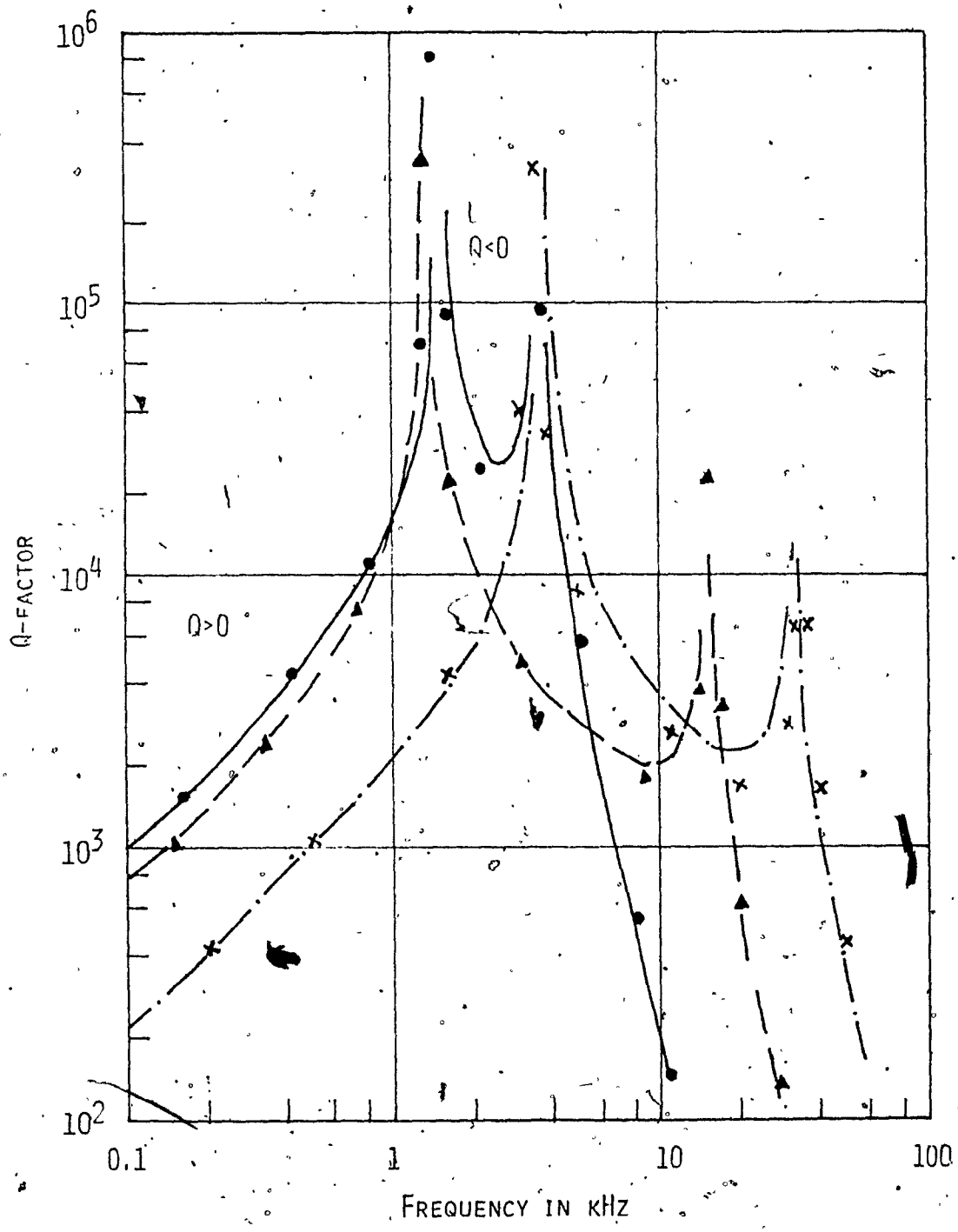

FIG.A.4B VARIATION OF Q-FACTOR WITH FREQUENCY FOR DIFFERENT NOMINAL INDUCTANCES (AMPLIFIER TYPE μA741C)

R=2.5K , L · EXACT ANALYSIS · MODEL ANALYSIS

1H ——— ● ● ● ●

0.1H — — — — ▲ ▲ ▲ ▲

0.01H —·—·— × × × ×

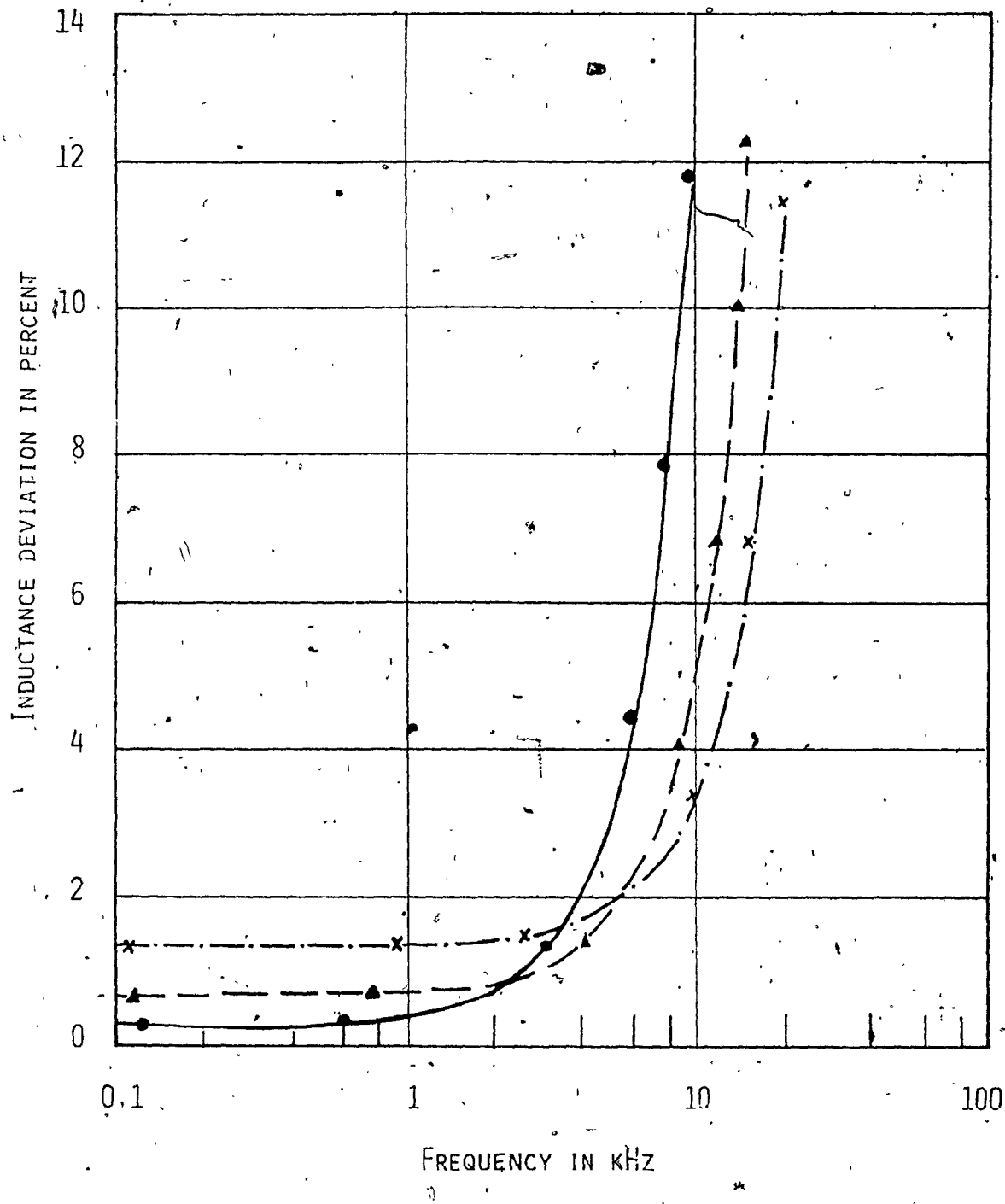

FIG.A.5A VARIATION OF INDUCTANCE DEVIATION WITH FREQUENCY FOR DIFFERNT GYRATION RESISTANCES(AMPLIFIER TYPE μA741C).

L_o=0.1H,R	EXACT ANALYSIS	MODEL ANALYSIS
1KΩ	———	● ● ● ●
2.5KΩ	— — — —	▲ ▲ ▲ ▲
5KΩ	— · — · —	x x x x

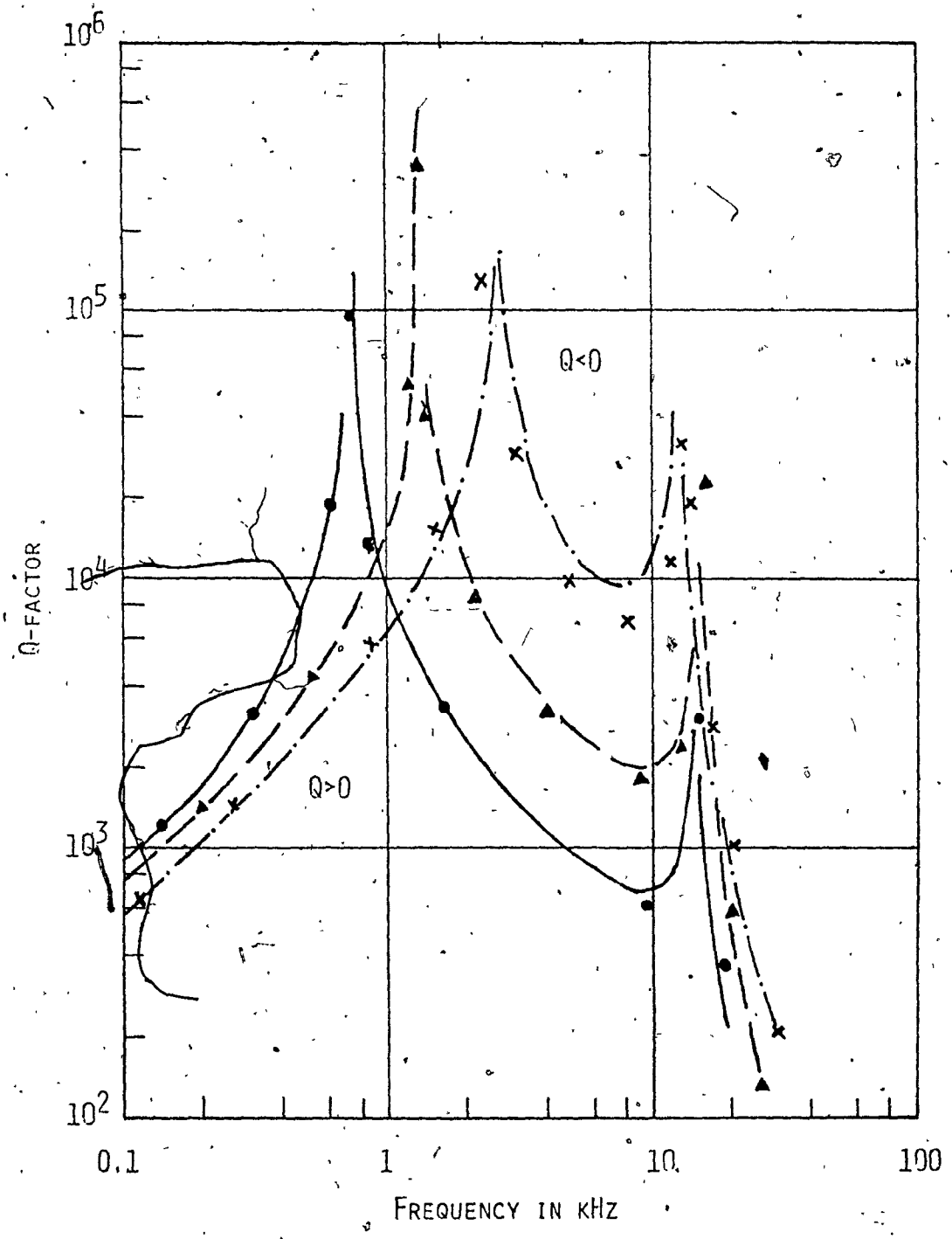

FIG.A.5B VARIATION OF Q-FACTOR WITH FREQUENCY FOR DIFFERENT GYRATION RESISTANCES(AMPLIFIER TYPE A741C).

L_o=0.1H,R — EXACT ANALYSIS — MODEL ANALYSIS

1K ——— • • • •

2.5K —.— — — ▲ ▲ ▲ ▲

5K —·—·—·— × × × ×

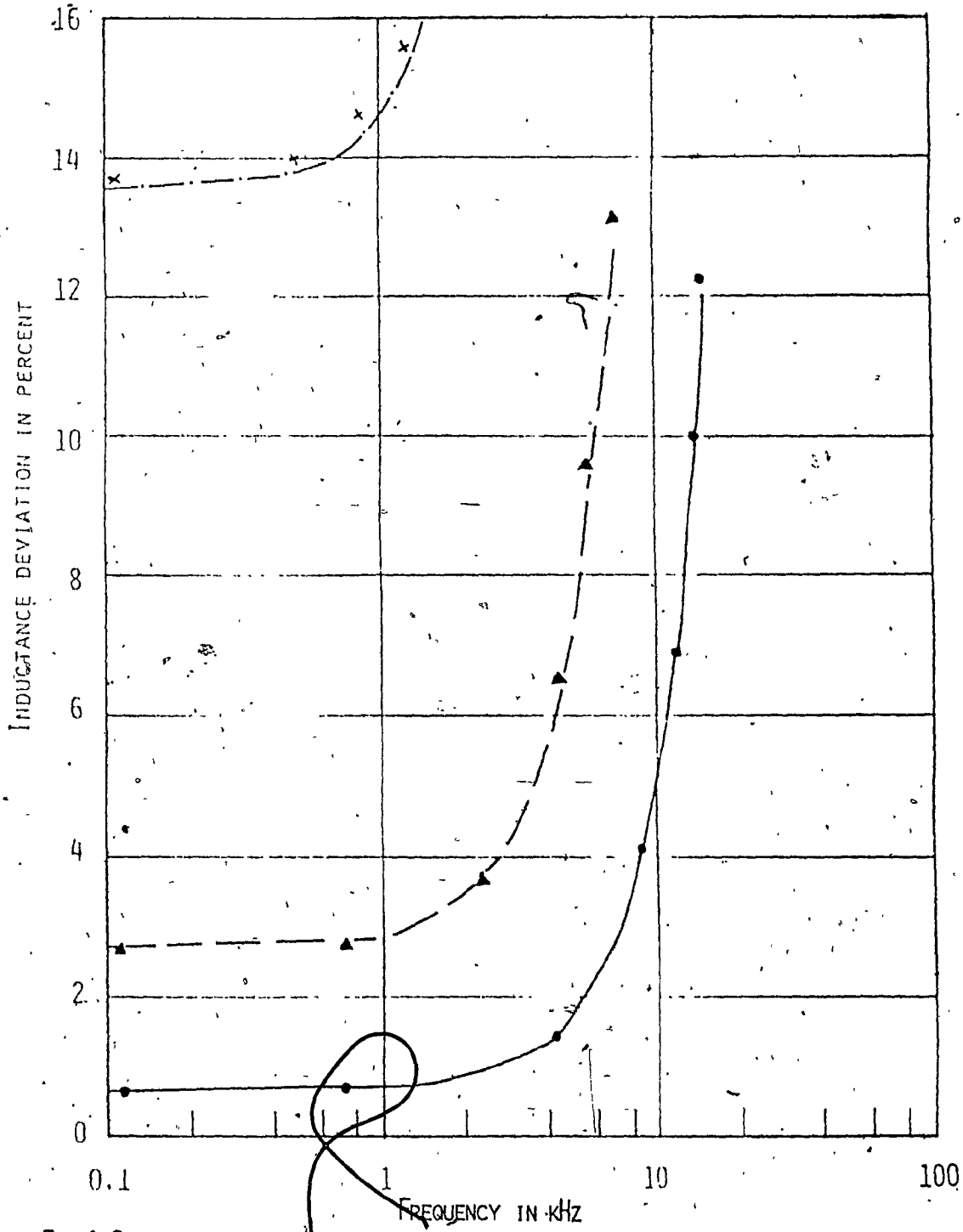

FIG.A.6A VARIATION OF INDUCTANCE DEVIATION WITH FREQUENCY FOR DIFFERENT DC GAINS(AMPLIFIER TYPE μA741C).
L_o=0.1H, R=2.5KΩ, A_0

A_0	EXACT ANALYSIS	MODEL ANALYSIS
200K	———	• • •
50K	— — —	▲ ▲ ▲
10K	—·—·—	× × ×

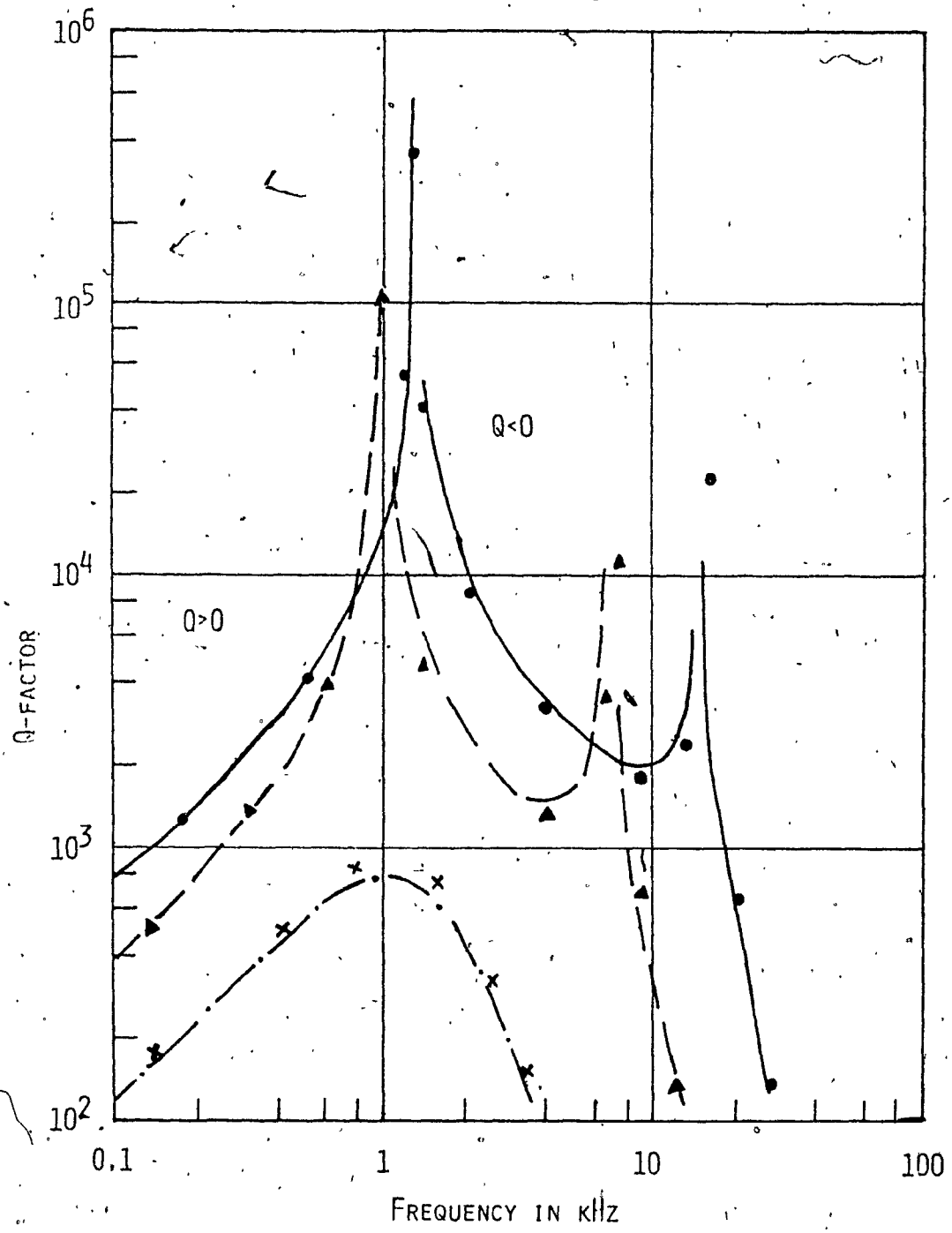

FIG.A.6B VARIATION OF Q-FACTOR WITH FREQUENCY FOR DIFFERENT DC GAINS(AMPLIFIER TYPE A741C).

L_o=0.1H, R=2.5KΩ, A_o EXACT ANALYSIS MODEL ANALYSIS

200K ——— ● ● ● ●

50K — — — ▲ ▲ ▲ ▲

10K — • — • — × × × ×

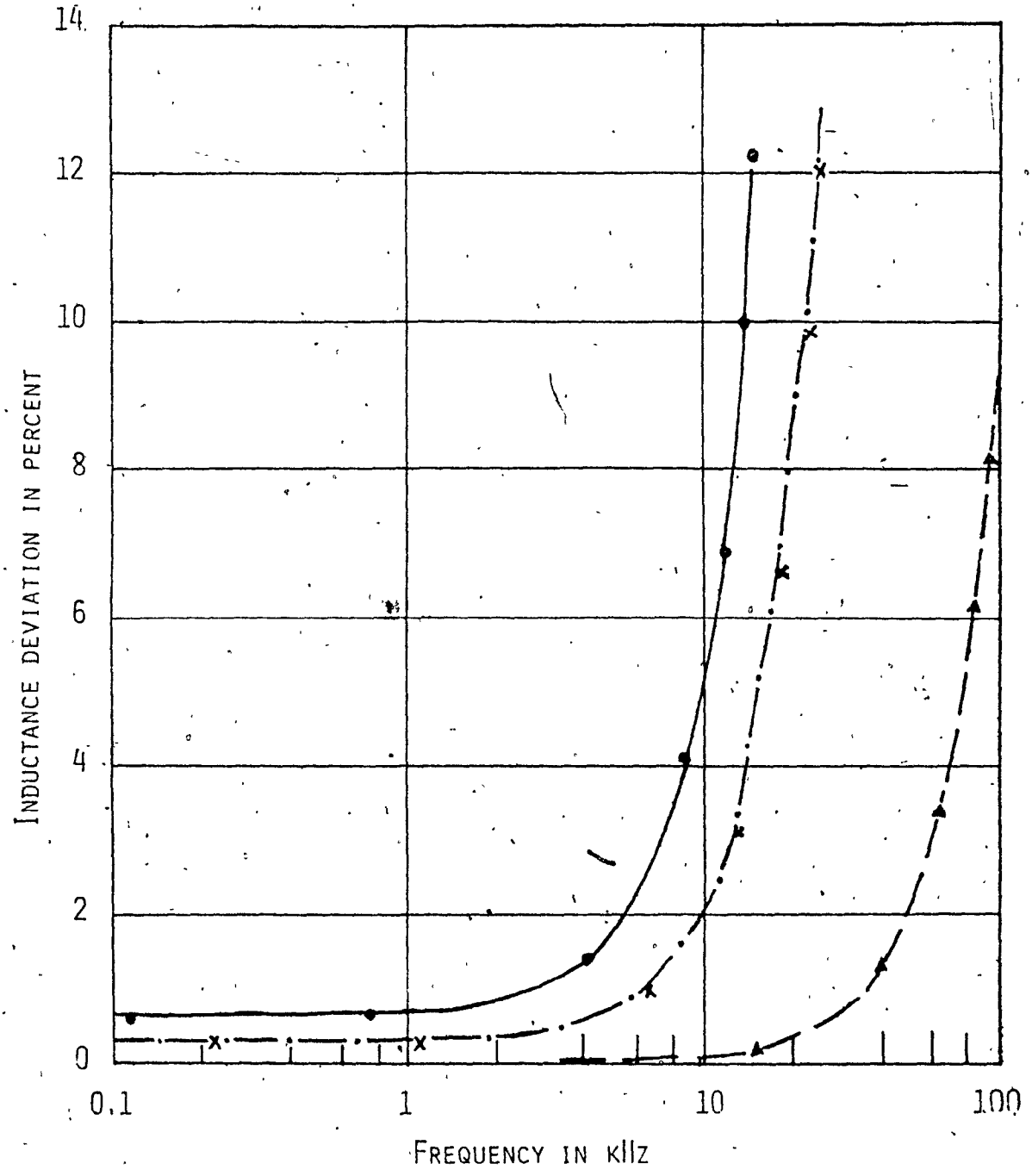

FIG.A.7A VARIATION OF INDUCTANCE DEVIATION WITH FREQUENCY FOR DIFFERENT OPERATIONAL AMPLIFIERS.

L_o=0.1H, R=2.5KΩ EXACT ANALYSIS MODEL ANALYSIS

μA741C

μA715

μA702

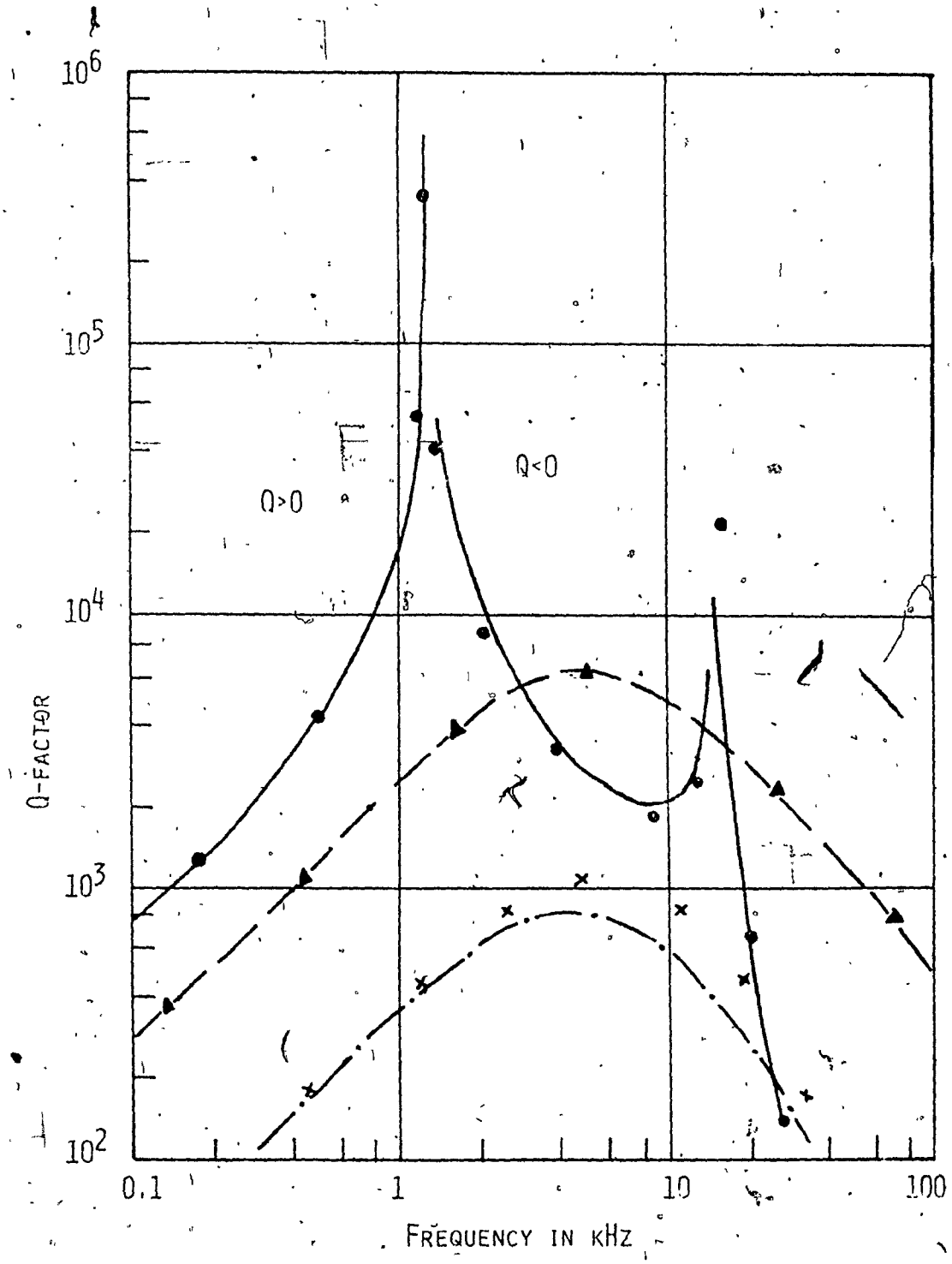

FIG.A.7B VARIATION OF Q-FACTOR WITH FREQUENCY FOR DIFFERENT OPERATIONAL AMPLIFIERS.

L_g=0.1H, R=2.5KΩ EXACT ANAEYSIS MODEL ANALYSIS

μA741C

μA715

μA702

APPENDIX B

MEASUREMENT OF THE PERFORMANCE OF A GYRATOR CIRCUIT

This appendix describes the method used to obtain the experimental results given in this thesis. The method can be applied for measuring the performance of any gyrator circuit.

B.1 The Test Circuit

The test circuit used is shown in Fig. B.1. The capacitance C_2 (decade capacitance box with a range 10pF to 1.11111μF) and the simulated inductance form a series resonant circuit. The resistances R_6 and R_7 form a low resistance drive to the resonant circuit. The capacitance C_1, resistance R_5 and amplifier A_3 are used to eliminate the dc off-set voltage present at the output of the signal generator. Amplifier A_5 is used to provide isolation between the simulated inductance and the attenuator. The resistance R_{10} is used to increase the effective load on amplifier A_5 so as to eliminate overloading. Amplifier A_4 is used to increase the level of V_1. By keeping lead CD as short as possible pick-up can be minimized. The frequency selective voltmeters (Siemens level meter-D354) is tuned automatically by a control signal from the decade signal generator (Siemens Digital level oscillator-G2004). The part of the test circuit shown enclosed in dotted lines in Fig. B.1 was enclosed in an aluminium box so as to minimize pick-up. Also all leads were kept as short as possible to minimize pick-up and unpredictable stray capacitances.

B.2 The Measurement Procedure

With switch S_1 at position A, the decade capacitance C_2 was adjusted for minimum meter reading. The output level of the signal

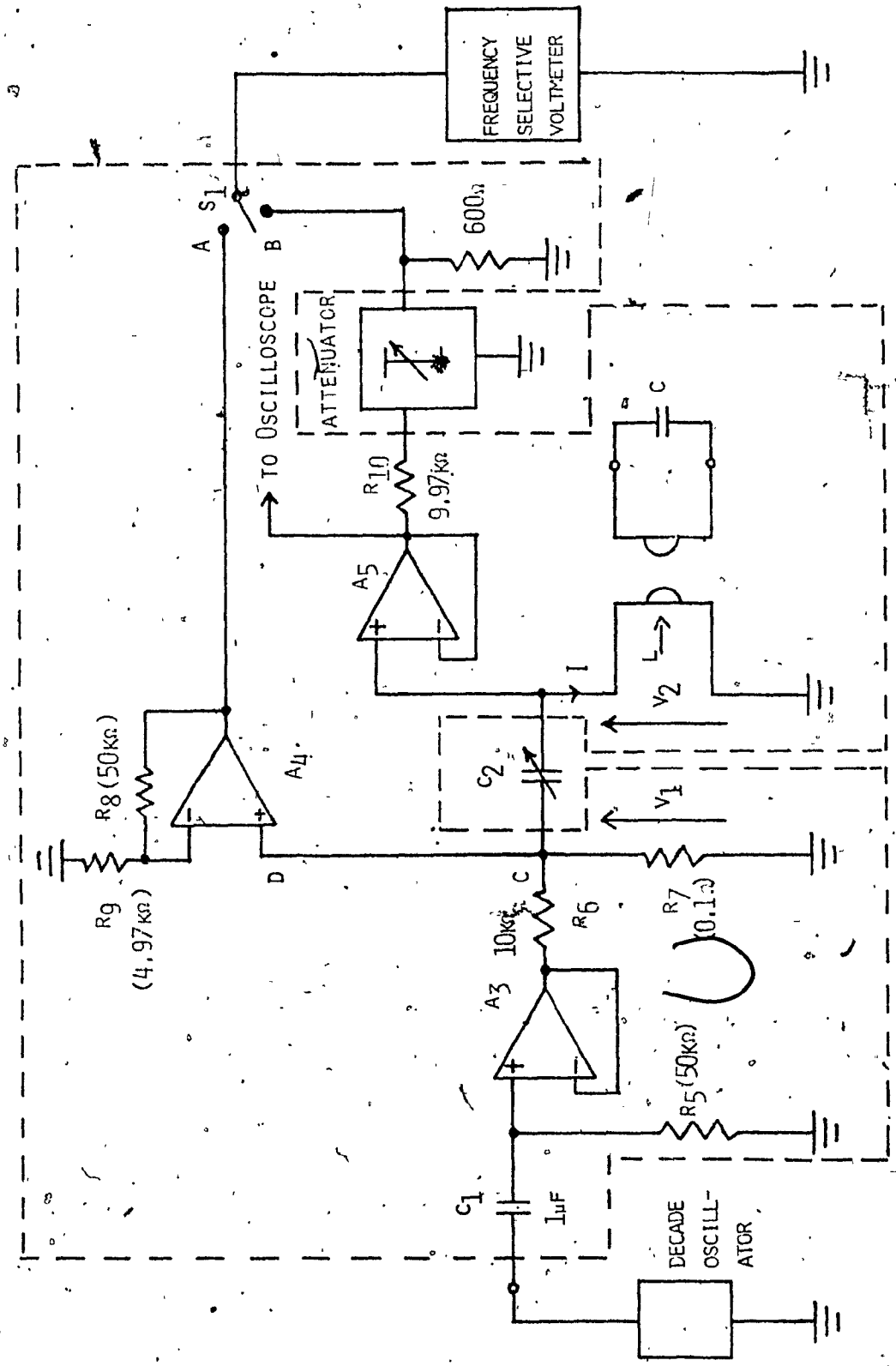

FIG.B.1 GYRATOR PERFORMANCE MEASURING SET-UP.

generator was adjusted to give a constant voltage of 0.3V. The tuning of C_2 was then checked for minimum meter reading. The meter reading was noted. Switch S_1 was then thrown to position B. By using only the attenuator, the level was adjusted to obtain the same reading on the voltmeter. Readings were then taken of the frequency, of C_2 and of the attenuator setting.

B.3 Calculations

At resonance

$$L = \frac{1}{(2\pi f)^2 C_2} \tag{B.1}$$

and

$$V_1 = Ir \tag{B.2}$$

$$V_2 = I(r + j\omega L) \tag{B.3}$$

where r is the series loss resistance of the simulated inductance L.

Hence

$$\left|\frac{V_2}{V_1}\right| = \frac{\sqrt{r^2 + (\omega L)^2}}{|r|} = \sqrt{1 + Q^2} \simeq |Q| \text{ for } |Q| > 10 \tag{B.4}$$

where

$$Q = \frac{\omega L}{r}$$

from Fig. B.1

$$|V_A| = \frac{R_9 + R_8}{R_9} |V_1| \tag{B.5}$$

$$|V_B| = \left\{ \frac{600}{(R_4 + 600)\left[\text{antilog}_{10}\left(\frac{\text{Attenuation}}{20}\right)\right]} \right\} |V_2| \tag{B.6}$$

and since $|V_A| = |V_B|$

$$\left|\frac{V_2}{V_1}\right| = |Q| = \frac{(R_9 + R_8)(R_{10} + 600)}{600R_2} \left[\text{antilog}_{10}\left(\frac{\text{Attenuation}}{20}\right)\right]$$

$$= 194.85 \left[\text{antilog}_{10}\left(\frac{\text{Attenuation}}{20}\right)\right]. \qquad (B.7)$$

the simulated inductance and Q-factor can be calculated by using Eqns. B.1 and B.7, respectively. The sign of Q-factor can be determined by observing the wave form of V_1 with reference to the wave form V_2. When the Q-factor is positive, and at frequencies less than the resonance frequency, V_1 will lag V_2. This angle of lag is decreased as the frequency is increased. At frequencies less than the resonance frequency V_1 will lead V_2 if Q-factor is negative. This angle of lead is decreased as the frequency is increased.

B.4 Precautions

The input level to the gyrator circuit and the dc supply voltages were maintained constant throughout the test. The residual capacitance of the decade capacitance box was 50pF. This was taken into account.

The dc voltage supply was decoupled by using ceramic capacitors of 0.1μF as close to the amplifiers as possible.

For high Q-factor, the voltage V_1 was slow to settle after any adjustment in C_2. Patience was thus needed.

APPENDIX C

MEASUREMENT OF AMPLIFIER DC VOLTAGE GAIN AND CUTOFF FREQUENCY

The open-loop gain of a compensated operational amplifier is given by

$$A = \frac{A_0\omega_0}{s + \omega_0} \qquad (C.1)$$

where A_0 and ω_0 are the dc voltage gain and cutoff frequency of the amplifier in rad./sec., respectively. The variation of 'A' with frequency is illustrated in Fig. C.1.

This appendix describes a method for the measurement of A_0 and ω_0.

C.1 The Test Circuit

The test circuit used is shown in Fig. C.2. The resistances R_{11} and R_{12} were chosen equal so as to give a unity closed-loop voltage gain between input and output. The resistances R_{13} and R_{14} from a potential divider. R_{14} was chosen to much smaller than the differential input-resistance of the amplifier (i.e. $R_{14} << R_I$) as a result e_n is proportional to e_s. The resistance R_{15} was a 10kΩ potentiometer and is used for offset voltage adjustment. The part of the circuit shown enclosed in dotted lines in Fig. C.2 was enclosed in an aluminium box so as to minimize pick-up. Also all leads were kept as short as possible to minimize pick-up and unpredictable stray capacitances.

C.2 The Measurement Procedure

Using R_{15}, the output voltage was adjusted to zero for zero input

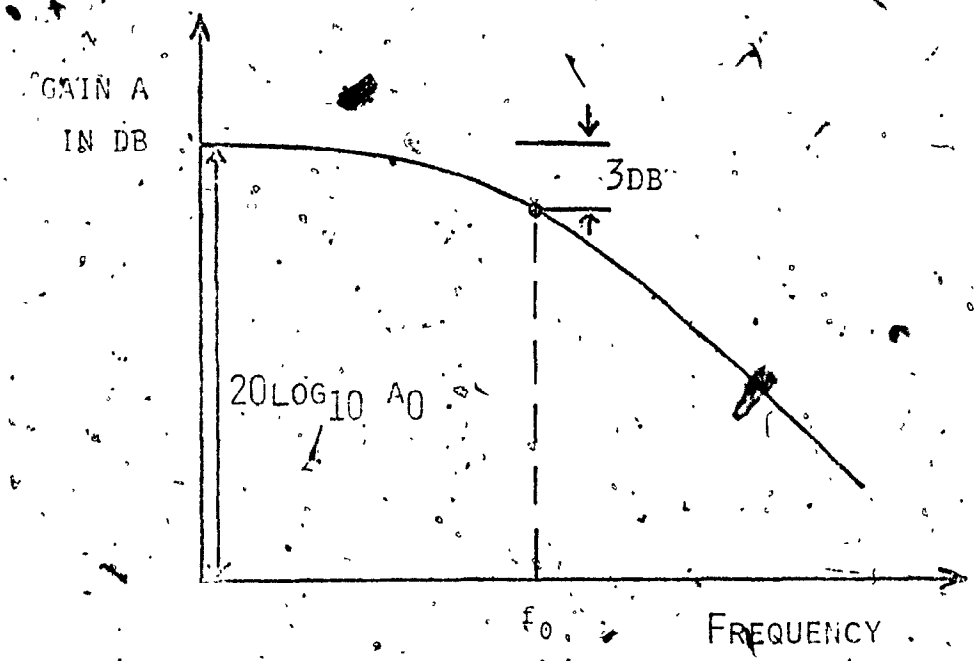

FIG.C.1 AMPLITUDE RESPONSE OF THE AMPLIFIER

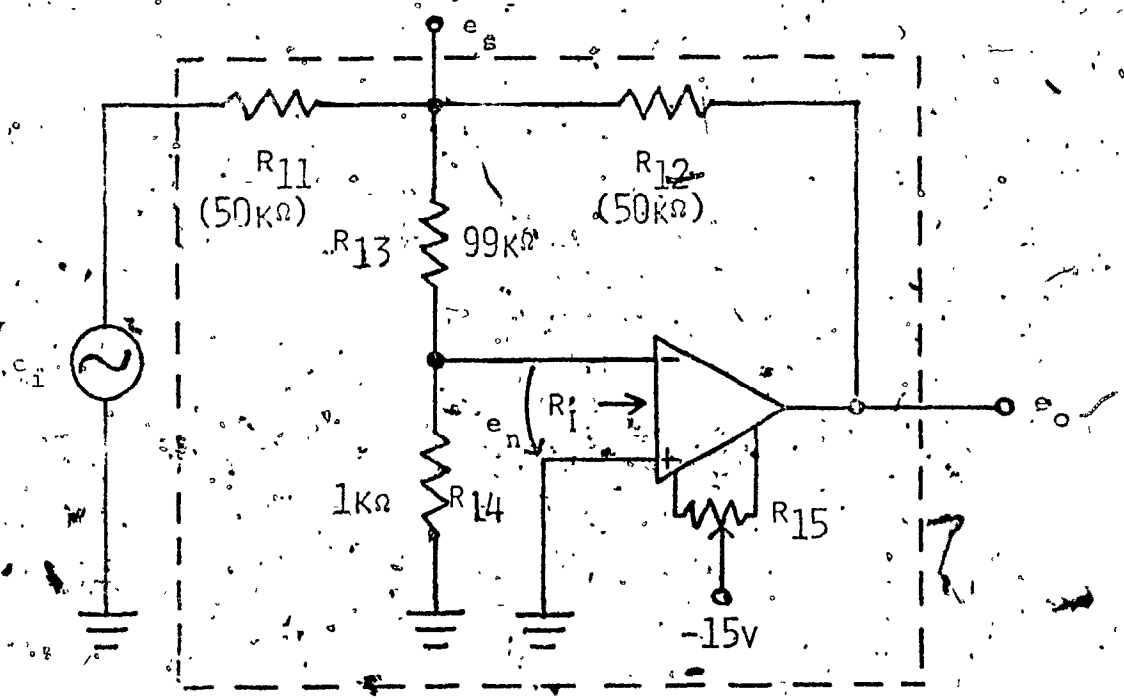

FIG.C.2 TEST CIRCIUT TO MEASURE AMPLIFIER OPEN-LOOP DC GAIN AND CUT-OFF FREQUENCY.

voltage. An input signal e_i was then applied and the level and frequency were adjusted to 1V and 0.5Hz respectively. The voltages e_s and e_o were measured using a digital voltmeter. This was repeated for a number of frequencies.

C.3 Calculations

By definition, the open-loop voltage gain is given by

$$A = \frac{e_o}{n} \qquad (C.2)$$

Since

$$R_I >> R_{14} \qquad (C.3)$$

we obtain

$$e_s = -\frac{R_{13} + R_{14}}{R_{14}} e_n \qquad (C.4)$$

Hence from Eqns. C.2 and C.4

$$|A| = \frac{R_{13} + R_{14}}{R_{14}} \left|\frac{e_o}{e_s}\right| \qquad (C.5)$$

This equation was used to obtain the modulus of the open-loop gain. The frequency response of the amplifier was then plotted. A_0 and ω_0 were determined from the frequency response.

C.4 Precautions

The input voltage level and the dc supply voltages were maintained constant throughout the test. The dc voltage supplies were decoupled by using ceramic capacitors of 0.1μF as close to the amplifiers as possible.

APPENDIX D

D.1 Voltage Handling Capacity of Gyrator GB

Using the notation of Section 4.5 for gyrator GB we obtain

$$T_1'(s) = \frac{2A(AR + R + Z_L)}{A^2R + 2(R + Z_L)A + 2(R + Z_L)} \tag{D.1}$$

Hence Eqns. 3.14, 3.26-3.27 and D.1 give

$$|T_1'(j\omega)| = 2\left\{\frac{\omega_0^2 + \omega^2(1 + A_0\omega_0RC)^2}{4\omega_0^2 + \omega^2(2 + A_0\omega_0RC)^2}\right\}^{(1/2)} \tag{D.2}$$

As $\omega \to 0$

$$|T_1'(j\omega)| \to 1 \tag{D.3}$$

and as $\omega > \omega_0$

$$|T_1'(j\omega)| \simeq 2\left(\frac{1 + A_0\omega_0RC}{2 + A_0\omega_0RC}\right) \tag{D.4}$$

If $A_0\omega_0RC >> 2$ then, for $\omega > \omega_0$ we obtain

$$|T_1'(j\omega)| \simeq 2 \tag{D.5}$$

Similarly

$$T_2'(s) = \frac{A^2(R - Z_L)}{A^2R + 2(R + Z_L)A + 2(R + Z_L)} \tag{D.6}$$

Hence Eqns. 4.25 and D.6 show that

$$|T_2'(j\omega)| = |T_2(j\omega)| \tag{D.7}$$

For $\hat{V}_{01} = \hat{V}_{02} = V_s$, Eqns. 4.19, D.5 and D.7 show that

$$V_{im} = \text{Min}\,(V_{im1}, V_{im2}) \tag{D.8}$$

where

$$V_{im1} = \frac{V_s}{2} \tag{D.9}$$

$$V_{im2} = \frac{V_s}{A_0\omega_0} \left\{ \frac{4\omega_0^2 R + \omega^2 (2R + A_0\omega_0 L_o)^2}{R^2 + \omega^2 L_o} \right\}^{(1/2)} \qquad (D.10)$$

Eqns. D.8-D.10 have been used to evaluate V_{im} for gyrator GB as shown in Figs. D.1-D.2. At low frequencies the performance of gyrator GB is identical to that of gyrator GA. At high frequencies, however, the voltage handling capacity of gyrator GB is smaller.

Figs. D.3-D.4 show experimental results for gyrator GB. The discrepancy between experimental and theoretical results at high frequencies is due to the internal loading on the amplifiers.

A comparison of the experimental results of Figs. 4.6-4.7 with those of Fig. D.3-D.4 shows that gyrator GA is superior as predicted by the theoretical approach.

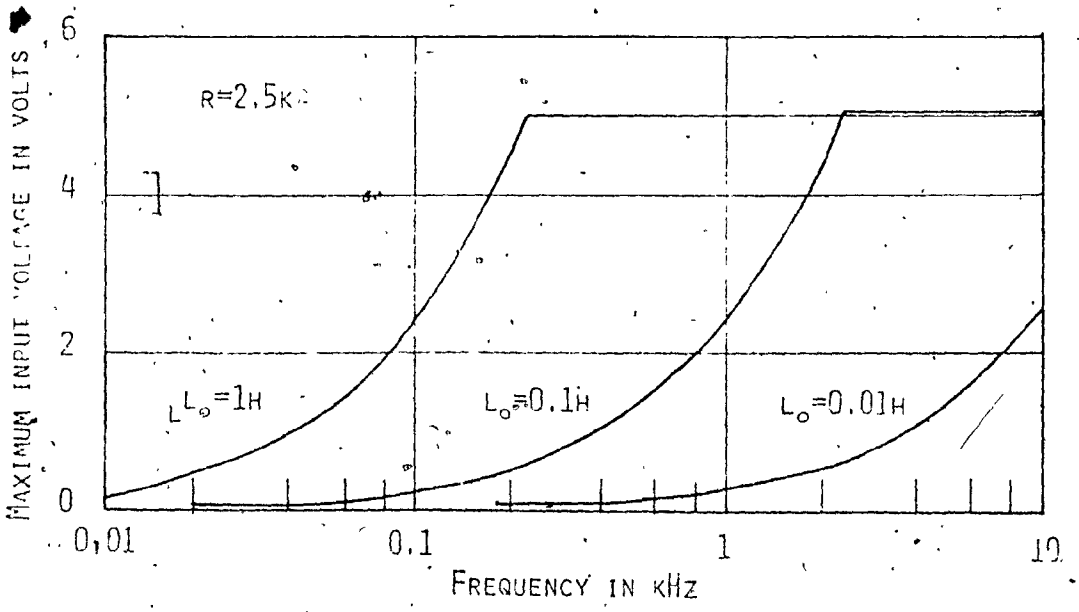

FIG.D.1 THEORETICAL MAXIMUM INPUT VOLTAGE AGAINST FREQUENCY FOR DIFFERENT NOMINAL INDUCTANCES (AMPLIFIER TYPE μA741C).

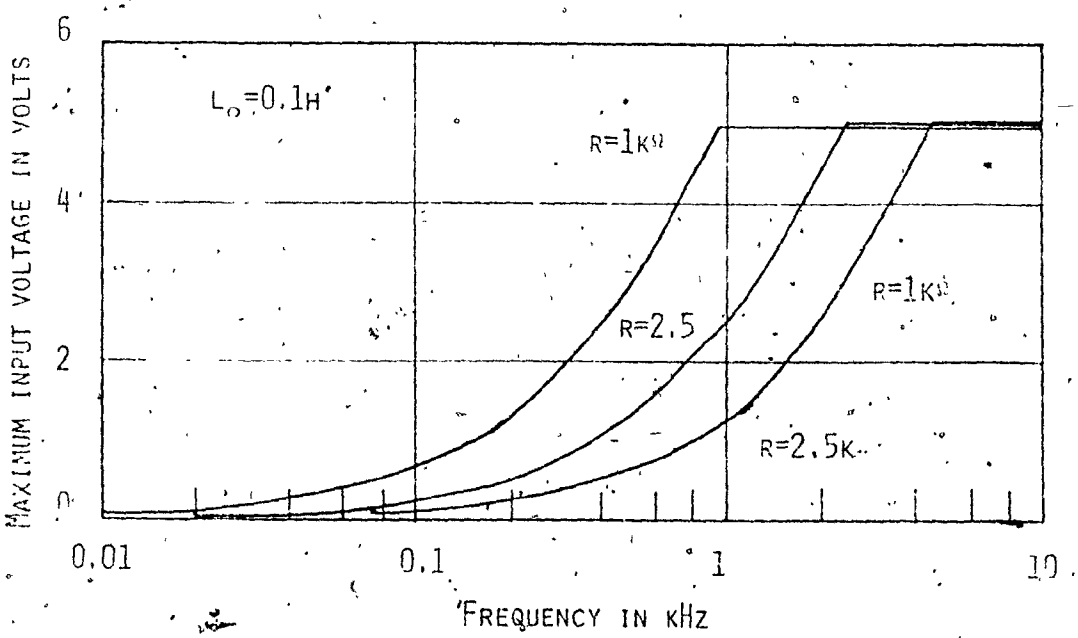

FIG.D.2 THEORETICAL MAXIMUM INPUT VOLTAGE AGAINST FREQUENCY FOR DIFFERENT GYRATION RESISTANCES (AMPLIFIER TYPE μA741C).

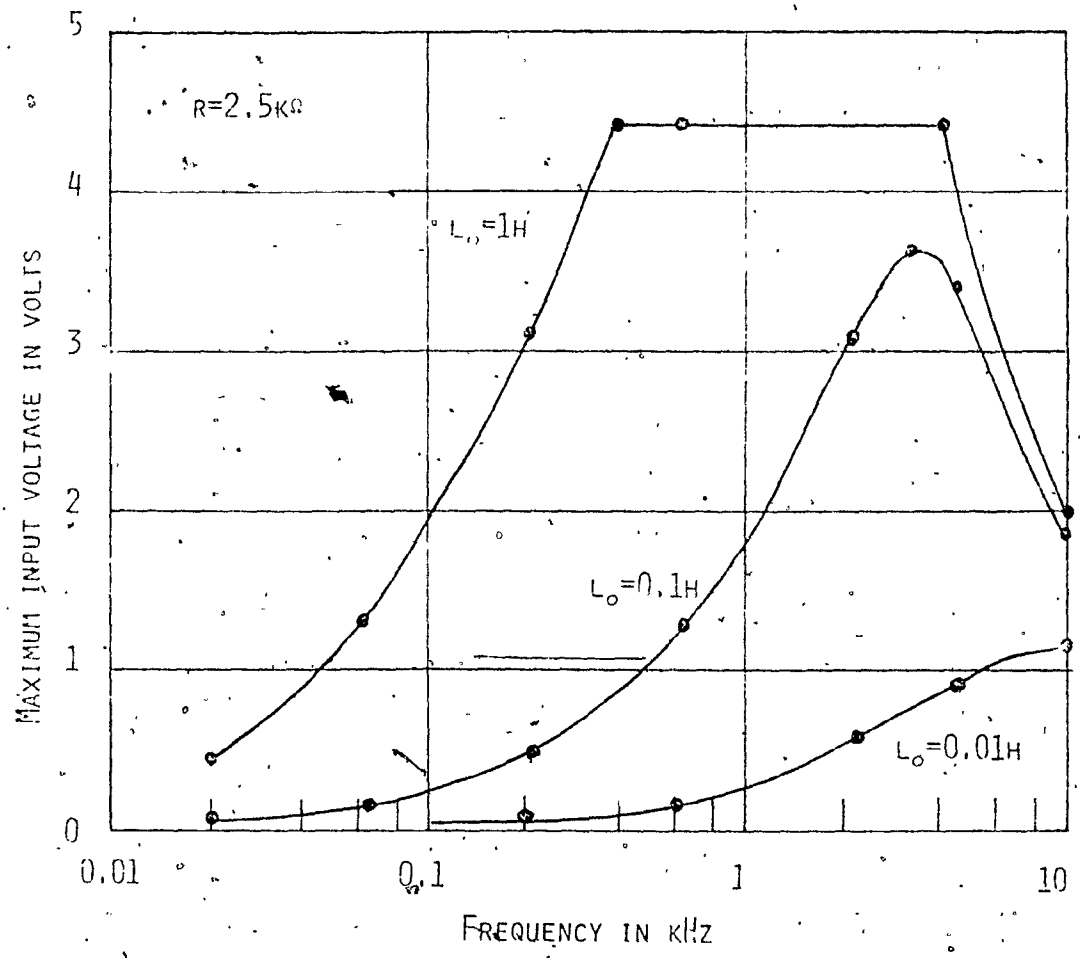

FIG.D.3 MEASURED MAXIMUM INPUT VOLTAGE AGAINST FREQUENCY FOR DIFFERENT NOMINAL INDUCTANCES (AMPLIFIER TYPE μA741C).

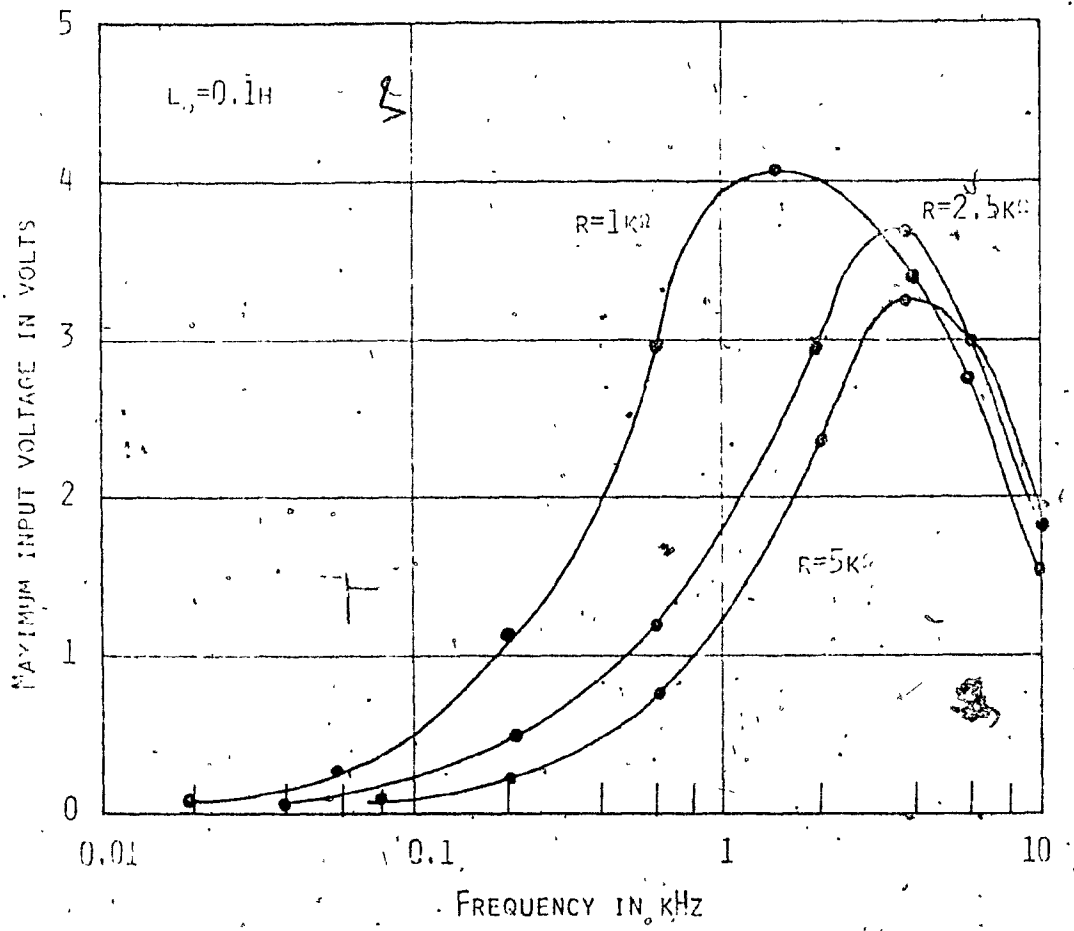

FIG.D.4 MEASURED MAXIMUM INPUT VOLTAGE AGAINST FREQUENCY FOR DIFFERENT GYRATION RESISTANCES (AMPLIFIER TYPE μA741C).